# STUDIA

## UNIVERSITATIS BABEŞ-BOLYAI

## CHEMIA

1

1987

CLUJ-NAPOCA

ANUL XXXII 1987

# STUDIA

## UNIVERSITATIS BABEŞ-BOLYAI

## CHEMIA

## 1

Redacţia: 3400 CLUJ-NAPOCA, str. M. Kogălniceanu, 1 ● Telefon 1 61 01

SUMAR — CONTENTS

STUDIA UNIV. BABEŞ—BOLYAI, CHEMIA, XXXII, 1, 1987

# FOREWORD

## REPORT OF MEETING

### II-nd Symposium on Colloid and Surface Chemistry

The II-nd Symposium on Colloids and Surface Chemistry — counted among the events devoted to the 65-th Anniversary of the Romanian Communist Party — was held at the University of Cluj-Napoca, Faculty of Chemical Technology, Department of Physical, Organic and Technological Chemistry, between September 8—10, 1986. The meeting was under the auspicies of the National Council for Science and Technology, The Central Institute for Chemistry, the Ministry of Education and Instruction, the Ministry of Chemical Industry and the Center of Physical Chemistry.

The proceedings fell under the following sections:

I. Interfacial Phenomena
II. Disperse Systems
III. Biological and Synthesis Membranes
IV. Colloid Systems in Technological Processes

As rightfully expected, the communications did succeed in evidencing the Romanian scientific research contribution to technological development, high revaluation of raw materials, obtainment of new products and materials, devising solutions meant to lower specific and energetic consumptions etc., in light of the exigences set forth by Academician Dr. engineer Elena Ceaușescu in the Congress of Science and Education.

The host-university Rector, Professor Aurel Negucioiu, in his opening speech, warmly welcomed the participants; he also pointed to the importance of such-like events in disseminating most recent achievements of science and technology, and; declaring the symposium open, he wished every success to the proceedings.

The participants in attendance enthusiastically acclaimed the message on behalf on the leadership of the National Council for Science and Technology (NCST) given by Mihail Florescu, minister-secretary of state in the NCST. His opening plenary lecture strongly and competently pointed to the particular importance of the colloid and surface chemistry for most varied branches of the presentday science and technology.

Some 155 communications were contributed by 332 scientists — covering wide areas of the colloid and surface chemistry, such as: stability of the colloid systems meant for complex industrial processes; achievement of high quality products; physico-chemical and mathematical modelling of certain biological processes; characterization and use of the synthesis membranes, as well as their correlation with the natural membrane; developing of technologies of which efficiency be closer to that of the processes in nature etc.

Plenary lectures were given on major themes: "Supermolecular Chemistry and Supermolecular Catalysis" (Professor Constantin Luca), "Some Topics of

Present Interest in the Chemistry of Liquid Interfaces" (Professor Emil Chifu), "Separation Processes and the Synthesis Membrane" (Dr. Gheorghe Rădulescu), "Interaction of Polymers with Surfactants" (Dr. Georgeta Popescu and Mircea Marinescu).

Debates on every communication were carried within an interdisciplinary frame. Varied in-practice-implementations of some new technologies and methodologies were cross-examined, as were made public notice at national level the aspects of great actuality in the field of colloid and surface chemistry.

The participants suggested that suchlike events be held periodically, and the III-rd Symposium meeting take place in the Universitary Center of Timişoara, in 1989.

This issue of the scientific journal, *STUDIA*, of our University is specially devoted to papers contributed in the above mentioned Symposium. The other papers communicated in the symposium will be published in "*Revue Roumaine de Chimie*", in one of its issues of this year.

On behalf of the
Organizing Committee,
EMIL CHIFU and MARIA TOMOAIA-COTIŞEL

*University of Cluj-Napoca*
*Faculty of Chemical Technology*
*Department of Physical, Organic and Technological Chemistry*
*3400 Cluj-Napoca, Romania*

STUDIA UNIV. BABEŞ—BOLYAI, CHEMIA, XXXII, 1, 1987

# SOME TOPICS OF PRESENT INTEREST IN THE CHEMISTRY OF LIQUID INTERFACES

**EMIL CHIFU***

*Received: September 8, 1986*

Some aspects of certain present-day topics in the chemistry of liquid interfaces are surveyed: dynamics of surface films, monomolecular films — membrane models, interfacial tension variations during the mass transfer through fluid interfaces. The applicability of the discussed phenomena, as well as some contributions to this field from the research group in colloid and surface chemistry at the Cluj-Napoca University are also reviewed.

Key-words: *dynamics, surface film, surface tension, interfacial tension, mass transfer, Marangoni effect, monomolecular film, membrane model*

The physical chemistry of liquid interfaces, closely related to colloid chemistry, covers a wide domain, involving the most various branches of science and technology such as: stability of emulsions and foams; polymerization in emulsion; retardation of water evaporation by means of monolayers; detergency; flotation of ores; etc. In the present work we shall limit ourselves to certain aspects of some current problems, namely: dynamics of surface films; monomolecular films — membrane models; interfacial tension variation during the mass transfer through fluid interfaces.

**Dynamics of surface films.** Local gradients of surface tension, caused — for example — by the presence of a surfactant the concentration of which varies from one site to another on a liquid interface, determine the motion of the latter. The area of the surface with large surface tension spontaneously decreases favouring the expansion of the surface with small surface tension. The fact is normal from the thermodynamic point of view and it results in a motion of the liquid interface, in whole. This motion also entails the draw of subjacent liquid layers, due to the lack of slippage between the surface and the "underlaying" bulk liquid. Local temperature changes — causing interfacial tension gradients —, as well as electrical charge variations — also affecting the surface tension — can lead to similar processes.

It was Plateau who first revealed the mobility of liquid interfaces but the interpretation he gave to the phenomenon was inaccurate. The merit of elucidating its nature is due to Marangoni and Gibbs [1]. Nowadays, this phenomenon is commonly known as the "Marangoni effect".

Some works elaborated at the Department of Physical Chemistry of the Cluj University [2] have also contributed to this field of research, since the early 1960s.

* *University of Cluj-Napoca, Faculty of Chemical Technology, Department of Physical, Organic and Technological Chemistry, 3400 Cluj-Napoca, Romania*

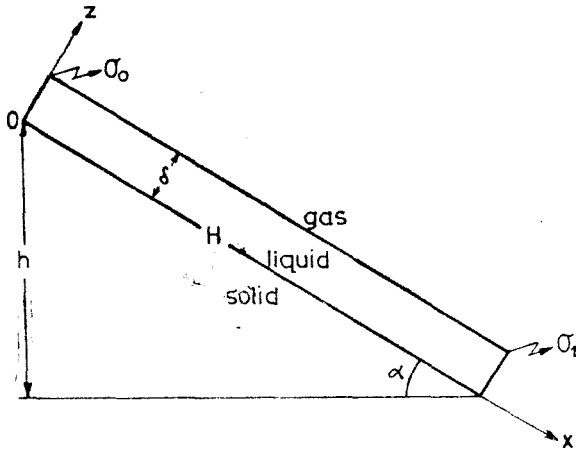


Fig. 1. The thin liquid layer acted by a surface tension gradient on an inclined plane.

Let us consider the model of a thin liquid layer (pellicle) — Fig. 1, of thickness $\delta$, and length H, having an indefinite width (semi-infinite pellicle); it is situated upon a solid inclined plane (the xy plane). The surface tension varies along the Ox axis, having constant values at the extremities of the pellicle: $\sigma_o$ (at x = 0) and $\sigma_1$ (at x = H). These surface tensions are selected so that $\sigma_1 < \sigma_o$. In this case the liquid/gas interface is moved with the negative direction of the Ox axis, and it draws with it subjacent layers of liquid, as well. Yet, a simultaneous draw of liquid occurs with the positive direction of the same axis, due to inclination of the plane. Thus, a concurrent flow is generated through the thin liquid layer, because of the simultaneous action of two forces of opposite directions: the surface tension and the gravity forces. In this relatively simple case of semi-infinite pellicle, one could possibly obtain the analytical solution of the equations governing the flow [3]; so, the velocity of the steady flow through the pellicle will be:

$$v_x = \frac{1}{\mu H}\left[-(\sigma_0 - \sigma_1) + \Gamma hg + \rho g h \delta\right] z - \frac{\rho g h}{2\mu H} z^2 \qquad (1)$$

where $\mu$ is the viscosity of the liquid, $\rho$ its density, $\Gamma$ the surface density, and $g$ the gravity acceleration. Correspondingly, the total flux through the thin liquid layer of section $1 \times \delta$ will be:

$$Q = \int_0^\delta v_x dz = -\frac{\sigma_0 - \sigma_1}{2\mu H}\delta^2 + \frac{1}{2\mu H}\Gamma g h \delta^2 + \frac{1}{3\mu H}\rho g h \delta^3. \qquad (2)$$

It is to be noticed that, due to the symmetry of the problem, the surface shear and/or dilatation viscosities do not intervene in Eqs. (1) and (2) [3].

Qualitatively, the above-presented model was experimentally verified when surface tension gradients were caused both by unequal concentrations of surfactant [2, 4] and by temperature differences [5]. The occurence of the two opposite fluxes in a given range of the level difference $h$ (Fig. 1) was clearly made evident [3].

The liquid pellicle experimentally realized in a surface canal was limited by two solid walls, then it has practically a triangular section (Fig. 2) [4—6]. As the analytical solution of the flow equation is very intricate in such cases, methods of numerical analysis were used, namely the simplex finite element method [5—6]. The corresponding algorithm was written out in a FORTRAN IV program and run on a Felix C 256 computer. As an illustration of the

obtained results, in Fig. 3 is represented the velocity ($v_x$) field corresponding to one set of values of the involved parameters [6]. The existence of the two fluxes of opposite directions can be well noticed (see the arrows), what generally agrees with the experimental data reported previously [4]. Also, the order of magnitude for the experimental rates of flow is found again by the used numerical analysis method

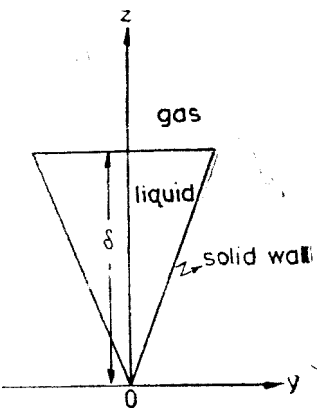


Fig. 2. Transverse section assumed for the thin liquid layer in the numerical calculations.

Important was also, in the model of a liquid pellicle situated on an inclined solid plane and acted by surface tension gradients, the immediate indication that at zero gravity ($g = 0$) — or in microgravity conditions — only the first term (in Eqs. 1—2), that is the Marangoni flow, would persist. This was in agreement with the fact that the intermolecular forces, exhibited in the surface tension forces, are remanent at zero gravity [7]; therefore they are determinant in the establishment of equilibrium and dynamical configurations of liquids in microgravity conditions. That is why our previous studies on this subject [2, 4] allowed us to project some experiments of importance in the space science and technology of liquids [8].

Because the equilibrium shape of a free liquid in microgravity conditions is a sphere, we considered two spherical masses of liquid (drops), linked by a canal. The canal contained a pellicle, along the liquid/gas interface of which acted a surface tension gradient. The examination of this model leads to the conclusion that, if the surface tensions $\sigma_0$ and $\sigma_1$ of the two liquids $L_0$ and $L_1$ (Fig. 4) are different, so that a surface tension gradient arises, there are two factors determining the flow of the liquid through the canal:

1 — the surface tension difference $\sigma_0 - \sigma_1$, causing the Marangoni flow from the drop with smaller to that one with greater surface tension;

2 — the pressure difference

$$p_0 - p_1 = 2\sigma_0/a_0 - 2\sigma_1/a_1, \tag{3}$$

which originates in the spherical shape of the liquid masses, $a_0$ and $a_1$ being the radii of the corresponding drops; this difference will determine the liquid motion termed capillary flow.

In terrestrial conditions, however, the flow between two spherical liquid/gas interfaces cannot be performed. Nevertheless, the behaviour of liquids at zero gravity can be simulated with the help of immiscible liquids of equal densities (neutral buoyancy). Evidently, in this case we shall have liquid/liquid, instead of liquid/gas, interfaces. The model in Fig. 4 can be experimentally performed by immersing the whole system (the canal and the two drops $L_0$ and $L_1$) in a third liquid $L_2$ (the continuous phase), immiscible with $L_0$ and $L_1$. The three liquids must have equal densities.

In interpreting the data it is necessary to take into account the fact that the two types of flow can develop in parallel, or in opposite directions.

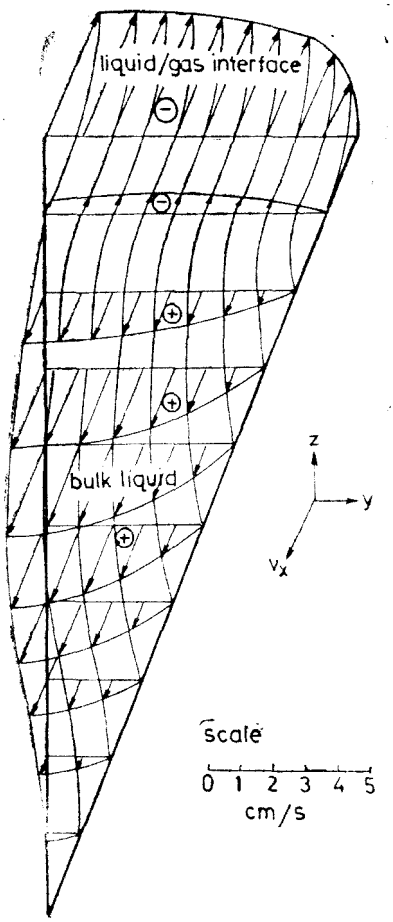


**Fig. 3.** The velocity field corresponding to a system with: $(\sigma_0 - \sigma_1) = 20.4$ dyn.cm$^{-1}$; $\mu = 9.98 \times 10^{-3}$P; $\rho = 0.9962$ g. cm$^{-3}$; $h = 1.8$ cm (Fig. 1); $\delta = 4.80 \times 10^{-2}$ cm; and $a = 3.87 \times 10^{-1}$ cm (Fig. 2); $\alpha = 40°$(Fig. 1); surface viscosities and surface density $\Gamma$ are neglected.

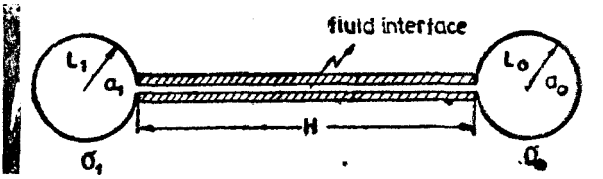


**Fig. 4.** Model of the flow between two spherical liquid/gas interfaces linked by a surface canal — slit.

Thus, when $\sigma_0 > \sigma_1$, the direction of the Marangoni flow will be from $L_1$ to $L_0$; in this case the capillary flow will be parallel to that of Marangoni type, if $p_1 > p_0$ throughout the process. This condition will be fulfilled if, at the initial moment,

$$\sigma_1/a_1 > \sigma_0/a_0 \text{ or } a_0/a_1 > \sigma_0/\sigma_1, \qquad (4)$$

since, afterwards, the values of the ratio $a_0/a_1$ permanently increase, while those of $\sigma_0/\sigma_1$ decrease.

If the initial condition (4) is not fulfilled, each drop becomes contaminated, by the flow, with liquid coming from the other drop and interpretation of the data is very complicated.

With the system of three equidense liquids we have succeeded in rendering evident the Marangoni flow occuring simultaneously and in parallel with the capillary flow. The results obtained for each of the flows, as well as those obtained for the total flux, have been conclusive [9].

In another type of experiment an undeformable drop with high viscosity is suspended in an immiscible liquid having the density equal to that of the drop. The interfacial tension of this "free" drop is then diminished at one of the poles — by injecting there a surfactant, — for example — and it becomes $\sigma_1$, while at the opposite pole it maintains its initial value $\sigma_0$ (Fig. 5). Along the drop meridians, the interfacial tension difference $\sigma_0 - \sigma_1$ determines the Marangoni flow, namely the movement of the interface with the draw of adjacent strata from the outer L, and the inner L′ liquid.

In microgravity conditions the external fluid L can be a gaseous phase. The system made up of a gas bubble (L′) in a liquid (L) is also thinkable.

By developing the theory we have shown — in a frame of spherical coordinates — $r$, $\theta$, $\varphi$ — that the velocities are not functions of the angle $\varphi$, because

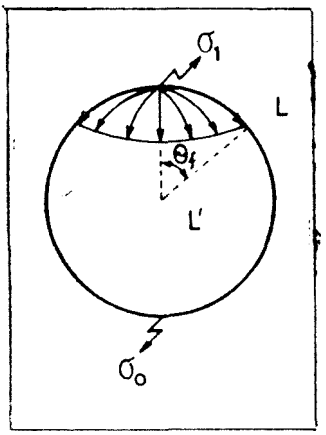


Fig. 5. The position of the surfactant front on the drop surface.

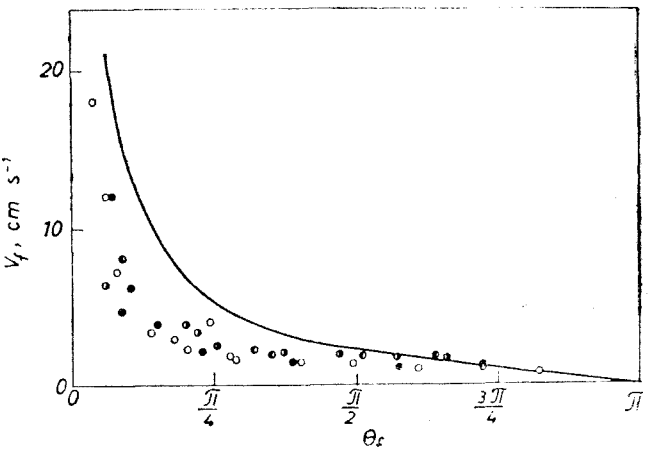


Fig. 6. Experimental (individual points) and calculated (solid line) front velocities along the drop meridians, at $(\sigma_0 - \sigma_1) = 5.5$ dyn. cm$^{-1}$; $(\mu + \mu') = 0.823$ P; and $2k/3a = 0$(Eq. 5); radius of the drop: ◑, 0.49 cm; ●, 0.62 cm; ◐ 0.84 cm; ○, 1.19 cm.

the Marangoni flow is symmetrical with respect to the Oz axis. The position of the surfactant front is characterized only by the value $\theta_f$ of the angle $\theta$ (Fig. 5). The movement forward of the surfactant front was recorded by filming with a camera of high speed (500 images/s) [10].

We have plotted in Fig. 6 the experimental values of the velocity $v_f$ of the surfactant front along the drop meridians, together with the theoretical values (solid line). Although the experimental points give a picture which is close to that obtained by theory, the more is the drop surface covered with surfactant, the better is the agreement. The fact is plausible, because in these conditions the flow can be supposed as quasi-steady, as it was assumed in the theoretical model. The theoretical curve in Fig. 6 was drawn in conformity with the equation proposed [10] in the above-mentioned assumption:

$$v_f = \frac{(\sigma_0 - \sigma_1) \sin \theta_f}{3[\mu + \mu' + (2k/3a)][1 - \cos \theta_f]} \tag{5}$$

where $\mu$ and $\mu'$ are the bulk viscosities of the two liquid phases (L and L'), $k$ is the surface dilatational viscosity and $a$ is the drop radius.

Due to the mobility of the interface (Marangoni effect), also involving the draw of the external liquid, the displacement of the entire drop is promoted as well, with a direction joining the point of maximum to that of minimum surface tension. This process is of interest in the space technology of liquids, as in microgravity conditions gas bubbles or dops suspended in an immiscible liquid are at neutral buoyancy.

When the surface tension gradients are high and the drop viscosity is small, deformations and oscillations are likely to happen, ending in the fission of the drop [10].

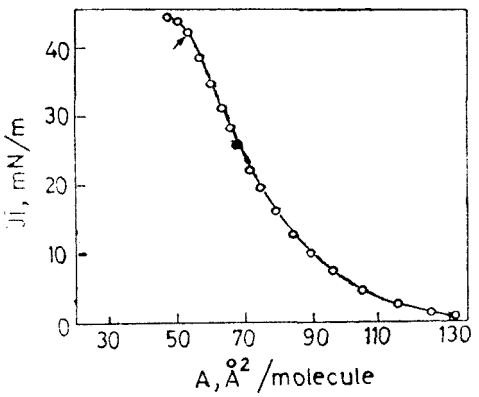


Fig. 7. Surface pressure — area curve of egg lecithin monolayer.

The experiments on the drop dynamics in microgravity conditions may be a matter of interest in modelling some systems such as atomic nuclei or star-type bodies.

The Marangoni flow and convection are very important at present in that branch of space technology of liquids which involves preparation of materials with special properties. For example, in space conditions containerless processes can be performed, and in this way the impurities resulted from possible chemical reactions between the (liquid) substance and the walls of the container are out of the question (see, for example, Ref. [11]).

**Monomolecular films — membrane models.** The biological membrane can be considered in a simplified manner as a lipid bilayer with proteins embedded both inside and outside it. The membrane lipids are natural surfactants and possess many of the synthetic surfactants properties. Most chemical aspects of cell membranes can be understood by means of model systems based on surfactants, and especially on those of the lipid-type. Such systems are plane monolayers and bilayers, as well as spherical bilayers (liposomes included) — see, for example, Ref. [12].

Generally, a liquid interface with an overlaying monomolecular film — monolayer — make up a half—membrane. Such a system has a great stability and it is suited to physico-chemical studies, with quantitative interpretations at the molecular level.

In this direction our research group has undertaken some investigations on phospholipid, galactolipid, fatty acid, protein and carotenoid films, especially in interpreting compression isotherms: surface pressure ($\pi$) — molecular area ($A$), like that in Fig. 7, where $\pi = \sigma_0 - \sigma$; $\sigma_0$ being the surface tension of the interface gas/pure subphase and $\sigma$ that of the film-covered interface [13—18].

The collapse of the monolayer — with formation of a bulk phase — occurs at high surface pressures (see the arrow in Fig. 7). In order to have a knowledge of the molecular interactions in mixed monolayers, we have studied the equilibrium: film — bulk collapsed phase. Taking into account the total ($m$) and partial ($p$) miscibility, as well as the immiscibility ($i$) of the surfactants of biological interest both in the monolayer ($M$) and in the collapsed phase ($C$), the following situations are possible [19], see Table 1.

*Table 1*

**Fundamental types of the equilibrium systems**

| | C | | |
|---|---|---|---|
| *M* | *m* | *p* | *i* |
| *m* | *mM — mC* | *mM — pC* | *mM — iC* |
| *p* | *pM — mC* | *pM — pC* | *pM — iC* |
| *i* | *iM — mC* | *iM — pC* | *iM — iC* |

To discriminate among reciprocal miscibilities of the components the two-dimensional phase rule can be used [20, 15, 18, 22]. In the case of plane interfaces, at constant temperature and external pressure it has the form:

$$w = (c - \varphi) + (\psi - s) \tag{6}$$

where $w$ is the variance of the system, $c$ is the number of independent chemical components of the system, $\varphi$ the number of bulk phases, $\psi$ the number of surface phases and $s$ that of the types of surface. For example, in the case of a two-component film at the air/water interface: $c = 4$ (the substratum — water; the inert gase — air; and the two monolayer-forming components); $\varphi = 3$ (water, air, the collapsed phase); $s = 3$ (the collapsed phase/water; the collapsed phase/air; air/water). If all the types of surface — the air/water interface included — carry only one surface phase then $\psi = 3$. In accordance with Eq. (6) the system is in this case monovariant, therefore $w = 1$. In consequence the surface collapse pressure varies as function of the monolayer composition and the two surfactants are completely miscible both in the monolayer ($M$) and in the bulk collapsed phase ($C$). When the components are immiscible the system is invariant.

In the following we shall refer to the case of two-component systems $mM - mC$ (see Table 1). From the equilibrium condition, namely from the equalization of the chemical potentials in the surface and in the collapsed phase it results that [19, 23]:

$$1 = \frac{f_1^M}{f_1^C} x^M \exp\left[\frac{(\pi_c - \pi_{c,1}) A_1}{kT}\right] + \frac{f_2^M}{f_2^C}(1 - x^M) \exp\left[\frac{(\pi_c - \pi_{c,2}) A_2}{kT}\right] \tag{7}$$

where $\pi_c$ is the collapse pressure of the mixed monolayer, $\pi_{c,i}$ that of the pure component $i$, $A_i$ are the molecular areas, $f_i^{M(C)}$ the activity coefficients and $x^M$ the molar fraction of the component 1 in the monolayer. Eq. (7) represents the curve of the monolayer $\pi_c = \pi_c(x^M)$, but that of the collapsed phase $\pi_c = \pi_c(x^C)$ can be obtained in a similar way, $x^C$ being now the molar fraction of the same component 1 in this phase.

If the interaction between the two components is not very strong, both equilibrium curves — making up a phase diagram — will be monotonous. Monolayer curves for systems of this type have been reported in some of our previous works [15, 22, 24—26].

A strong attraction or repulsion between molecules of the two types of surfactants leads to the occurence of extreme values (maxima or minima) on the equilibrium curves, what corresponds to formation of some kinds of surface "azeothrope".

In the approximation of perfect solutions of the two components in both phases one introduces $f_i^{M(C)} = 1$ in Eq. (7). In Fig. 8 is given the curve of the monolayer for the system β—cryptoxanthin ($A_1 = 23$ Å$^2$): egg lecithin ($A_2 = 54$ Å$^2$) at 295 K. The solid line represents the theoretical curve calculated about Eq. (7) in the approximation of perfect solutions. It can be seen that the experimental points fit well this theoretical curve [19, 22].

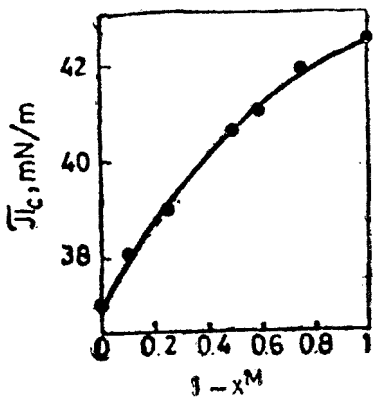


Fig. 8. Monolayer curve of the system β—cryptoxanthin: egg lecithin (see the text).

The nonconformity with the perfect behaviour can be interpreted in different approximations. Thus, assuming that the two surfactants form regular solutions both in the monolayer and in the collapsed phase, the following equations are valid [19, 23]:

$$\ln x^C + \xi^C(1 - x^C)^2 = \ln x^M + \xi^M(1 - x^M)^2 + \\ + (\pi_c - \pi_{c,1})A_1/kT$$

$$\ln (1 - x^C) + \xi^C(x^C)^2 = \ln (1 - x^M) + \\ + \xi^M(x^M)^2 + (\pi_c - \pi_{c,2})A_2/kT \qquad (8)$$

Here $\xi^M$ and $\xi^C$ are the interaction parameters, in the monolayer and the collapsed phase, respectively. The equations (8) allow us to derive $\xi^M$ and $\xi^C$ values ensuring the best description of the experimental $\pi_c = \pi_c(x^M)$ curves [27].

The interaction parameters can be correlated with the molecular structure of the studied surfactants. Being a quantitative measure of molecular interactions they are able to furnish valuable information, at least when surfactants having similar structures are to be compared [27].

Excess free energies of mixing can also be considered for the above-mentioned purpose [22, 24 — 26].

The model of regular solutions is applicable when the positive deviations from the perfect behaviour are recorded for $x_M > 0.5$ provided that $\pi_{c,1} > \pi_{c,2}$. In case the deviations arise at values $x_M < 0.5$, if the condition $\pi_{c,1} > \pi_{c,2}$ is fulfilled, one can resort to the model of molecular associates [28].

On certain systems we succeeded in obtaining information concerning the conformation and packing in monolayers for molecules of biological interest [26, 29].

When there is interaction of the monolayers with electrolytes from the aqueous subphase [30], formation of complexes could possibly occur, as in the case of xanthophylls with ions of the transition metals [31].

Protolytic equilibria in biosurfactant monolayers are also of present interest [32 — 34]. The apparent surface acidity constants are usually smaller than those in the bulk phase, what could be due to preferential accumulation of neutral molecular species in the interface then to a shift of equilibrium, favouring the species with greater surface activity [35].

**Interfacial tension variation during mass transfer through fluid interfaces.** During mass transfer — for example in the liquid/liquid extraction — when one component of the system passes from one phase to the other, an interfacial tension variation can occur at the moment the extraction process starts and persist till distribution equilibrium is established. This variation will be:

$$\Delta\sigma = \sigma^{(e)} - \sigma \qquad (9)$$

where $\sigma^{(e)}$ and $\sigma$ stand for the interfacial tension values when the distribution equilibrium is reached, and at a moment $t$ of the process out of equilibrium, respectively. This problem was only little investigated, as yet [36 — 43].

On the other hand, the process of mass transfer is generated and maintained by the chemical potential difference $\Delta\mu$ between the two phases, with regard to the compound subjected to transfer.

By appealing to the thermodynamics of irreversible processes, let $X_1=\Delta\mu$ be the primary thermodynamic force, and $J_1$ its conjugated thermodynamic flux of substance. Consequently, a variation of the interface area, that is the coupled flux $J_2$, can occur in the system, and then arises the secondary thermodynamic force $X_2 = -\Delta\sigma$.

In order to establish the relationship between the two thermodynamic forces $(\Delta\mu)$ and $(-\Delta\sigma)$ the following linear equations will be used:

$$\begin{aligned} J_1 &= L_{11}\Delta\mu + L_{12}(-\Delta\sigma) \\ J_2 &= L_{21}\Delta\mu + L_{22}(-\Delta\sigma) \end{aligned} \tag{10}$$

in which $L_{ij}$ are the phenomenological coefficients. By taking into account Onsager reciprocity relationships one obtains:

$$\Delta\sigma = M\Delta\mu \tag{11}$$

where $M = L_{21}/L_{22}$ is the so-called surface transfer number [36]. It is to be noted that its dimensions are those of adsorption (mol cm$^{-2}$).

In the case of simple passage of one component between two fluid phases, by making explicit the chemical potential difference, in the approximation of perfect solutions Eq. (11) becomes [37, 38]:

$$\sigma^{(e)} - \sigma = MRT \ln K_D \frac{V_o}{V_w} - MRT \ln \frac{c_w}{c_o} \tag{12}$$

where $c_w$ and $c_0$ are the concentrations of the component subjected to transfer — in the water phase $(w)$ and oil $(o)$, respectively — at a moment $t$ of the process, out of equilibrium; $V_w$ and $V_0$ are the molar volumes of the liquid phases in question; $K_D$ is the distribution constant defined as the ratio of the molar fractions of the given component in the two phases, at equilibrium $(K_D = x_w^{(e)}/x_o^{(e)})$; $R$ and $T$ have their usual meanings.

Being well-known that in some oil phases certain molecules (acids, aliphatic alcohols etc.) are associated we have taken this also into account. By considering a process in which the molecules of the component subjected to transfer are simple in the aqueous phase and predominantly dimer in the oil phase, we have proposed the equation [39—43]:

$$\sigma^{(e)} - \sigma = MRT \ln K \frac{\sqrt{V_o}}{V_w} - MRT \ln \frac{c_w}{\sqrt{c_o}} \tag{13}$$

where $K = x_w^{(e)}/\sqrt{x_o^{(e)}}$.

We mention that Eqs. (11 — 13), foreseeing the linear depenence between the interfacial tension variation and the chemical potential difference, that

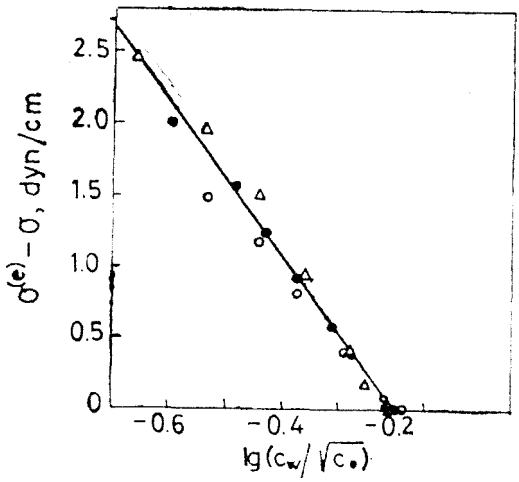


Fig. 9. Interfacial tension variation ($\sigma^{(e)} - \sigma$) *vs.* $\log(c_w/\sqrt{c_o})$, in the course of butyric acid transfer from hexane into water. Initial concentrations ($M$): △, 0.312; ●, 0.532; ○, 0.813.

is the very determinant of the transfer process, will be valid only in conditions not far from equilibrium; the fact agrees with the linear form of the equations like (10).

The experimental control of Eqs. (12) and (13) on the case of monocarboxylic aliphatic acids in various oil/water systems led us to conclusive results. Simultaneous measurements of interfacial tension $\sigma$ and of concentrations $c_w$ and $c_o$ were needed, at different time intervals during the process, until the establishment of distribution equilibrium [38, 39].

In Fig. 9 we give, as an example, the results obtained in the transfer of butyric acid from hexane into water [39]. Even if the initial concentrations of butyric acid were different, a unique "correlation" straigh tline $\sigma^{(e)} - \sigma - \log(c_w/\sqrt{c_o})$ was obtained, in accordance with Eq.(13). Table 2 gives the values $M$ and $K_{calc}$ calculated correspondingly from the slopes and intercepts of the experimental straight lines like that in Fig. 9, according to Eq.(13). The agreement between the constants $K$ calculated like this and those experimentally determined ($K_{exp}$) by dosing the given acids, at equilibrium, in the two phases, is fully satisfactory [39 — 43]. On the other hand, in the transfer of propionic acid from butyl acetate into water, for example, equation (12) is observed [38].

In this view, our results [38 — 43] differ from those of other authors [37] who made use only of a type (12) equation when interpreted experimental data of both systems with simple transfer and systems in which intervened molecular associations.

The above facts contribute to elucidation of the mass transfer mechanism, namely of the liquid-liquid extraction, from the point of view of the interfacial tension variations arising in the process.

*Table 2*

**Surface transfer numbers and distribution constants on extracting some monocarboxylic aliphatic acids from hexane into water.**

| Acid | $M \times 10^{11}$ mol cm$^{-2}$ | $K_{calc}$ | $K_{exp}$ |
|---|---|---|---|
| Propionic acid | 17.0 | 0.118 | 0.134 |
| Butyric acid | 9.3 | 0.031 | 0.033 |
| Valerianic acid | 2.3 | 0.009 | 0.008 |

* * *

Although, at first sight, the three above-discussed items seem different, there are intimate connexions among them. So, the Marangoni effect plays a special role in the space technology of liquids [8 — 11]. It is also invol-

ved in the modelling of deformations and of other movements at the level of biosurfaces [44]. On the other hand, in the mass transfer through fluid interfaces spontaneous convective motion may occur, also related to the Marangoni effect [45].

## REFERENCES


1. Plateau, J., *Phyl. Mag.* Ser. *4*, **38**, 445 (1869); Marangoni, C., *Ann. Phys (Poggendorf)*, **142**, 337 (1871); *Nuovo Cimento*, Ser. *2*, **5—6**, 239 (1872); Gibbs, J., *Trans. Connecticut Acad.*, **3**, 343 (1878).
2. Chifu, E., and Cădariu, I., *Stud. Univ. Babeş—Bolyai, Chem.*, **6**(2), 19 (1961); Chifu, E., *ibid.* **8**(1), 49 (1963); Chifu, E., and Oniciu, L., *ibid.* **9** (1), 95 (1964); Deutsch, R., and Chifu, E., *ibid.* **9**(1), 101 (1964); Chifu, E., *ibid.* **10** (2), 85 (1965); Deutsch, R., Sandru, P., and Chifu, E., *ibid.* **10**(2), 91(1965); Deutsch, R., Szőcs, H., and Chifu, E., *ibid.* **10**(2), 99 (1965); Chifu, E., and Deutsch, R., *Rev. Roumaine Chim.*, **11**, 873 (1966).
3. Chifu, E., and Stan, I., *Rev. Roumaine Chim.*, **27**, 703 (1982).
4. Chifu, E., and Albu, I., *Stud. Univ. Babeş—Bolyai, Chem.*, **13** (1), 99(1968).
5. Chifu, E., Albu, I., Gheorghiu, C. I., Gavrilă, E., Sălăjan, M., and Tomoaia-Cotişel, M., *Rev. Roumaine Chim.*, **31**, 105 (1986).
6. Chifu, E., Gheorghiu, C. I., and Stan, I., *Rev. Roumaine Chim.*, **29**, 31 (1984).
7. Li, T., *J. Chem. Phys.*, **36**, 2369(1962); Painter, H. L., *AIAA Journal*, **2**, 1627 (1964); Otto, E. V., *Chem. Engng. Progr. Symp. Ser.*, **62**, 158(1966); Serebryakov, V. N., *Kosm. Isled.*, **4**, 713 (1966); Seebold, J. G., Holister, M. P., and Satterlee, H. M., *J. Spacecraft*, **4**, 101 (1967).
8. Chifu, E., "Surface flow of liquids in the absence of gravity", 19+20 pp, proposal selected by NASA's Office of Aeronautics and Space Technology, 1977.
9. Chifu, E., Finta, Z., Sălăjan, M., and Gavrilă, E., *Rev. Roumaine Chim.*, **26**, 1345 (1981).
10. Chifu, E., Stan, I., Finta, Z., and Gavrilă, E., *J. Colloid Interface Sci.*, **93**, 140 (1983).
11. Mc. Neil, T. J., Cole, A., and Subramanian, R. S., *J. Amer, Ceram. Soc.*, **68**, 254 (1985).
12. Hiemenz, P. C., "Principles of Colloid and Surface Chemistry", pp 477—481, Marcel Dekker, Inc., New York and Basel, 1986.
13. Chifu, E., Tomoaia, M., and Ioanette, A., *Gazz. Chim. Ital.*, **105**, 1225 (1975).
14. Chifu, E., Tomoaia-Cotişel, M., Andrei, Z., and Bonciu, E., *Gazz. Chim. Ital*, **109**, 365(1979).
15. Tomoaia-Cotişel, M., and Chifu, E., *Gazz. Chim. Ital.*, **109**, 371 (1979).
16. Chifu, E., Tomoaia-Cotişel, M., and Ioanette, A., *Gazz. Chim. Ital.*, **109**, 397 (1979).
17. Chifu, E., Tomoaia-Cotişel, M., and Andrei, Z., *Stud. Univ. Babeş—Bolyai, Chem.*, **24**(2), 63 (1979).
18. Tomoaia-Cotişel, M., *Ph. D. thesis*, University of Cluj-Napoca, 1979.
19. Zsako, I., Tomoaia-Cotişel, M., and Chifu, E., *J. Colloid Interface Sci.*, **102**, 186(1984).
20. Defay, R., Prigogine, I., Bellemans, A., and Ewerett D. H., "Surface Tension and Adsorption", pp 75—79, Longmans, Green, London, 1966.
21. Chifu, E., Zsako, I., and Tomoaia-Cotişel, M., *J. Colloid Interface Sci.*, **95**, 346 (1983).
22. Tomoaia-Cotişel, M., and Chifu, E., *J. Colloid Interface Sci.*, **95**, 355 (1983).
23. Joos, P., and Demel, R. A., *Biochim. Biophys. Acta*, **183**, 447(1969).
24. Chifu, E., and Tomoaia-Cotişel, M., *Rev. Roumaine Chim.*, **24**, 979(1979).
25. Chifu, E., and Tomoaia-Cotişel, M., *Rev. Roumaine Chim.*, **27**, 27(1982).
26. Chifu, E., and Tomoaia-Cotişel, M., in "Surfactants in Solution", (Mittal, K.L., and Lindman, B., eds.), vol. 2, pp. 1349—1364, Plenum Press, New York and London, 1984.
27. Tomoaia-Cotişel, M., Chifu, E., and Zsako, I., *Colloids Surf.*, **14**, 239 (1985).
28. Chifu, E., Chifu, A., Tomoaia-Cotişel, M., and Zsako, I., *Rev. Roumaine Chim.*, **32**, 627 (1987).

29. Zsako, I., Chifu, E., and Tomoaia-Cotişel, M., *Gazz. Chim. Ital.*, **109**, 663 (1979); Tomoaia-Cotişel, M., Zsako, I., and Chifu, E., *Ann. Chim. (Rome)*, **71**, 189 (1981); Tomoaia-Cotişel, M., Chifu, E., and Zsako, I., in "Water and Ions in Biological Systems", (Pullman, A., Vasilescu, V., Packer, L., eds.), pp. 243–250, Plenum Press, New York and London, 1985.
30. Tomoaia-Cotişel, M., Zsako, I., Chifu, E., and Quinn, P. J., *Chem. Phys. Lipids*, **34**, 55 (1983).
31. Chifu, E., Zsako, I., Tomoaia-Cotişel, M., Sălăjan, M., and Albu, I., *J. Colloid Interface Sci.*, **112**, 241 (1986).
32. Chifu, E., Tomoaia-Cotişel, M., Mocanu, A., Andrei, L., and Zsako, I., *Stud. Univ. Babeş—Bolyai, Chem.*, **31**(1), 74 (1986).
33. Zsako, I., Tomoaia-Cotişel, M., Mocanu, A., and Chifu, E., *J. Colloid Interface Sci.*, **110**, 317 (1986).
34. Tomoaia-Cotişel, M., Zsako, I., Mocanu, A., Lupea, M., and Chifu, E., *J. Colloid Interface Sci.*, **117**, 464 (1987).
35. Chifu, E., *Stud. Univ. Babeş—Bolyai, Chem.*, **17**(2), 143 (1972).
36. Zhukhowitskii, A. A., Grigoryan, V. A., and Mikhalik, E., *Doklady Akad. Nauk SSSR*, **155**, 392 (1964); Grigoryan, V. A., Zhukhowitskii, A. A., and Mikhalik, E., *Zhur. fiz. Khim.*, 39, 1179(1965).
37. Frumin, G. T., Ostrovskii, M. V., and Abramzon, A. A., *Zhur priklad. Khim.*, **40**, 1328(1967).
38. Chifu, E., and Albu, I., *Stud. Univ. Babeş—Bolyai, Chem.*, **19**(2), 83 (1974).
39. Chifu, E., and Albu, I., *Ann. Chim. (Rome)*, **65**, 519 (1975).
40. Chifu, E., and Albu, I., *Rev. Chim. (Bucureşti)*, **30**, 1004 (1979).
41. Albu, I., and Chifu, E., *Rev. Roumaine Chim.*, **25**, 459 (1980).
42. Albu, I., and Chifu, E., *Stud. Univ. Babeş—Bolyai, Chem.*, **28**, 46 (1983).
43. Albu, I., *Ph. D. thesis*, University of Cluj-Napoca, 1984.
44. Marquez Garcia, A. R., Dalle Vedove, W., and Sanfeld, A., *J. Chem. Soc., Faraday Trans.*, **77**, 2303 (1981); Dalle Vedove, W., and Bisch, P. M., *J. Physique*, **43**, 1(1982).
45. Hennenberg, M., Bisch, P. M., Vignes-Adler, M., and Sanfeld, A., *J. Colloid Interface Sci.*, **69**, 128 (1979); Dalle Vedove, W., and Sanfeld, A., *ibid.*, **84**, 318 (1981); *ibid.*, **84**, 328 (1981).

STUDIA UNIV. BABEŞ—BOLYAI, CHEMIA, XXXII, 1, 1987

# INTERACTION OF POLYMERS WITH SURFACTANTS

**GEORGETA POPESCU* and MIRCEA MARINESCU***

*Received: September 8, 1986*

Some comparative data obtained on varied systems are presented, wherein tensioactive substances and polymers not only are component parts with special characteristics but also play an important role in the development and transformations of the system. An account is thus given of the interaction and the systems in which it evolves. Discussion is focused upon the possibilities to apply studies upon the interactions of polymers with surfactants, in following directions: employing characteristics of the disperse systems in reactions of interest (polymerization in heterogeneous systems, micellar catalysis, fine synthesis), mimetic systems — as structure or function — of some biosystems (chemical capture and stocking of solar energy — the mimetic function of synthesis —, micelle photocatalysis), specific molecular transportation (liposomes type), employing characteristics of the disperse systems in medical, analytic scopes or in perfectioning investigation techniques etc.

Key-words: *polymer-surfactant interaction, association colloids, disperse systems, membrane phenomena, photosynthesis*

The incipient restricted study of such physico-chemical systems as association colloids has been developing steadily enlarging its content so that what one calls today the polymer-surfactant interaction (PSI) covers a wide range of the phenomena involved in very diverse systems: physico-chemical, chemical, biological.

Delimitation of the fields in which PSI is encountered may be achieved by the following scheme:

Polymer-surfactant interaction was studied in relation with the properties of association colloids, with modification of micellization phenomena on introduction of polymer into the system. The study of disperse systems represents a major application of PSI. The obtaining, stabilization as well as modification of structure and properties of a disperse system (emulsion, suspension or microemulsion) are often possible, taking into account of PSI in systems in which both surfactants and polymers are present. This interaction should also be considered in case of chemical reactions occurring in heterogeneous or microheterogeneous media (disperse systems); these reactions (in suspension, emulsion, microemulsion) find many applications in preparation of substances with special properties which are useful in the industry of paper, dyes, in printing, photography, in the industry of oil extraction, wherever soluble polymers and surfactants coexist in the same medium.

Several decades of assiduous research have evidenced the important role of PSI both in achieving the structure of biological membranes and especially

**ICECHIM, Center of Physical Chemistry, 7 Bucharest, Romania*

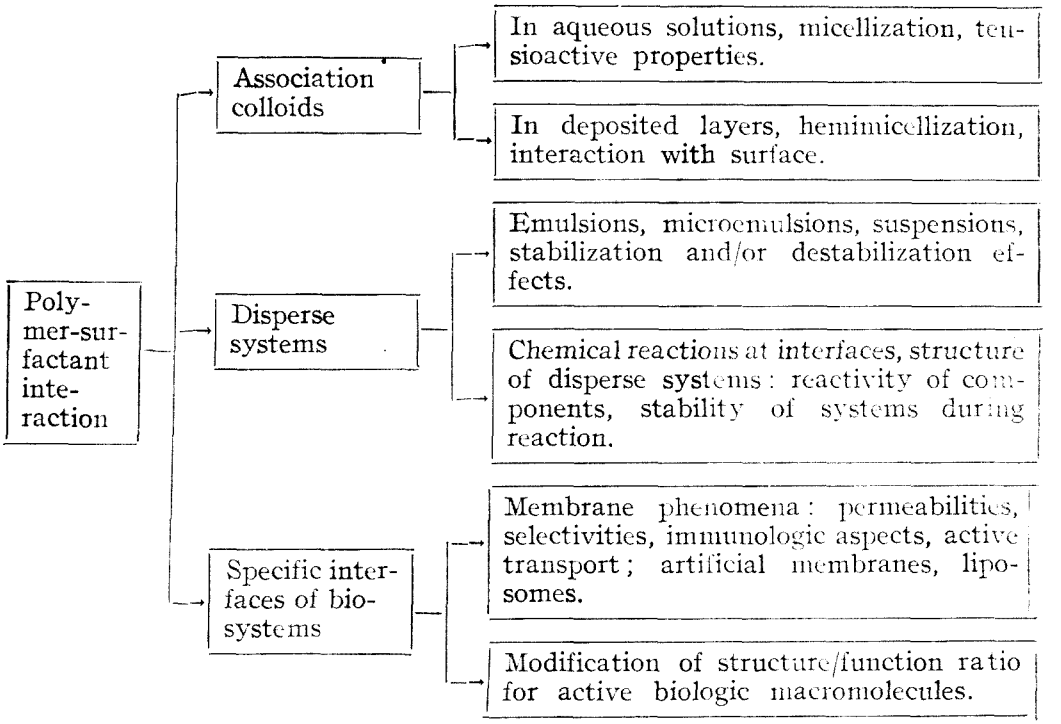


in ensuring their function, and so the function of living systems of which membranes are a part. This is very important not only because it facilitates the understanding of intra- or intermolecular living systems, but because it allows reproducing them in analogous, mimetic systems for the practical purposes of bioengineering: the designing of useful devices. All these aspects will be considered further.

First of all, one should specify the physico-chemical character of PSI. Table 1 [1] lists the types of intermolecular interactions (in case of intramolecular polymers as well). They are all electrostatic and strongly dependent on inter- or intramolecular distance: at small distances, of the order of ionic or charge radius, the repulsions are exerted as in ion-ion or ion-dipole interactions; at larger distances one deals with long-range interactions which are attractions including ion-dipole, dipole-dipole, dipole-induced dipole or ion-induced dipole interactions, also called Keesom or dispersion London forces.

*Table* 1

**Potential functions**

| Interaction type | Potential function |
|---|---|
| Ion — Ion | $1/R$ |
| Ion — Dipole | $1/R^2$ |
| Ion — (Haotic orientation) | $1/R^4$ |
| Dipole — Dipole | $1/R^3$ |
| Dipole — (Haotic orientation) | $1/R^6$ |
| Ion — Induced Dipole | $1/R^4$ |
| Dipole — Induced Dipole | $1/R^6$ |
| Dispersion forces | $1/R^{6*}$ |

* London type interactions

The last two types of interactions proportional to $1/R^4$ and $1/R^6$, respectively, are referred to as Van der Waals interactions, inspired by the name of the correction term which describes the behaviour of a real gas against that of an ideal gas written without the correction terms.

All these interactions act nonspecifically yet synergetically in some instances are called a generic name in colloidal physical chemistry, i.e. *hydrophobic bonds* (excluding water as a solvent).

I. **The role of PSI in association colloids.** It is known that the molecules of amphiphilic substances, as surface active substances, associate in solution to form micellar aggregates which are different as shape, size and number of molecules included depending on the concentration of PSI in water [2]. The aggregation occurs when concentration in solution exceeds the so-called critical micellar concentration (CMC). Studies of the variation of physico-chemical properties as surface tension, electrical conductivity, light scattering with PSI concentration in solution have evidenced the existence [3] of a critical micellar concentration domain (Fig. 1).

In studies on association colloids one has always to do with large molecules (macromolecules). Hydrophobic type interactions were evidenced and, therefore, we consider useful recalling some of our results on the matter.

Professor Eugen Angelescu has conducted through studies on micellar aggregation of association colloids of soap type; his studies have been continued by coworker [4–6]. We refer to the interaction between soap molecules and organic aromatic molecules (e.g. cresols, phenols) evidenced by modification of solution properties (viscosity, electric conductivity) with the amount of additive as *"Angelescu Effect"*. Fig. 2 shows the variation of relative viscosity and electric conductivity of sodium stearate and elaidinate with the concentration of cresol [7] added. Two regions are obvious: I — at low O-cresol concentrations, the viscosity ($\eta$) rises and conductivity ($\lambda$) decreases, and; II — at high concentrations (above 3%) the variations are inverse: $\eta$ decreases and $\lambda$ increases. These results were explained by penetration of O-cresol molecules in micellar aggregates of soaps in water (solubilization).

Angelescu effect depends both on the PSI as well as on the solubilized molecule nature [8]. This is shown in Fig. 3.

The colligative properties (Fig. 1) change when in PSI—water system one introduces polymer. The polymer may be soluble polyelectrolyte with groups that dissociate in water or

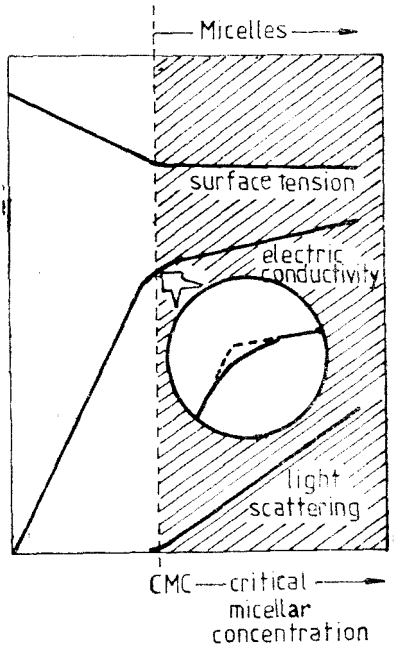


Fig. 1. Critical micellar concentration (CMC) of an aqueous surfactant solution, evidentiation by some experimental methods as: surface tension, electric conductivity and light scattering measurements.

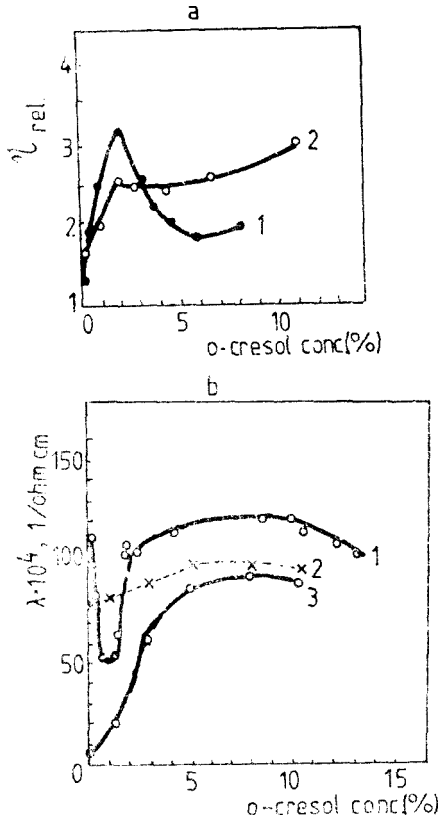


Fig. 2. Experimental indication of *„Angelescu effect"*:
a) the dependence of relative viscosity of aqueous surfactant solutions on percent concentration of added O-cresol: 1 — 0.2 M sodium stearate; 2 — 0.2 M sodium elaïdate; temperature 50 °C;
b) the dependence of electric conductivity of aqueous surfactant solutions on the percent concentration of added O-cresol: 1 — 0.4 M sodium elaïdate; 2 — 0.4 M sodium oleate; 3 — 0.4 M sodium stearate; temperature 30 °C.

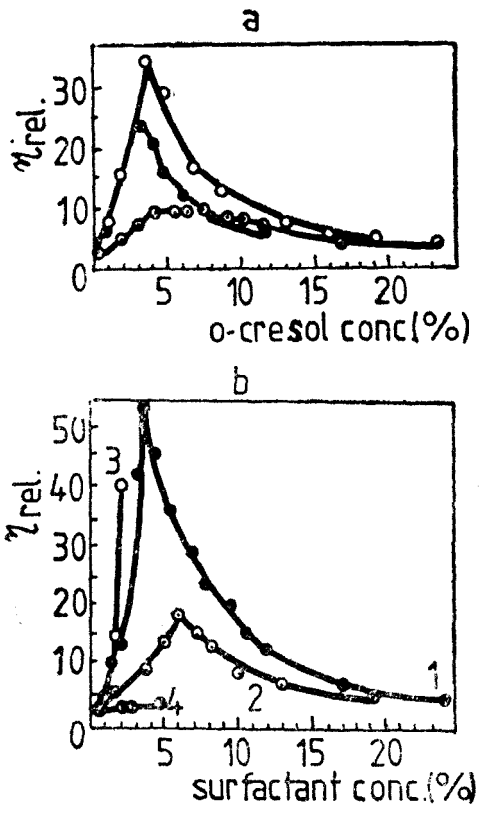


Fig. 3. Dependency of relative viscosity of some soap aqueous solutions on percent concentration of O-cresol:
a) 1 — 0.4 M sodium stearate; 2 — 0.4 M sodium linoleate; 3 — 0.4 M sodium linolenate; temperature 50 °C;
b) the dependence of relative viscosity of 0.4 M sodium linolenate on the concentration of added substance: 1 — O-cresol; 2 — cyclohexanol; 3 — α—naftol; 4 — cyclohexane; temperature 30 °C.

a non-ionic polymer. Fig. 4 evidences a PSI for a system consisting of sodium dodecylsulfate (SDS) as PSI and polyvinylpyrolidone (PVP) as polymer [9]. A change of the dependence of solution surface tension on SDS concentration at PVP addition is obvious. Fig. 5 shows another example: the adsorption of a water-insoluble dye, dimethylazobenzene (DMAB) versus the surfactant concentration in solution [10]. The amount of solubilized DMAB rises as the surfactant concentration increases; the effect turns stronger when polymer is

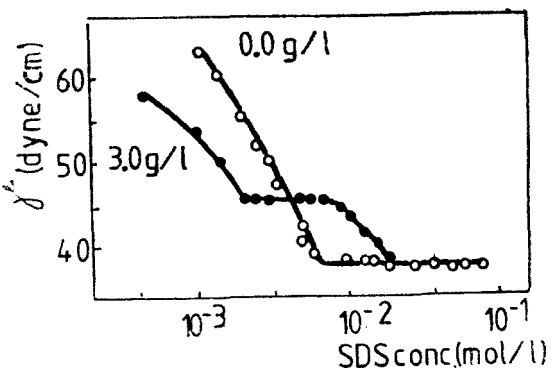


Fig. 4. The surface tension variation of a sodium dodecylsulphate (SDS) aqueous solution without and with 0.3% added polyvinylpyrrolidone; (PVP) with the surfactant (SDS) concentration.

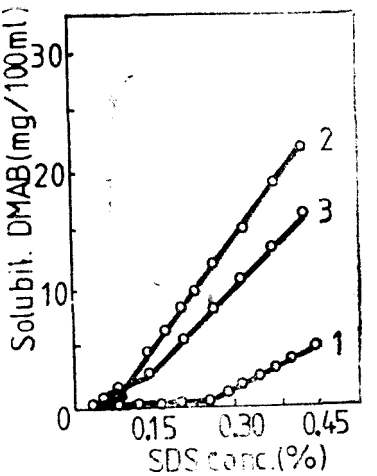


Fig. 5. Solubilization of a dye-dimethylazobenzene (DMAB) — in some SDS aqueous solutions without and with PVP added: 1 — without PVP; 2 — with 0.5% PVP; 3 — with 0.5% PVP-Ac (vinyl copolymer pyrrolidone-acetate) added.

added. These data were interpreted in terms of surfactant adsorption on polymer macromolecules, adsorption ensured by long range London dispersion forces.

In case the polymer bears charges, being a polyelectrolyte, the dipole-dipole or dipole-induced dipole attractions may become more important than dispersion forces.

These are global experimental findings which do not allow a quantitative description of PSI. Experimental methods as diffusion at equilibrium, ion-specific electrodes or fluorescence of specific markers have yielded diagrams which characterize quantitatively PSI, i. e. bonding isotherms.

Fig. 6 shows two such isotherms [11] obtained at different ionic strengths: the number of surfactant molecules adsorbed per lisozyme molecule (a protein whose molecular weight is 14500) versus the surfactant (SDS) concentration; this latter is expressed as concentration of free surfactant molecules not adsorbed on protein. The inset of the figure represents the bonding isotherm for the same system at concentrations below and above CMC. These rezults prove that the gradual adsorption of SDS molecules on protein macromolecule occurs below and above CMC. One should take into account that above CMC the surfactant participates in two associations: one in the polymer and the second in micelle. The inset in Fig. 6 proves just this behaviour, the bonded fraction $\bar{\nu}$ recording a maximum at CMC. Above CMC $\bar{\nu}$ decreases slightly which attests a redistribution of adsorbed SDS molecules among the free fraction, the adsorbed one and that associated in micelle.

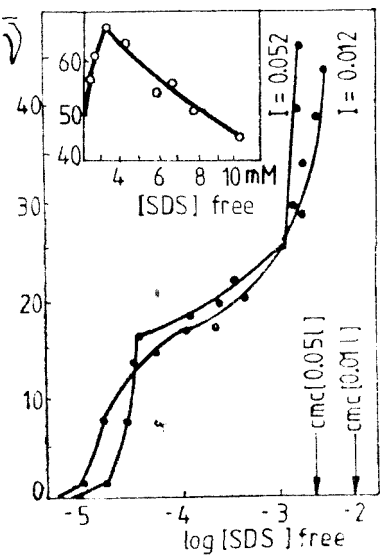


Fig. 6. Representation of two bounding isotherms of SDS on lysozime: 1 — at ionic strength I = 0.012; 2 — at ionic strength I = 0.052; inset representation: the dependence of $\bar{\nu}$, bounding ratio on SDS concentration around CMC of SDS ($5 \cdot 10^{-3}$M/l).

Utilization of the equation:

$$\frac{\bar{\nu}}{[\mathrm{SDS}]_{\mathrm{free}}} = K\,(n - \bar{\nu})$$

for the two bonding isotherms in Fig. 6 yields: $n$ — the number of bounding sites (in this case they are 18—20) and $K$ — the bonding constant; knowledge of the latter allows one to find $\Delta H$, $\Delta G$, $\Delta S$ which give a thermodynamic description of the system [11].

II. **Polymer-surfactant interaction in disperse systems.** The polymer-surfactant interaction play an important part in evolution of some disperse systems in which chemical reactions take place, such as emulsion, microemulsion polymerization. We refer for an example to polymerization of acrylamide in heterogeneous system [12]. One starts from a disperse system which may be an emulsion or a microemulsion and notes that the initial structure of the system modifies when the reaction starts. Figures 7 and 8 evidence the modification of structure during polymerization. Fig. 7 shows the conductometric titration of organic phase (white spirit or cyclohexane and non-ionic emulsifier) with aqueous phase (acrylamide in water 50%). As the phase ratio changes, the conductivity of the system records jump increases which confirms restructuring of emulsion during titration.

In this system, during polymerization at given phase ratio (0 · 3), introduction of initiators into the reaction medium entails a sudden increase of conductivity shortly after the reaction starts; this increase proves that the inversion of emulsion from W/O to O/W type shows transformation of initial emulsion into a forming polymer suspension in the nonpolar solvent (Fig. 8).

This finding supported by other observations (optical and electron microscopy) [12] is accounted for by the appearance of the polymer in the reaction medium which, at very low concentrations, causes an important decrease of interface tensions initially ensured by the nonionic emulsifier employed. The decrease of interface tension causes an immediate inversion. The way the polymer is distributed on the interface initially occupied by emulsifier is not yet known.

III. **Polymer-surfactant interaction at specific interfaces of biosystems.** Most of the structure and part of living membrane operation were elucidated as belonging to a whole. Over the years various alternatives have been advanced for membrane structure; however, throughout the past decade the mosaic model of membrane gained unaninous recognition [13]. The bilipidic layer is two ways or one way crossed by associated proteins which have precise role (Fig. 9). This insertion is ensured by polymer-tenside specific interaction.

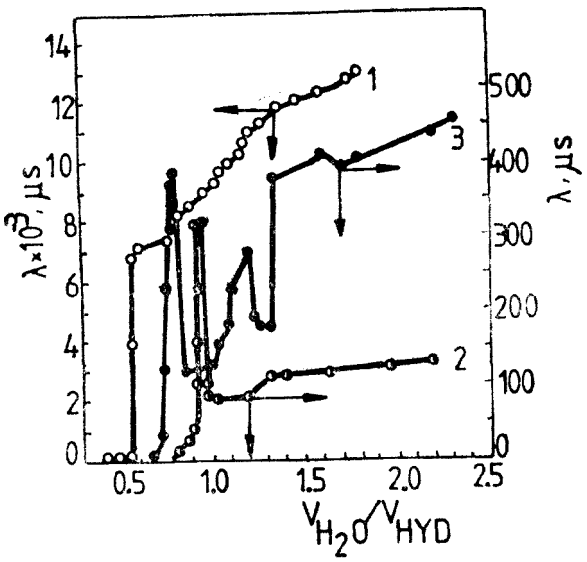


Fig. 7. Conductometric titration of the organic dispersion medium (white spirit + ethoxylated stearine with 8 moles EO 3%): 1 — acrylamide and sodium acetate solution ($H_2O/AA = 1$, moles acetate/moles acetate+moles acrylamide = 0.1); 2 — water; 3 — acrylamide solution ($H_2O/AA = 1$).

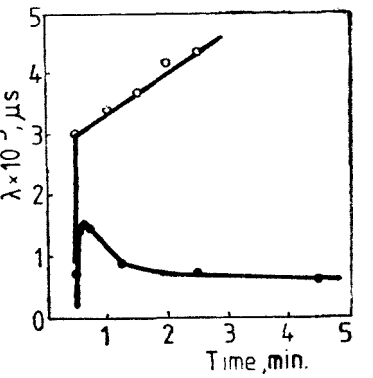


Fig. 8. Conductometric evidence of the inversion of phases during the polymerization reaction: (●) moles acetate/moles acetate + moles acrylamide = 0.02; (○) moles acetate + moles acrylamide = 0.1

The living world exists because solar light is taken over and this is achieved through membranes. Utilization of solar energy which is endless, cheap and nonpolluting, is not recent attempt. In the 3 billion years of living world evolution, countless systems have been tested most of which have survived to our days. Almost all green plants, algae, bacteriae, utilize this source of energy which is sun, in presence of water, air, $CO_2$, as well as sources of nitrogen, in the synthesis of all raw materials that make up the organic matter existing on the planet. Moreover, according to theories admitted today, the activity of plants in warmer geologic eras has remeted in the energy resources strongly exploited today: coal, oil, natural gas.

The existing data prove the importance of photosynthesis in fixing $CO_2$ as well as freeing atmospheric oxygen. Perhaps it is not uninteresting to recall that oxygen, carbon dioxide and water in terrestrial atmosphere are recycled

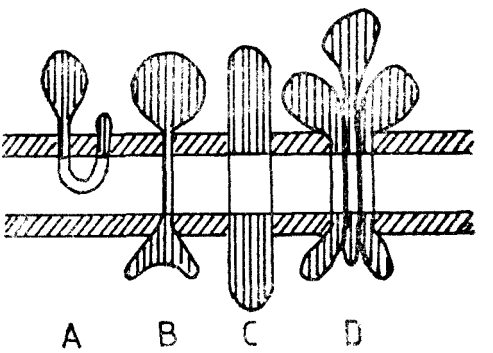


Fig. 9. Schematic representations of membrane-bound proteins. Shaded portions have hydrophilic surfaces and unshaded portions have hydrophobic surfaces in contact with the hydrocarbon core of the bilayer. Protein may lie entirely on one side of the membrane (A), or may have portions exposed on both sides.

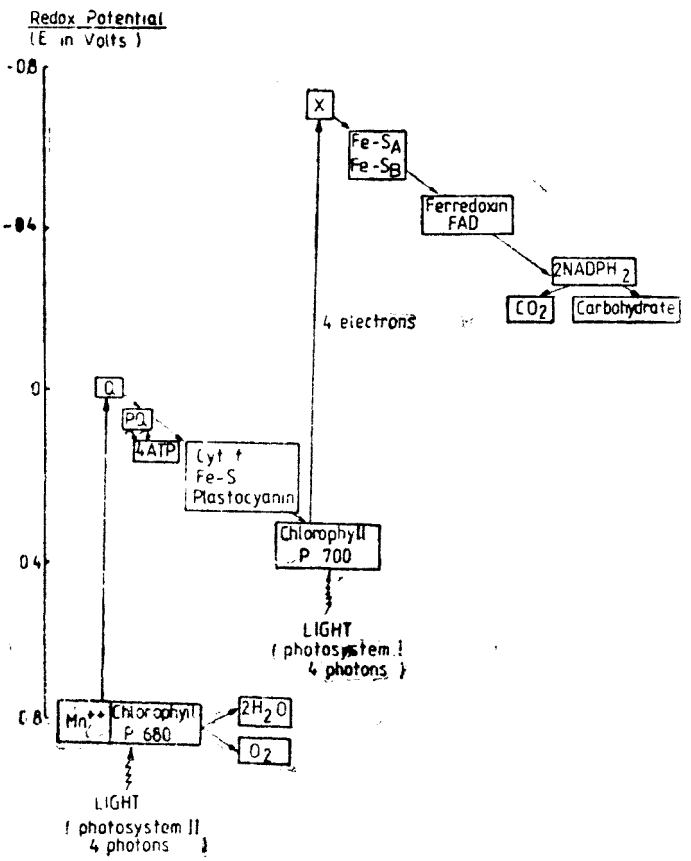


Fig. 10. Proposed photosynthetic electron transport scheme. One quantum of light (photon) activates each electron at each photosystem. A minimum of 8 photons activate 4 electrons through the two photosystems to liberate one $O_2$ and fix one $CO_2$.

continuously through plants: once in 300 years $CO_2$, in 2 000 years $O_2$ and in 2 million years the whole water [14].

The efficiency of photosynthesis amounts to 5—6%, if one takes account of losses and efficiencies of each stage of solar energy processing (from sea level to the energy incorporated in the plant). In spite of all these, the amount of organic matter produced each year is enormous.

Figure 10 shows the general scheme admitted today for the photolysis of water — PHOTOSYSTEM I (PhS I) — and fixing $CO_2$ in carbohydrates (glucides) by algae and higher green plants — PHOTOSYSTEM II (PhS II) a minimum of 8 photons (4 for PhS I and 4 for PhS II) activates the electrons in the two photosystems an free oxygen fixing $O_2$ (one molecule of $O_2$ and

one of $CO_2$) [14]. The same scheme is presented in a simpler form in Fig. 11 [16]. It is worth to note that each of the two stages PhS I and PhS II requires light: with water first and with $CO_2$ second. In both photosystems the first chemical product of light absorption is an excited substance which passed on a higher level following absorption of a quantum.

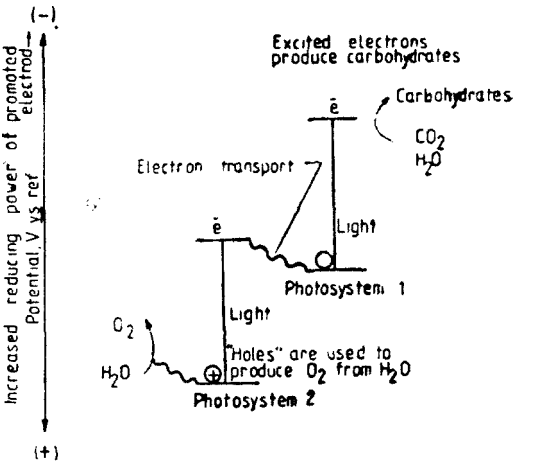


Fig. 11. Illustration of the mechanism of natural photosynthesis. In both photosystems shown, the primary chemical result of light absorbtion is excited-state electron transfer.

The structures which ensure the photosynthetic function in most green plants and algae are referred to as chloroplasts; they are made up as specialized cell-organelles (in bacteria they are called chlorosomes). The chloroplasts are provided with membrane striations organized as stacks, called *grana*, which increase the active surface of the membrane hundreds to thousand times.

The main component of these membrane is a tetrapyrrolic porrfirine cycle that coordinates a magnesium atom a scentral ion and possesses at one pyrrol a hydrocarbonate radical saturated or partially unsaturated called *phytol*. Although the organizing of chlorophyll in chloroplast membranes is fairly diversified, it is generally associated with special ensembles in which a proteic component together with a determined number of chlorophyll molecules (about 250) ensure a so called *„attached reaction centre"* incorporated in the chloroplast membrane through polymer-surfactant interaction as well (Fig. 12) [14]. The figure shows how the P 700 bacterioprotein crosses the whole membrane ensuring a predetermined orientation for chlorophyll molecules. This membrane schematically shown in Fig. 13 [17] is the key of photosynthesis, because the light is absorbed there and mostly because the membrane separates the charges on its two sides. Fig. 13 shows how separation of charges is achieved; this is, in fact, how light energy is collected and stored. Water is thus photolyzed into oxygen and protons with major implications in the geology of earth and structure of biosphere.

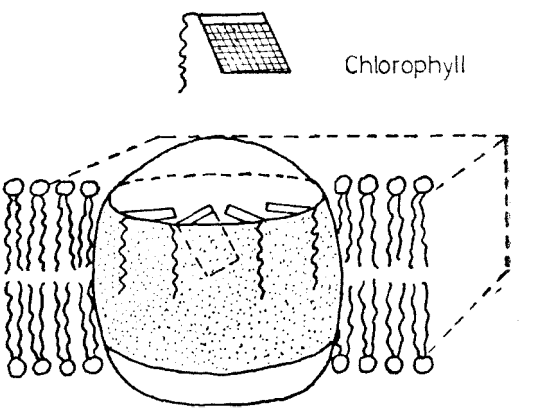


Fig. 12. Proposed orientation of protein particle and chlorophyll molecules in chloroplast membrane.

The reactions of charge separation occur across the membrane; P 700 belongs to PhS I while P 680 to the PhS II. One may also notice in Fig. 13

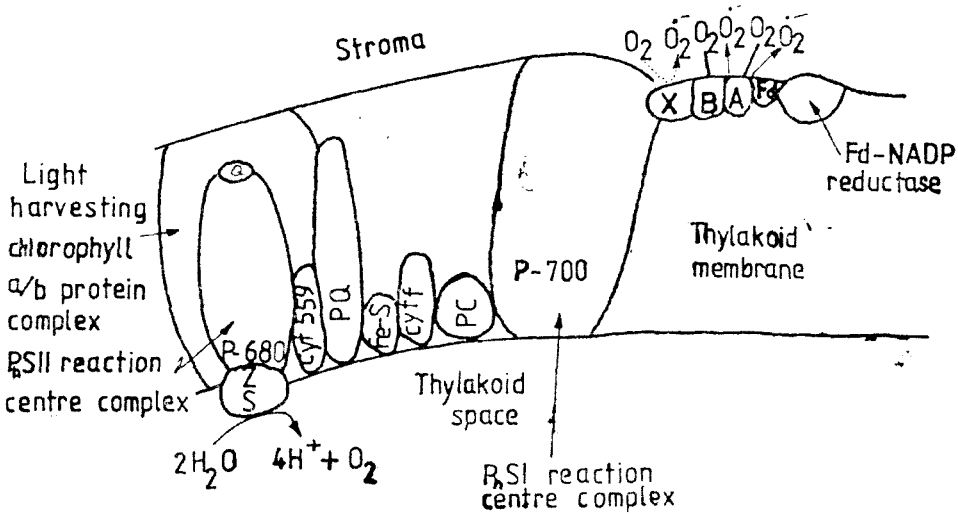


Fig. 13. Schematic representation of the electron transport system in chloroplasts showing the points of interaction with oxygen.

that the chloroplast membrane contains cytochroms b, c, as well as other electron donors and acceptors, unknown substances denoted by Z and X.

These few data regarding the way solar energy is collected and stored by living systems were presented here because at membrane level there exist simultaneously, amphyphilic substances (surfactants specific to biosystems) and proteins; they are present in the microunits making up the living membranes and any other cellular organellae. The attempts at achieving physico-chemical

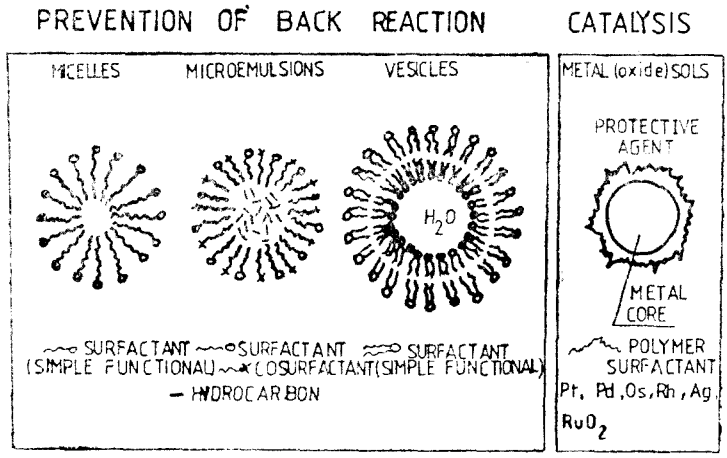


Fig. 14. Structural features of colloidal assemblies employed in light-induced charge separation and redox catalysis.

systems analogous to the photosystems designed to collect and store solar energy have also utilized the components mentioned.

Figure 14 shows several types of disperse photosystems (micellar aggregates, vesicles etc.) utilized to achieve an increase of stability [18]; they are throught to prevent back reactions from occurring at dark, which happens in homogeneous systems containing photosensitive components.

The reversible reactions limit the lasting operations of the system, because they deplete rapidly and irreversibly the components. To avoid such circumstances one separates charges at interface by utilizing surfactants. Fig. 14 also shows how catalysts (rare metals) are conditioned as sols on protection colloids consisting of surfactants and polymers.

The final section of this contribution has emphasized the presence of PSI in the structure of all living systems whose functional possibilities are amplified by them; the ways of collecting and storing solar energy through photosynthesis were also analyzed. The latter example shows that this solution characterizing the living world was also utilized in designing artificial solar energy storage systems. This is how the ring closes and solutions that have been functioning for geological eras are nowadays involved in modern technologies designed to solve the energy problems of the future.

## REFERENCES


1. Z. Simon, „Biochimie cuantică și interacții specifice", Ed. Științifică, Cluj, 1973.
2. K. L. Mittal, P. Mukerjee, in "Micellization, Solubilization and Microemulsions" vol. 1, pp. 1–21, K. L. Mittal Editor, Plenum Press, New York, London, 1977.
3. K. J. Mysels, P. Mukerjee, *Pure and Applied Chemistry*, **51**, 1083–1089, 1979.
4. E. Angelescu, and G. Popescu, *Studii și Cercetări de Chimie*, **VI (2)**, 233–273, 1958; **VI (4)** 617–618, 1958; **VII (2)** 187–196, 1959.
5. E. Angelescu, and G. Popescu, *Rev. Roumaine Chim.*, **11**, 503–508, 1966; **11**, 1389–1396, 1966.
6. G. Popescu, *Rev. Roumaine Chim.*, **15**, 431–440, 1970.
7. E. Angelescu, and G. Popescu, *Proceedings of the IV-th International Congress on Surface Active Substances*, Brussels, September, 1964; Gordon § Breach Science Publishers Inc., London, New York, Paris, vol. II, pp. 641–650.
8. E. Angelescu, and G. Popescu, *Rev. Roumaine Chim.*, **13**(9), 1207–1214, 1968.
9. H. Lange, *Chemiker Zeitung*, **96**, 192, 1972.
10. G. Popescu, M. Radu, D. Anghel, *Proceedings of the VI-th International Congress on Surface Active Substances*, Zürich, Sept. 1972.
11. M. N. Jones, and Ph. Manley, *J. C. S. Faraday Trans. I*, **75**, 1736, 1979.
12. C. M. Boghină, C. I. Cincu, N. N. Marinescu, M. N. Marinescu, M. V. Dimonie, M. Leca, G. Popescu, C. G. Oprescu, A. Roșanu, and M. Lungu, *J. Macromol. Sci. Chem.*, **A22(5–7)**, 591–618, 1985.
13. C. Tanford, *Journ. of Polymer Science: Polymer Symposium* **62**, 189. 1978.
14. D. O. Hall, *Nature*, **278**, 114–117, 1979; *Solar Energy* **22**, 302–324, 1979.
15. D. O. Hall, "Biological Solar Energy Conversion" Symposium, oct. 1978, Diepenbeek, Belgium.
16. M. S. Wrighton, *Chemical and Engineering News*, **57**, 29–47, 1979.
17. D. O. Hall, "Trends in Biochemical Sciences", pp. 188–191, July, 1980.
18. M. Grätzel, in: "Photochemical Conversion and Storage of Solar Energy, Edited by J. S. Connolly, Acad. Press, New York, London, 1981.

STUDIA UNIV. BABEŞ-BOLYAI, CHEMIA, XXXII, 1, 1987

# SEPARATION PROCESSES AND THE SYNTHESIS MEMBRANE

**GHEORGHE RĂDULESCU***

*Received: September 8, 1986*

A general account is given on the separation processes (microfiltration and ultrafiltration that take place in the membrane representing a barrier between two phases, with implication on the transport processes of matter. Reference is made to the mechanics of such processes, its applicableness, as well as to the membrane nature.

Key-words: *membrane processes, microfiltration, ultrafiltration*

Through their characteristics, membranes have called for less conventional procedures and technologies, and in so doing they have entailed the presentday development of many a field of science and technics, wich would have been impossible without the progress achieved in the knowledge of membrane processes.

Presently, the membrane phenomenon-based procedures and technologies such as osmosis, reverse osmosis, dialysis, hemodialysis, electrodialysis, ultrafiltration, diffusion and gas permeation have spread on a large scale and allow for a more economical solving of certain processes which other technologies fail to adequately do.

Not long before the 60's, researchers of the University of California (Los Angeles) [1, 2] found that a cellulose acetate membrane was able to separate salt from water, what later would lie at the basis of desalination industry by reverse osmosis process, perfectioning such types of membranes [3, 4]. Proceeding from this findings, new membranes have been developed of which use allow of purifying industrial residues, they could also be successfully used in food industry processes, in yielding chlorine and sodium hydrate, for obtainment of high purity chemicals, as well as in medicine.

The semipermeable membrane separation techniques have long been known, yet it was during the last twenty-five years only that they have known large-scale developement. These changes have been prompted by the researches conducted at the Office of Saline Water in the United States, as well as by the Délégation Générale à la Recherche Scientifique et Technique in France, which collaboratively with some Universities and specialized companies have synthesized new types of polymers whose macromolecular state allows for film characteristics. If dissolved in suitable solvents, they form a viscid solution which, after spreading on a plane surface can solidify through solvent evaporation, or through solvent evaporation in a precipitation bath, yielding fine films that represent some sort of permiability — and selectivity — related to high performance barriers,

* *University of Cluj-Napoca, Faculty of Chemical Technology, 3400 Cluj-Napoca, Romania*

existing thus the possibility to obtain a large number of synthetic membranes with neededly imparted characteristics.

Theoretically, it can be admitted that most of the exchanges and separations in the homogene and heterogene phases are accounted for by the membrane technique, which, in fact, reproduces what nature has optimised at the level of exchanges and permeations through the selective natural walls, termed biological membranes.

Needless to particularly insist upon the principles of these techniques or upon the mathematical description of the physical processes lying at their base since they can be found in numerous reference works [5—13], we only review some aspects that enable us to get an insight in the presentday development of the two above mentioned processes, which are today applied on an industrial scale.

**What is a membrane?** The membrane is considered a phase or structure that is interposed between two phases or compartments, being able to make the substance transport through it more difficult or even hamper it, or allowing for permeation of certain species of particles only. Therefore, it is some sort of a barrier, an imperfect discontinuity region between two phases, respectively, the constituents of the phase mass being likely to be unequally transported through the membrane what entails their separation. As seen, difference is made in the membrane definition between region and interface so that they are not taken for each other. Generally, membranes can be considered as gel-like, lamellar systems of thickness depassing molecular dimensions and opposing some resistence to breaking [11, 14, 15].

**Membrane processes.** In general, a membrane process-based functioning system consists of two fluid, uniform and homogeneous phases wherein matter and energy can be exchanged at rates generated by the characteristics of the phase or of the group of phases, by the barrier separating them, respectively, which is the membrane itself.

A membrane process consists in permeation of a constituent or group of similar constituents from the fluid in contact with one surface of the membrane onto the liquid in contact with its second one, what can lead to separation of the fluid phase constituents.

In separation processes, membrane plays the role of some selective barrier for the constituents of a mixture. The microscopic processes characterizing membrane phenomena are due to the molecular interaction between membranes and fluids, and the differing affinity grade entails a differing transport coefficient for the constituents, what allows of their separation. Obviously, separation takes place on the surface of the membrane or within it where molecular interactions can take place, and clarification of the phenomena occurring there allows for ascertainment of the permeability mechanism. In the main, the permeability through the membrane involves both the diffusion phenomena through the membrane and solubility of the species diffusing through it, the latter phenomenon being the consequence of the molecular interactions.

However, some propelling force is needed so that the transfer of the components through membrane take place.

Lakshminarayanaiah [16] has given a very suggestive sketch of the transport phenomena likely to emerge in adjacent membrane — fluid systems, when one considers the action of some chemical potential difference ($\Delta \mu$), electric potential difference ($\Delta E$), temperature difference ($\Delta T$) or pressure difference ($\Delta P$), as seen in Fig. 1.

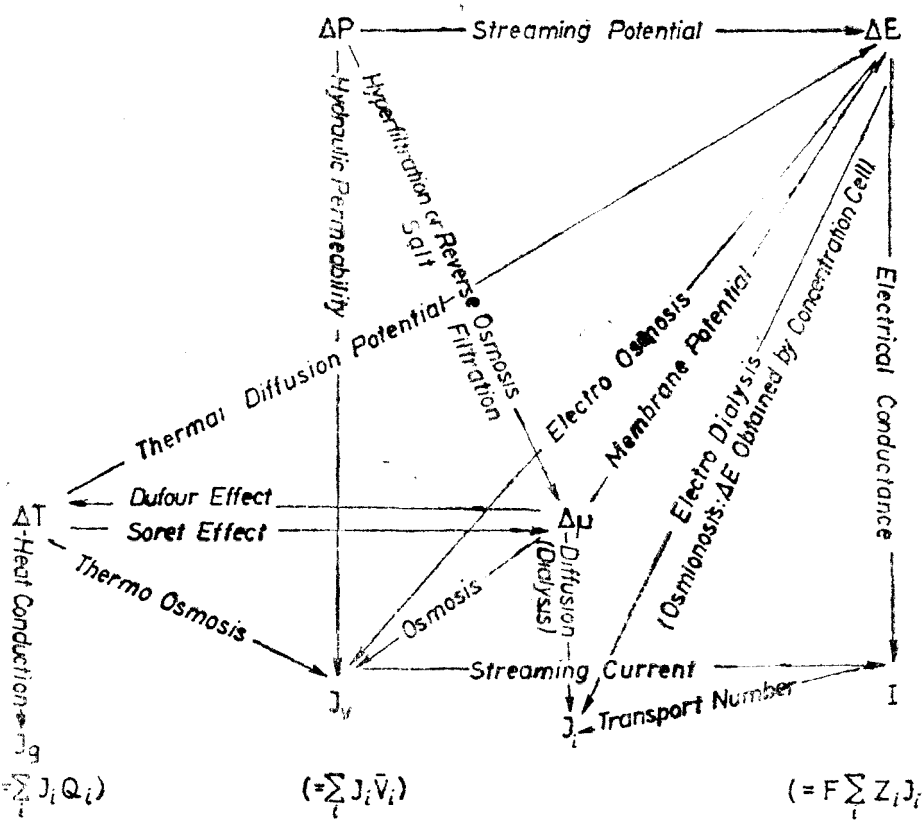


Fig. 1. Scheme of various transport phenomena arising across membranes: $J_i$ — flow of the $i$ type particles; $Q_i$ — heat quantity transferred by species $i$; $V_i$ partial molar volume of the species $i$ in membrane, and; $z_1$ — task of species $i$ [16].

Therefore, if the motive power is generated by a concentration gradient, the through-membrane-separation phenomenon is dialysis; the separation entailed by an electric potential gradient is electrodialysis, while the pressure gradient gives rise to reverse osmosis (hyperfiltration), and ultrafiltration and piezodialysis, thermo-osmosis respectively, ensue when a temperature gradien is involved.

**Why membrane?** From the very beginning, it must be emphasized that the replacement of extant processes by new ones, based on membrane processes, secures to the latter an as important role in the future as has been the one held by laser or carbon fibre. Albeit any industrially-obtainable polymer can also be turned into a membrane, it must however answer to the desired purpose and to a certain production cost. Economically, a system requires membranes with selective properties, as well as corresponding membrane assembling, membranes which can be designed either planar-like, or as lumen (canal) fibres-forms meant to provide large membrane surface in a small volume modulus.

The interest in membrane separation processes lies in that the separation of the substances dissolved into one another, as well as solvent separation do not imply physical state changes, allowing thus to economize the amount of heat necessary to such changes, hence separation turning economically

advantageous. To put it differently, unlike evaporation or crystallization, membrane processes do not consume vaporization or crystallization latent entalpy — non-heat-consuming separations being involved. However, their main shortcoming lies with a slow transmembrane transfer, what makes it difficult to conceive repeated systems comprising a large number of rounds of elements analogous to plates, which are very simply assembled in a distillation column. This hindrance cannot be surmounted but by high selectivity. All in all, the membrane processes are energy-economizing, especially in the intensive-energo fields wherein they have gained most ground.

That is why the industrial separation through membranes has emerged in sea water desalination by reverse osmosis where it takes up only 25% of the energy consumed by the competing technologies.

**Microfiltration.** Microfiltration is a technique allowing for the clearing up of a liquid containing very fine suspensions, under a transversal pressure gradient along the microporous membrane. The modulus used is similar to the one employed in continuous filtration using planar membranes of very fine porosity (0,1—10 μm), which are able to retain microorganisms on the filtering element. That has of late made filtration become a sterilization method in cool that is ever more being used in food industry and pharmaceutics.

Historically, this technique can be considered as a first important application of membranes. Thus in 1929 the German Company „Membran Filtergesellschaft Sartorius Werke" (Göttingen) started producing microfilters endowed with acetate and cellulose nitrate microporous films. Such material was then principally provided to bacterological laboratories. Later, between 1960—1962, this technique was taken over by Lowel Chemical Co in the United States that later became Millipore Co., which reproduced and perfected the German-originating membranes [17].

The ultrafiltration membranes have been much diversified, being used as filter-membrane, in-profusion filters, respectively. Thus one can distinguish:

— Membranes obtained by filtration of some pulverulent material: metals, metal oxides, coal, polytetrafluoroethylene etc.;

— Membranes prepared by selective erosion or degradation of a film formed by filtration of a mixture of two differently originating powders;

— Films presenting microfractures of controlled form. Thus PP or PTFE sheets are subjected to some mechanical and thermic treatment which causes oriented microsplits of well defined amplitudes;

— Membranes obtained by coagulation;

— Membranes obtained by drilling. A thin homogeneous polycarbon film is irradiated by a beam of parallel α-particles or of accelerated hard ions which leaves sensible fraits in the material, followed by chemical revealing;

— Randomly oriented fibre or compressed balls matrices, welded or bound, so that a network of canals is made (glass, wool, azbestos, dicetom clay etc.;

— Mixtures of cellulose esters, polyvinylidene fluoride, cellulose acetate, PVC, PTFE.

Microfiltering membranes are characterized by uniformity of the pores, between 10 μm and 0.025 μm and a thickness of 90—170 μm, they also have high porosity — each $cm^2$ of the filtering surface contains millions of pores which represent 80% of the total filter volume, what allows for obtainment of important flows on unit surface, having a wide application range: sterilization of the preparations used as medicine, high quantity water processing

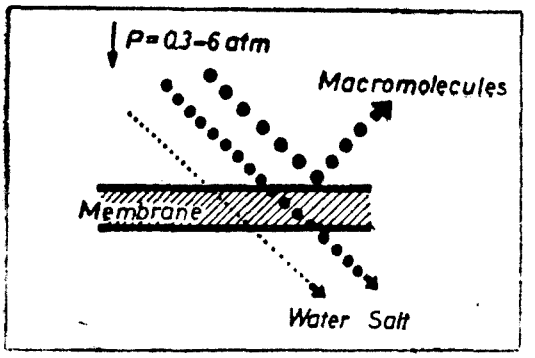


Fig. 2. The ultrafiltration process through membrane

necessary to wash the components used in electronics, in wine and juice processing etc.

**Ultrafiltration.** Ultrafiltration (UF)is a membrane process that allows of solvent and salt elimination from a macromolecular solution, without phase, temperature or ionic force change.

UF is an apparently analogous process to microfiltration yet distinquished in that ultramicroporous membranes are used with very fine pores of which nominal bore ranges between 0.0004 μm (40 Å) and 0.1 μm. These micropores whose bore is beyond the optic microscope perception threshold can be evidenced by an electron microscope.

UF became operant after the technique allowing for obtainment of selective yet very permeable barriers had been set up properly, able to ensure under a pression of 1 bar a flow of thousands of litres per day and $m^2$. Principally, the UF process is given in Fig. 2.

The main characteristics of a membrane are: distribution of the magnitude of the pores defining the selectivity and the solvent flow that determine the performance, which conventionally is obtained from the rejection coefficient.

The membranes used in UF may be of cellulose, polysulphose which work at pH = 1 — 14 and temperatures of up to 80 °C, of polyviliden fluoride, polyamide, copolymers acrylonitrile as well as of other compounds.

The effect of screening through pores (passing through a sieve) is considered as UF mechanism. Retention of some substances depends both on its characteristics (shape, magnitude etc.) as well as on the membrane. The process is carried at external pressures between 0.3 to 6 atm.

The ultramicroporous UF membrane must be resistant, fine, selective and permeabile.

The through-membrane flow is given by

$$J = K \frac{SP}{l\eta} \tag{1}$$

where $J$ stands for through-membrane flow expressed in day/$m^2$ (20 °C) at 2 bars; $K$ is the membrane permeability coefficient; $S$ — membrane surface; $l$ — membrane thickness; $\eta$ — solution viscidity, and the rejection output ($R$) by the relation:

$$R\,\% = \frac{C_0 - C}{C_0} \cdot 100$$

where $C_0$ and $C$ represent the initial concentration and that after UF in the component to be removed.

One of the major difficulties encountered in the UF is the polarization of concentration, that is accumulation of macromolecular solute in the liquid layer situated upstream of the retaining membrane. In this case the phenomenon has a particular importance because the transfer flow is high and also the macromolecular solute, which si collected at the interface, does not but slowly retrodiffuse towards the inside of the treated liquid. A local increase in concentration results, which si translated by an osmotic effect directed in reverse direction of the transport imposed by the applied motive pressure. The accentuated polarization in UF is due to the molecular diffusion constants, which are 2—3 times smaller than those of the salts in the saline waters.

In extreme cases it is observed the less reversible formation of a gelatinized film that adds to the membraue resistence beside that of its own. Therefore, polarization entails considerable reduction of the apparent permeability of the ultrafiltrating barrier.

The effect of this disturbing phenomenon can be imposed onto the treated liquid. This is what accounts for the sometimes intricate geometry of the ultrafilters, of which achievement gives rise to numerous processing difficulties. The choosing of a modulus is finally determined by the use for which it is meant to. It is also demanded consideration of varied parameters namely: nature and concentration of the liquid mixture to fraction; ability of the retained solute to gelatinize; surface/volume ratio, the requested frequency of cleaning the membraues; necessity to sterilize the equipment and the cost of the device. According to necessities, planar, spiral, tubular, capillary moduli or systems endowed with holed fibres of which internal bores range between 200—30 μm have been deviced. No equipment is simultaneously satisfactory for all potential uses, the producers' involvement being given by one of the particular applications.

The UF is widely spread in food industry, pharmaceutics, waste water filtration etc. We thus find it used in concentrating and purifying filtrable viruses or bacteriums, in concentrating enzymes, hormons, eggwhite, in clearing and sterilizing drinks from fruit juice. A particular application is also found in milk industry. Thus, the remaining liquid after coagulation in cheese processing (whey) contains 5—7 g/l of soluble proteins (albumines, globulines) mixed on a great ration with lactose (50 g/l) and with varying quantities of mineral salts and fat matter. Due to their solubility and dilution it is hard to retrieve these proteines which dry by an atomizing process. The such obtained proteic powder may contain 80—85% proteines, being thus a highly valuable nutriment used in human feeding or in preparation of dietetic stuffs.

By ultrafiltration, milk separates in two phases:

a) The reject rich in soluble proteines: casein and some fat matters;

b) The ultrafilltrate containing the majority of the components with small molecular weight (water, lactose, mineral salts etc.).

The reject can be used after drying in processing highly protein-rich compounds meant for food.

The UF is also used in preparing a reject of which composition is equal or close to that of cheese. This reject is coagulated by fermentation and under pression, and cheese is obtained providing final subjection to dry [17, 18].

## REFERENCES

1. Reid, C.E., Breton, E.J., *J. Appl. Polymer Sci.*, **1**, 133(1959).
2. Breton, C.J. Jr., Reid, CE., *A.I.Ch.E., Chem Eng.* Symp. Ser. **24**, 171, (1959).
3. Loeb, S., Sourirajan, S., *U.S.A Licence* 3133132 (1964).
4. Loeb, S., Sourirajan, S., Weawer, D.E., *U.S.A. Licence*, 3133137 (1964).
5. Lakshminarayanaiah, N., *Transport Phenomena in Membranes*, Academic Press, New York, 1969.
6. Merten, U. (ed.), *Desalination by Reverse Osmosis*, MIT Press, Cambridge, Mass., 1966.
7. Bier, M., (ed.), *Membrane Processes in Industry and Biomedicine*, Plenum Press, New York, 1971.
8. Flinn, J.E., (ed.), *Membrane Science and Technology*, Plenum Press, New York, 1970.
9. Eisenmen, G., (ed.), *Membranes*, Vol. 1, 2, Marcel Dekker Inc., New York, 1973.
10. Kesting, R.E., *Synthetic Polymeric Membranes*, McGraw-Hill Book Co., New York, 1971.
11. Hwang, L.T., Kammermeyer, K., *Membranes in Separations*, Wiley—Interscience Publ. New York, 1975.
12. Meares, P., (ed.), *Membranes Separation Processes*, Elsevier Sci. Publ. Co., New York, 1976.
13. Liteanu, C., Rădulescu, Gh., *Bazele Membranologiei*, Ed. ştiinţifică şi enciclopedică, Bucureşti, 1984.
14. Sollner, K., *J. Phys. Chem.*, **49**, 47(1945).
15. Mândru, I., Ceacăreanu, D.M., *Chimia coloizilor şi suprafeţelor*, Ed. tehnică, Bucureşti, p. 40, 1976.
16. Lakshminarayanaiah, N., *Chem., Rev.*, **65**, 491 (1965).
17. Néel, J., *Information Chimie*, **248**, 111(1984).
18. Jacquemet, J.C., *Sciences et Techniques*, **52**, 13 (1978).

STUDIA UNIV. BABEŞ-BOLYAI, CHEMIA, XXXII, 1, 1987

# MONOMOLECULAR FILMS AND COLLAPSE STRUCTURES AS BIOMEMBRANE MODELS

MARIA TOMOAIA-COTIŞEL*, JÁNOS ZSAKÓ*, EMIL CHIFU* and PETER J. QUINN**

*Received: September 8, 1986*

The membrane model systems such as monomolecular films and collapsing monolayers have been usefully employed to investigate the structure and some properties of the biological membranes. Monolayers of lecithins, galactolipids, fatty acids and carotenoids at air/water interfaces are stable, and can be exploited to investigate the conformation and packing of biosurfactant molecules in two-dimensional lattice, as well as the interaction energies between the molecules, under conditions analogous to those that prevail *in vivo*. Structures obtained upon the collapse of galactolipid monomolecular films have been visualized by shadowing techniques and examined under the electron microscope, and they appear to closely resemble liposomes in aqueous systems. The surface characteristics of biosurfactants derived from studies on the behavior of monomolecular films and the collapse structures formed therefrom can be correlated with the conformation of the molecules in natural membranes or to some structural arrangements involved in certain membrane-associated processes.

Key-words: *monomolecular film, collapse structure, membrane model, interaction energy*

**Biomembrane Models.** We do not intend to give a detailed account on the development of structural models ascribed to biological membranes as suffice it to present the simplified molecular architecture of biological membranes, illustrated in Fig. 1 [1]. It can therefrom be inferred that cell membranes consist of a lipid bilayer in which the membrane proteins are either embedded [1], or adsorbed [2] in its surface. It is noteworthy that the first indication of lipid bimolecular arrangement in natural membranes was obtained using monomolecular films at the air/water interface [3].

A bilayer structure is now generally recognised as a basic structural feature of the lipid components of many membranes which either form the boundary of living cells (plasma membrane) or constitute many of the membranous subcellular organelles within cells. Apart from providing the matrix in which the various membrane proteins are supported, the lipid bilayer fulfils an essential barrier function which, because of its semipermeable nature, regulates the passage of solutes between the various subcellular compartments, and between cell and its environment [4]. The dynamic state of a lipid bilayer is a central feature of the fluid-mosaic model of membrane structure, which renders lipids and proteins mobile in such an architecture by virtue of the fluid nature of

* *University of Cluj-Napoca, Faculty of Chemical Technology, Physical Chemistry Department, 3400, Cluj-Napoca, Romania*
** *University of London, King's College, Department of Biochemistry, Campden Hill, London W8 7AH, U.K.*

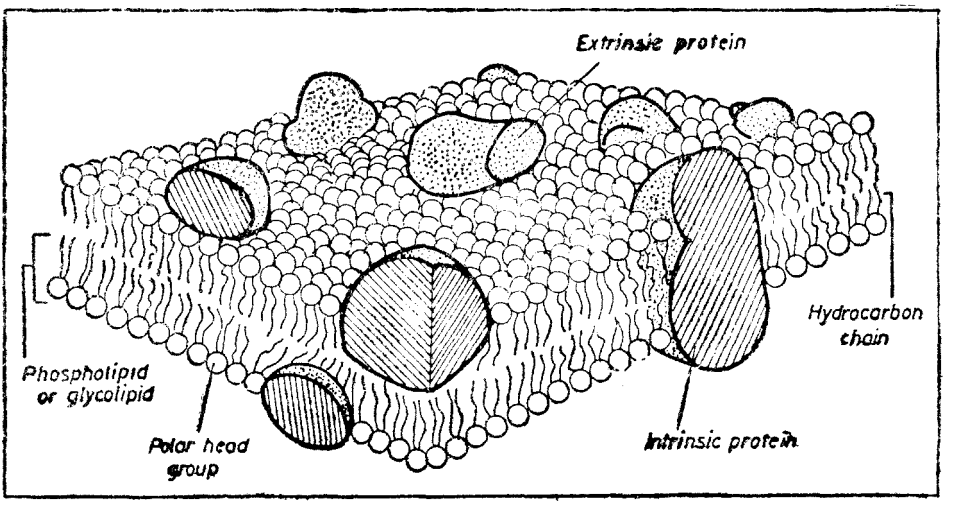


Fig. 1. Fluid mosaic model for biomembrane.

the lipid bilayer (Fig. 1). The relative mobility of the molecules varies from one membrane to another — from states with rapid lateral diffusion and rotation to rigid almost crystalline structures as is in the case of the purple membrane of *Halobacterium halobium* in which bacteriorhodopsin is disposed in a highly regular array and motion is strongly hampered [5].

Given the simplified structure shown in Fig. 1, various model systems can be devised to investigate membrane phenomena. Planar bilayers (black membranes, or BLM) closely resemble the structure of natural membranes, but they are generally unstable and break down within a few minutes. Although useful information has been obtained from studies of such films particularly on their electrical and permeability properties [6], their utility is relatively limited because the composition of these structures cannot be controlled and serious difficulty is encountered in getting them asymmetrical [7]. As a matter of fact, open bilayer lipid membranes can hardly offer a bilayer structure outside the central part, and generally their obtention requires the presence of organic solvent.

Spherical bilayers, or liposomes, — which can be single- or multi-bilayer structures — have proven useful as models of biomembrane structure, especially when employed in reconstituted systems in which solubilized membrane proteins can be reincorporated to form a functional membrane system. These closed lipid membranes — called vesicles — have also proven satisfying in the study of transport phenomena, because of their geometry. The vesicles — or liposomes — can be used in drug incorporation as they display a large interaction surface, yet sometimes disadvantages may arise, such as oxidation of the lipids in the process of their obtention by sonication method etc. [7].

Another membrane model is the planar monolayer — or monomolecular film — at the air/water interface, which stems in the pioneering work of

Langmuir [8]. These structures are relatively stable over long periods of time and suitable for a variety of studies on their molecular characteristics. The use of monolayers as membrane models appears to be justified as they represent one half of a bilayer [4, 9, 10]. Nevertheless, monomolecular films can provide useful information, at molecular level, on conformation and packing of the molecules with biological significance in the natural membrane, under conditions allied to those encountered *in vivo* [9—14]. Monomolecular films also offer an adequate structural arrangement for the experimental investigation of physico-chemical parameters including quantitative examination of the interactions between the film-forming molecules [14—22] as well as between the film and the subphase components such as soluble proteins [23], electrolytes [24], drugs [25] etc.

It is worth mentioning that monolayers are often employed to obtain some artificial membranes — monomolecular [11, 26, 27], or bilayer [7, 28—30] — using different variants of the classical deposition method of a single monolayer or multi-layers onto varied surfaces, developed by Langmuir and Blodgett [31]. Such artificial membranes have been used for the study of the monomolecular film structures at certain constant surface pressure values, as well as for the study of their collapse processes and of the phenomena associated with cell membranes. However, we should mention that special caution must be taken such that artifacts related to the transfer of monolayer films are avoided and the 'built-up film' structure is maintained like that at the air/water interface.

In the following we are giving an account of the results of our researches on the monolayer properties of some biosurfactants both in "pure state", viz. monocomponent films, and in "mixture", i.e. mixed monolayers at the air/water interface.

**Structure of the Biosurfactant Monomolecular Films.** Herein are reviewed the results we have obtained by means of compression isotherms: surface pressure ($\pi$, mN/m) as function of molecular areas ($A$, Å$^2$) on some biosurfactants — major structural and functional components of natural membranes —, such as: galactolipids (monogalactosyl 1,2-distearoyl glycerol: MGDG, and digalactosyl 1,2-distearoyl glycerol: DGDG); lecithins (1,2-dipalmitoyl L-α-phosphatidyl choline: DPL, and 1,2-distearoyl L-α-phosphatidyl choline: DSL); fatty acids [stearic (octadecanoic) acid: SA, oleic (*cis*-9-octadecenoic) acid: OA, and linoleic (*cis*, *cis*-9,12-octadecadienoic) acid: LA]; and carotenoids (equinenone: 4-oxo-β-carotene: E, canthaxanthin: 4,4'-dioxo-β-carotene: CX, β-cryptoxanthin: 3-hydroxy-β-carotene: C, zeaxanthin: 3,3'-dihydroxy-β-carotene: ZX, astaxanthin: 3,3'-dihydroxy 4,4'-dioxo-β-carotene: AX). Experimental details have already been published [14, 17, 18, 27, 32—35]. To illustrate, compression curves of some biosurfactants, namely DGDG, DSL, AX and SA have been plotted in Fig. 2. From the compression isotherms parameters characteristic of the behavior of biosurfactants, such as limiting molecular areas ($A_0$) and surface compressional moduli ($C_{so}^{-1}$), were estimated — the former (dashed lines in Fig. 2) by extrapolating the high surface pressure linear portion of the isotherms to $\pi = 0$, while the latter [36, 37] from the slope of the straight

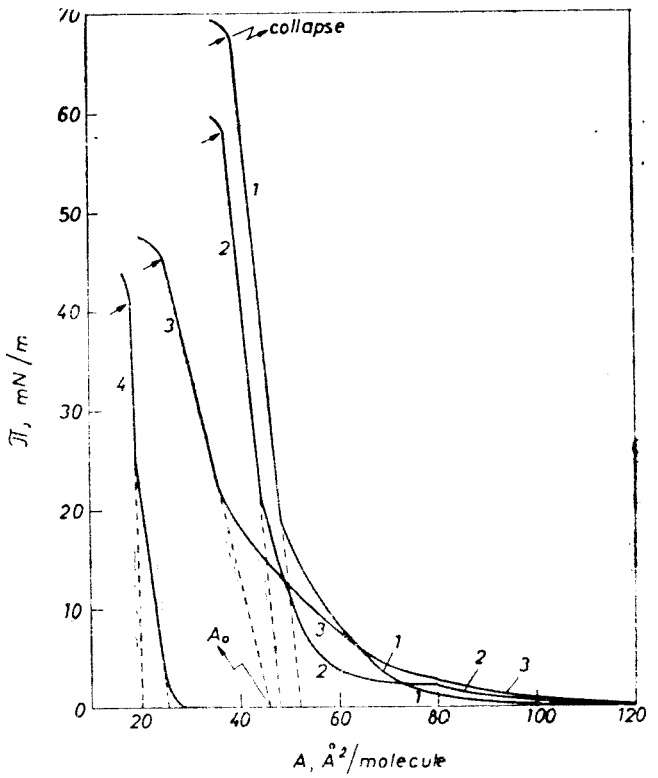


Fig. 2. Surface pressure-area isotherms of DGDG (1), DSL(2), AX(3) and SA(4), at the air/water interface.

line of the curve by the formula $C_{so}^{-1} = -A_0\left(\frac{\partial\pi}{\partial A}\right)_T = A_0\left(\frac{\pi_c}{A_0 - A_c}\right)$. Also, from the $\pi$ vs. $A$ isotherms, the collapse pressures ($\pi_c$) were obtained, as highest pressures to which monomolecular films can be compressed without detectable expulsion of the molecules to form a new, tri-dimensional phase termed as collapsed bulk phase — what is indicated on the curves by a slope change at highest surface pressures —, and the corresponding collapse areas ($A_c$) (arrows in Fig. 2).

The experimental monolayer characteristics $A_0$, $A_c$, $\pi_c$ and $C_{so}^{-1}$ are given in Table 1.

It is to be observed from Table 1 that the $C_{so}^{-1}$ values for carotenoids (1—5), for SA (6, at intermediate surface pressures), and for fatty acids (7 and 8, with unsaturated chains) are near by the lower limit of the values ascribed to condensed-liquid two-dimensional state [36], while for biosurfactants (9—12) of which molecules have each two saturated hydrocarbon chains, they range within the upper limit allowed for condensed surface liquid. As for SA at very high surface pressures, $C_{so}^{-1}$ indicates a two-dimensional solid state.

*Table 1*

**Calculated and experimental molecular areas (Å²); $C_{so}^{-1}$ and $\pi_c$ values (mN/m)**

| Crt. no. | Surfactant | $A_4$ | $A_0$ | $A_6$ | $A_c$ | $A_p$ | $C_{so}^{-1}$ | $\pi_c$ |
|---|---|---|---|---|---|---|---|---|
| 1. | Equinenone (E) | 61 | 60 | 53 | 48 | 38 | 151 | 32 |
| 2. | β — Cryptoxanthin (C) | 40 | 42 | 35 | 23 | 24 | 82 | 37 |
| 3. | Canthaxanthin (CX) | 61 | 60 | 53 | 44 | 38 | 145 | 36 |
| 4. | Zeaxanthin (ZX) | 42 | 49 | 36 | 30 | 29 | 103 | 40 |
| 5. | Astaxanthin (AX) | 42 | 46 | 36 | 25 | 29 | 99 | 45 |
| 6. | Stearic acid* (SA) | 25.5 | 25.5<br>20 | 22 | 18 | 17.6 | 102<br>455 | 40.8 |
| 7. | Oleic acid (OA) | 39 | 41 | 34 | 27 | 26 | 88 | 30 |
| 8. | Linoleic acid (LA) | 47 | 48 | 41 | 31 | 30 | 74 | 26 |
| 9. | DPL** | 69 | 55 | 60 | 42 | 40 | 229 | 55 |
| 10. | DSL** | 69 | 48 | 60 | 37 | 40 | 257 | 58 |
| 11. | MGDG*** | 69 | 49 | 60 | 38 | 35 | 208 | 49 |
| 12. | DGDG*** | 69 | 52 | 60 | 39 | 37 | 240 | 68 |

* $A_0 = 20$ Å² for solid state and $A_0 = 25 \cdot 5$ Å² for condensed liquid monolayers [34];
** Calculated values are for folded „internal salt" (γ) conformations of the lecithin molecules [33];
*** Calculated values are for parallel conformation of polar headgroups of the galactolipid molecules [35].

These results point to the importance of the flexible saturated hydrocarbon chains in providing compact, hardly compressible monolayers at high $\pi$ values.

In interpreting $A_0$ and $A_c$ values geometric molecular models were used [14, 17, 18, 32—35], in accord with the molecular structures of biosurfactants. Thus, a "rigid plate" model has been proposed for carotenoids [14, 17, 32], since the delocalized $\pi$-bond-system of the polyene chain entails the rigidness of their molecules. As regards the biosurfactants with saturated chains (lecithins, galactolipids, stearic acid), or with a smaller number of isolated double-bonds (oleic and linoleic acids) in the hydrocarbon chain, a "*quasi*-rigid prism" model was proposed [14, 33—35] because the collisions between the molecules presumably lead to conformational transitions in both their hydrocarbon and polar regions and during compression the hydrocarbon chains adopt gradually a most extended conformation and a vertical orientation. According to either geometric model, the biosurfactant molecules at the air/water interface are oriented with their polar headgroups toward the aqueous phase whilst their hydrocarbon chains extend into the gaseous phase.

The linear dimensions of the molecules for their most favourable conformation in monolayer were computed from the geometry of the molecules taking into account the internuclear distances, valence angles and the van der Waals radii of the atoms. Area necessities of the vertically oriented molecules were calculated to different approximations. In the case of rotating molecules a tetragonal close packing ($A_4$), or a hexagonal compact packing ($A_6$) of some molecular cylinders obtained by rotation of the oriented molecules were presumed. Also calculated was the area of the non-rotating, closest packed molecules $A_p$ that corresponds to the parallel orientation of the polar headgroup horizontal axes. As for the significance of the rotation, it can be a real one, yet a random, dynamic orientation of the terminal polar group axes can also be imagined. The computed areas $A_4$, $A_6$ and $A_p$, for the twelve biosurfactants studied, are also given in Table 1.

It can be noticed in Table 1 that the experimental area $A_0$ is in good agreement with the $A_4$ value relating to compounds (1—3), (7) and (8). Mention should be made that two values are given for SA because of the two sequential linear portions that occur on the compression isotherm (Fig. 2, curve 4). Thus, the first linear portion, corresponding to a condensed liquid state, gives $A_0 = 25.5$ Å$^2$/molec., equal to $A_4$, while the second one, standing for the solid state of the film (Table 1), leads to $A_0 = 20$ Å$^2$/molec. — the latter ranging between $A_6$ and $A_p$ values. Similarly, $A_6 < A_0 < A_p$ is found with biosurfactants (9—12) having also saturated hydrocarbon chains. Thus, a tetragonal close packing of vertically oriented "rotating" molecules, can be presumed at the molecular area value of $A_0$ in the case of molecules with some rigidity (carotenoids and unsaturated fatty acids) or even for a surface lattice of the saturated long chain molecules (SA), but at intermediate surface pressure only. In the latter alternative phase transition from condensed liquid to solid was evidenced [34]. For the solid state film of SA and for surfactants (9—12) at $A_0$, a hexagonal lattice can be presumed with a close packing of the molecules having a restricted "rotation" (Table 1).

There are however two exceptions, with AX (5) and particularly with ZX (4) where $A_0$ is greater than $A_4$. That is reasonable since both carotenoids

(4 and 5) have polar groups in the air phase, and especially the OH group which allows for dimerization of biosurfactant molecules. Consequently, the area necessity increases greatly if the dimer rotates and seemingly $A_0 > A_4$. This dimerization does not alter the area necessity if the "rotation" of the molecules is restricted as happens at collapse. Therefore, with ZX $A_c \approx A_p$, and with AX $A_c$ is even smaller than $A_p$.

Thus, apparently, ahead of film collapse an almost regular two-dimensional lattice of the "non-rotating" molecules develops, as generally $A_c$ does not differ much from $A_p$.

However, some exceptions can be noted with, for example, biosurfactants (1) and (3) where $A_c$ is greater than $A_p$. These substances have the same hydrocarbon chain, yet they differ by the number of polar groups C = O. Thus, in the case of the film of equinenone (the molecule has one single polar headgroup C = O anchored in the aqueous phase) $A_c$ is by about 10 Å$^2$ greater than $A_p$, while with canthaxanthin (symmetrical molecule with two polar headgroups C = O at each extremity) the experimental collapse area increment — compared to the calculated one — diminishes to about half of that of equinenone, which would illustrate the role of the air phase dipole-dipole forces in film stabilization. As regards zeaxanthin (with symmetrical molecular structure that carries one hydroxyl group at each extremity, i.e. β-ionone ring) $A_c$ is about equal to $A_p$, and with astaxanthin (having one carbonyl and one hydroxyl group at each extremity) the enhanced molecular interactions lead to values of $A_c < A_p$. Therefore, it is likely that the polarity of the terminal groups also interfere in the film-stabilizing complex phenomena.

Experimental results are in good agreement with the above given geometric models relating to both conformational transitions of the molecules (either in the polar portion and in the hydrocarbon one) during monolayer compression, and the transition from one surface lattice type to another.

We mention, at the same time, that these calculations employing molecular geometric models have evidenced the most stable conformation of the molecules in both condensed — and expanded — liquid state of the monolayer, and allowed for explaining the nature of the phase transitions observed on the compression isotherms, if they are caused by conformational transitions (DSL, curve 2 in Fig. 2, Table 1). The phase transitions that appear in biosurfactant monolayers are likely to correlate in a certain way [10] to the fluidity and phase separation characteristics of cell-membrane systems.

At low surface pressures e.g. for $\pi < 15$ mN/m for carotenoid films, i.e. in the expanded — liquid state of the monolayer, the compression isotherms can be well described by means of the van der Waals-type two-dimensional state equations [15, 17, 18]:

$$\left[\pi + \frac{\alpha}{A^{3/2}}\right](A - A'_0) = kT \tag{1}$$

where $\alpha$ and $A'_0$ are empirical parameters that can be derived from experimental $\pi - A$ curves; $\alpha$ is a measure of the intermolecular attractive forces and $A'_0$ is correlated with area necessity of the molecules, also referred to as co-area; the other magnitudes having the known significances. Some examples of computed values for carotenoid films are given in Table 2.

*Table 2*

**Surface characteristics of some surfactants**

| Surfactant | $\pi_c$, mN/m | $C_{so}^{-1}$, mN/m | $\alpha \times 10^{30}$ Nm² | $A_0'$, Å² |
|---|---|---|---|---|
| Equinenone (E) | 32 | 151 | 9.02 | 43.8 |
| Canthaxanthin (CX) | 36 | 145 | 8.74 | 43.2 |
| β — Cryptoxanthin (C) | 37 | 82 | 3.08 | >42.0 |
| Zeaxanthin(ZX) | 40 | 103 | 5.46 | 35.3 |

Having in mind that in the expanded state of the films the main role comes to dipole-dipole intermolecular forces, the parameter $\alpha$ can be taken as a measure of the intermolecular attractive forces dominated by dipole-dipole interactions, and as seen from Table 2 it increases in the order: β-cryptoxanthin < zeaxanthin < canthaxanthin < equinenone. This order also corresponds to the increase of $\overline{C_{so}^{-1}}$, what renders $C_{so}^{-1}$ to be first determined by the structure of the polar end group.

The high $\alpha$ values observed with equinenone and canthaxanthin might be due to the polarizing effect of the carbonyl group upon the $\pi$-electrons, entailing enhanced dipole-dipole interactions in the film.

Comparing the $\pi_c$ values in Table 2 one observes that these values increase in the order: equinenone < canthaxanthin < β-cryptoxanthin < zeaxanthin, what, at high surface pressures, points to the role of the intermolecular hydrogen bondings in the complex stabilizing phenomenon of surfactant films — fact also evidenced in the molecular area values (see Table 1).

Upon the collapse of the monolayer, apart from the dipole-dipole interactions between surfactant molecules and the interaction of the polar group with the subphase liquid, an important role is held by the dispersion forces and the collapse pressure is the resultant of all these cooperative effects. The $\pi_c$ value is greater in the case of saturated long chain molecules (9—12; Table 1) because the dispersion intermolecular forces are much stronger than with unsaturated chain biosurfactants (1, 7, 8).

In order to correlate the values of $\pi_c$, $\alpha$ and $C_{so}^{-1}$ with the electron structure of the molecules, HMO calculations have been performed for the molecules of carotenoids [18]. Of the values of $\pi$-electron densities and of the bond-order, dipole moments of each bond were computed. Taking into account the most stable conformation of the molecules oriented at the interface — as shown above —, the total dipole moments were calculated which characterize the polarity of the headgroup anchored in the aqueous subphase. The determined values of the dipole moments are in good agreement with the experimentally obtained parameters $\pi_c$, $C_{so}^{-1}$ and $\alpha$, allowing for interpretation of the monolayer structure in terms of dipole-dipole interactions and of the dispersion forces.

Given the above and taking into account that the function of the biological membranes is related to the membrane structure, to the presence of molecules in a particular, preferred orientation, further detailed investigation is necessary on biosurfactant molecular conformations in monolayers, on their

molecular organization exhibited in both surface lattice correlated to their packing and orientation in the monomolecular film, and in the collapsing structures emerging from the monolayers "compressed" to surface pressures greater than $\pi_c$.

**Collapse Structures in Monomolecular Films.** Upon compression of the monolayer, after the linear portion of the $\pi - A$ isotherms (of highest surface pressures), a slope change is observed — what points to film collapse, i.e. a new phase emerges — the collapsed bulk phase. During collapse, a part of the surfactant molecules are ejected from the monolayer (the surface lattice) toward a tri-dimensional bulk phase.

Generally, the coordinates of the collapse point, $\pi_c$ and $A_c$ (Fig. 2), are quite reproducible in a wide range of compression rates, that is thermodynamic equilibrium can be presumed between the monolayer and the freshly collapsed bulk phase.

To visualize the collapse structures that form up upon the collapse of the biosurfactants, for example galactolipid film, at the air/water interface shadow-cast electron microscopy was employed. This method lies in the deposition of a monolayer from a galactolipid film at the air/water interface on the surface of a carbon-coated copper electron microscope grid [27] by a modified Langmuir—Blodgett technique [31]. The grid was vertically raised through the film held at a certain surface pressure, at a speed of 0.25 mm.min$^{-1}$. After air-drying the grids are transferred to a vacuum chamber and the surface coated with a thin layer of platinum by shadow-cast at an angle of about 10°. The structural features were examined directly under the electron microscope.

The reproducibility of the images obviously shows that the collapse structures have great stability, maintaining thus their architecture against the thermal and mechanical shocks (transfer, degassing and shadow-casting). The stability of the collapse structures and of the monolayers, as observed on electron micrographs recorded at greater surface pressure than the surface collapse pressure, is likely to be entailed by the cohesion forces of the saturated hidrocarbon chains accompanied by the intermolecular forces through the hydrogen bondings between the galactosyl groups of the lipids or between their polar headgroups and water.

Films of MGDG and DGDG in expanded-liquid and condensed-liquid states have a characteristic appearance in shadow-cast form [27]. The collapse structures are also typical of each of the two lipids. Figs. 3 and 4 show collapsed structures obtained from highly compressed monolayers of MGDG and DGDG, respectively, at greater surface pressures than $\pi_c$. In the case of MGDG the observed structure (Fig. 3) is similar to freeze-fracture replicas prepared from dispersed lipid in the lamellar-gel phase. DGDG, on the other hand, forms multilamellar liposome structures in the dispersed aqueous systems which do not directly resemble the shadow-cast films in the region where the film has collapsed (Fig. 4). The detailed structural arrangement of the lipid in collapsed DGDG monolayers are likely to be entailed by the formation of bilayers from monolayers, and these bilayers are directed toward the aqueous phase, not to the air phase, as is probably the case with MGDG, where even formation of inverted micelles from the monolayer is likely since they occur in dispersed systems under certain conditions [33]. The collapse structure for DGDG see-

mingly relates to the greater polarities of the head groups which consequently lead to enhanced interactions with the aqueous phase, so that, finally, liposome structures are formed at the interface, as obtained with other biosurfactants [39].

It is, however, difficult to make as of now a detailed description of the collapse stages of an overcompressed condensed galactolipid monolayer. Further investigation is needed to elucidate the collapse phenomenon, and the "crumple patterns" that are observed when the films are collapsed.

Yet, relating to collapse mechanism, some conclusions can be drawn from the kinetics of relaxation phenomena of galactolipid films, phenomena occuring in monolayers at constant molecular area values, by recording the surface pressure vs. time curves [27] and from the structure of collapsed phases. From such studies one can infer that MGDG monolayers collapse by a fracture process whereas the DGDG ones by nucleation and a subsequent growth process [27].

Using the example of galactolipids, we have shown that studies on the behavior of these biosurfactants in monolayer can provide important data concerning the physico-chemical properties of molecules in oriented structures at the air/water interface. These, in turn, can be correlated with their behaviour in dispersed systems and ultimately provide a model for understanding their structural and functional role in the biological membrane.

**Mixed Monolayer Films. Miscibility.** Obtaintion of information relating to the way in which individual constituents interact with each other in mixed monomolecular films is important for understanding the structural arrangements in membranes and the specific complexes required for certain membrane phenomena.

Taking into account the major role played by biosurfactants in living cells, we employed monolayer techniques for the beginning, in view of getting data relative to the prevailing interactions between carotenoids and their lipid environment in some biological membranes of plant and animal cells.

Five systems of two-component monolayers are reviewed, consisting of lipid ($A$) and carotenoid ($B$), namely: (1) egg lecithin (EL): β-cryptoxanthin (C); (2) EL: β-cryptoxanthin palmitate (CP); (3) EL: zeaxanthin monopalmitate (ZP); (4) 1,2-distearoyl lecithin (DSL): astaxanthin (AX); and (5) 1,2-distearoyl digalactosyl glycerol (DGDG): AX, investigated by both compression isotherms and ejection curves [20—22, 40, 41].

The miscibility of two components, $A$ and $B$, in monolayer is an important problem that can be interpreted by the additivity rule of molecular areas and by the Gibbs free energies of mixing [14, 42, 43] — either of them being applicable at varied constant values of the surface pressure, yet smaller than the collapse surface pressure of component $B$ in its monocomponent film ($\pi_B$) if $\pi_B < \pi_A$, where $\pi_A$ stands for collapse pressure of the "pure" $A$ monolayer.

Upon collapse the monolayer ($M$) is in equilibrium with a new phase — the collapsed bulk phase ($C$). At high surface pressures the miscibility can be also discussed by employing the phase rule and the collapse pressure method [14, 19—22, 40, 41, 43—46].

In the case of total miscibility of the components in both $M$ and $C$, the shape of the monolayer curve, also termed as collapse isotherm (i.e. collapse

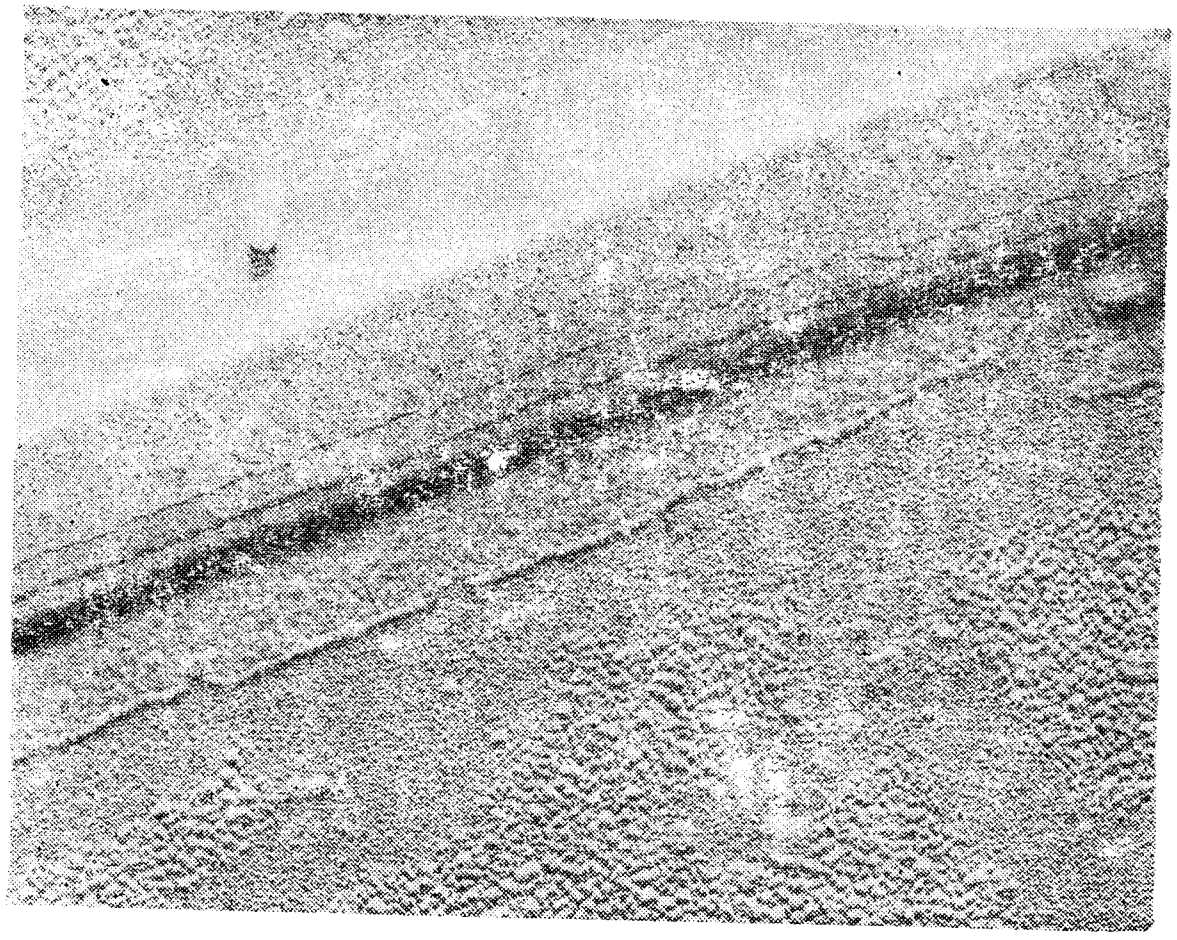

Fig. 3. Electron micrographs of shadow-cast collapsing monomolecular films of MGDG spread on aqueous subphase and compressed to $\pi$ greater than 50 mN/m. Magnification of 91,000 ×.

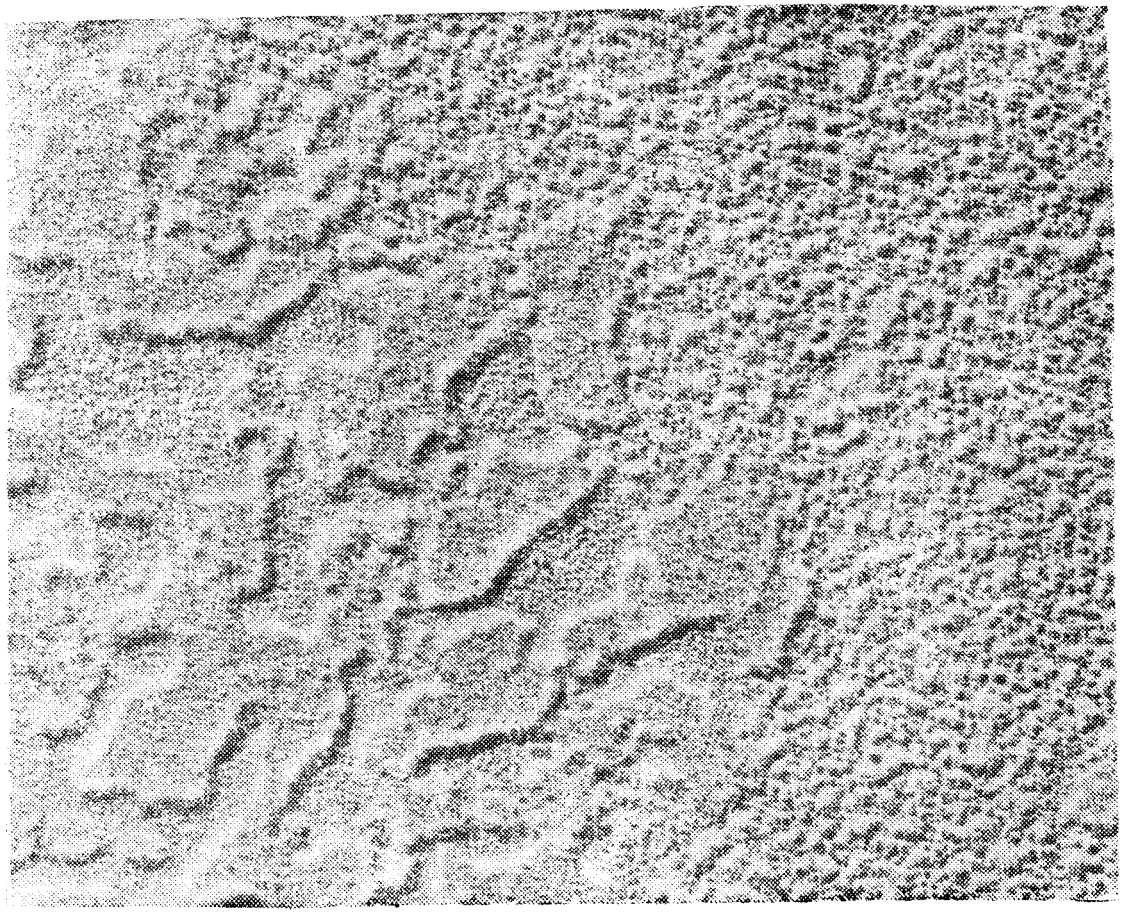

Fig. 4. Electron micrographs of shadow-cast monomolecular films of DCDG on aqueous subphase and compressed to a surface pressure of 69 mN/m, i.e. after collapse. Magnification of 94,000 ×.

surface pressure of the mixed monolayer ($\pi$) as function of monolayer composition ($x_i^M$), where $x_i^\varphi$ is the molar fraction of component $i$ in phase $\varphi$), can be described by using various approximations.

By most simple approximation both phases $M$ and $C$ are considered as perfect solutions of two components and the equation depicting the shape of the monolayer curve has the form:

$$x_A^M \exp\left[(\pi - \pi_A)A_A/kT\right] + (1 - x_A^M) \exp\left[(\pi - \pi_B)A_B/kT\right] = 1 \qquad (2)$$

In Eq. (2) $A_i$ represents the collapse area in the pure monolayer of component $i$. The other magnitudes have the wellknown significance. The $\pi_i$ and $A_i$ values are derived from the experimental compression isotherms of the pure films (some of them are given in Table 1). It has been found experimentally that collapse pressure is a unique function of the monolayer composition, systems (1—5) being monovariant. This means that components $A$ and $B$ are miscible in both phases ($M$ and $C$), in accord with surface phase rule [20—22, 40, 41, 44, 45]. Deviation of the experimental data from the curve given by Eq. (2) points to existence of some specific interactions between components in monolayer.

With system (1) Eq. (2) describes very well the experimental curve (no specific interactions between EL : C in monolayer) [20, 41], while with all other systems positive deviations occur from the perfect system curve (Fig. 5) [21, 22, 40].

For cases wherein the maximum deviation from perfect behavior was recorded at $x_A^M > 0.5$, we reported that the theory of regular solutions could be applied in both $M$ and $C$. The following equations are valid [21, 22, 41, 47]:

$$\begin{aligned} \ln\left(1 - x_A^C\right) + \xi^C \left(x_A^C\right)^2 &= \ln\left(1 - x_A^M\right) + \\ &+ \xi^M \left(x_A^M\right)^2 + (\pi - \pi_B)A_B/kT \\ \ln x_A^C + \xi^C \left(1 - x_A^C\right)^2 &= \ln x_A^M + \\ &+ \xi^M \left(1 - x_A^M\right)^2 + (\pi - \pi_A)A_A/kT \end{aligned} \qquad (3)$$

where $x_i^C$ and $\xi^C$ stand for the molar fraction of component $i$ and the interaction parameter (that characterizes the interaction between $A$ and $B$), respectively, in the collapsed bulk phase ($C$), while $x_i^M$ and $\xi^M$ stand for the values of the same parameters in monolayer ($M$). Eq. (3) allowed to compute the $\xi^M$ and $\xi^C$ values, ensuring the best description of the expe-

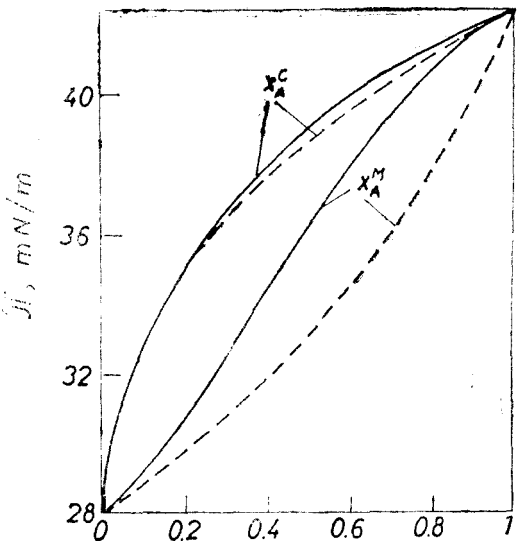


Fig. 5. Phase diagram for EL:CP monolayers. Full lines — regular solution approximation calculated by $\xi^C = -1.73$ and $\xi^M = -2.65$. Dashed lines — perfect solution approximation computed for $\xi^C = \xi^M = 0$.

*Table 3*

**Collapse pressure ($\pi_i$) and area per molecule at collapse ($A_i$); for „pure" monolayers; interaction parameters in monolayer ($\xi^M$) and in collapse phase ($\xi^C$); and minimum standard deviation ($\Delta$).**

| System | Component | | $\pi_i$, mN/m | | $A_i$, Å²/molec. | | $\xi^M$ | $\xi^C$ | $\Delta$, mN/m |
|---|---|---|---|---|---|---|---|---|---|
| | $A$ | $B$ | $A$ | $B$ | $A$ | $B$ | | | |
| (1) | EL | C | 42.5 | 37 | 54 | 23 | 0 | 0 | — |
| (2) | EL | CP | 42.5 | 28 | 54 | 44 | −2.65 | −1.73 | 0.169 |
| (3) | EL | ZP | 42.5 | 35 | 54 | 52 | −9.48 | −8.67 | 0.105 |

rimental monolayer curve, for the system (2, full line in Fig. 5), and for system (3) (see Table 3). By using the regular solution approximation and phase diagrams (of the type of those in Fig. 5), the theoretical ejection curves were calculated for both systems (2) and (3) employing the obtained interaction parameters (Table 3). These theoretical curves were compared with the experimental ones, and conclusions were drawn relative to the nature of collapse equilibria and area necessity of the $C$ phase [22].

With systems (4) and (5), maximum experimental monolayer curve deviations from the perfect behavior were recorded at $x_A^M < 0.5$ [40]. This situation could not be interpreted by means of the approximation of regular solutions. In order to explain the molecular interactions between components, we presumed the forming of some $AB_n$-type molecular associations. Obviously, the collapse pressure of the monolayers containing only $AB_n$-type molecular species must be greater than $\pi_A$ and the position of the maximum deviation from perfect behavior is dependent on both $n$ and the stability of the $AB_n$ associations.

Assuming that both $M$ and $C$ are perfect solutions, which contain $A$ and $B$ and all the molecular species of $AB_i$-type ($1 \leqslant i \leqslant n$), the collapse pressure of the mixed monolayer will obey the relation:

$$x_A^M \exp\left[(\pi - \pi_A)\frac{A_A}{kT}\right] + \sum_{i=1}^{n} x_{AB_i}^M \exp\left[(\pi - \pi_{AB_i})\frac{A_{AB_i}}{kT}\right] + x_B^M \exp\left[(\pi - \pi_B)\frac{A_B}{kT}\right] = 1 \tag{4}$$

Eq. (4) contains the molar fractions of all the molecular species from the monolayer, their collapse pressures $\pi_{AB_i}$ as well as the corresponding molecular areas $A_{AB_i}$, as unknown magnitudes, which are practically impossible to measure directly. It follows thus from Eq. (4) that eighteen parameters are to be computed from one single experimental curve. The computing of molar fractions would imply the knowledge of equilibrium constants for each of the $n$ molecular associations, according to reaction: $AB_{i-1} + B \rightleftharpoons AB_i$ characterized by the equilibrium constant $K_i$.

In order to overcome the above difficulties we employed the approximation of perfect solutions of the regular molecular associations, [48], which allowed for interpretation of the behavior of systems (4) and (5). Therefore, we have

advanced the following simplifications [49] that lie at the basis of regular molecular associations: the molecular areas are additive, i.e. $A_{AB_i} = A_A + iA_B$; the attachment of each $B$ molecule to $A$ molecule, or to the $AB_{i-1}$ complex association brings about the same collapse pressure increment, $\Delta\pi$, of the pure monolayer consisting of $A$ i.e. $\pi_{AB_i} = \pi_A + i\Delta\pi$ and the equilibrium constants have the same value for each $i$ complexing step ($K_i = K$). In this simplified method only two parameters, namely $K$ and $\Delta\pi$, must be computed from the experimental data of the monolayer curve. Using a double minimization procedure for the standard deviation, the $K$ and $\Delta\pi$ values were calculated for the system (4) and (5) (Table 4), taking a maximum value of $n = 6$ in accord with the molecular models and the surface lattice of pure lipid monolayers (Table 1).

The $AB_n$-type associations for $1 \leqslant n \leqslant 6$ in systems (4) and (5) appear to have approximately the same stability (see $K$ values in Table 4), which may suggest that the intermolecular interactions lie in the hydrogen bondings with participation of the OH-group from AX and of the O-atoms from the stearic ester of glycerol. The slightly enhanced stability of the DSL:AX associations in system (4) might be entailed by the induction effect of the negative charge localized in the DSL phosphatidyl group.

As concerns the stabilizing effect of the mixed monolayer given by the collapse pressure increment $\Delta\pi$ (Table 4), the greater value observed for the mixed films of carotenoid and DSL as compared to that of DGDG films also seems reasonable. The greater value of the collapse pressure of the DGDG pure monolayer is rendered by the particularly strong intermolecular forces that act between galactosyl groups (see Fig. 4, collapse structures). Therefore, the stabilizing effect of the associations DGDG : $(AX)_n$ is relatively low in system (5). In the case of the DSL pure monolayer, which has a smaller collapse pressure as compared to that of DGDG (see Fig. 2 and Table 1), the intermolecular attraction is weaker, and thus the forming of associations with AX could have a greater stabilizing effect. Consequently, the values of the stability constants and of the collapse pressure increment are in accord with the theoretical results envisaged on the basis of the molecular structures and of the electron effects.

Thus, by employing the two-component monomolecular film techniques, we have been successful in evidencing the existence of the caroteno-lipid specific interactions in the monolayer at the air/water interface, which could be correlated with the overall role of the carotenoids as membrane stabilizers [50].

However, we cannot foretell the possibly quantitative consequences of these caroteno-lipid interactions relative to the *in vivo* systems: namely membranes with excitable structures. In such natural membranes — i.e. photoreceptors — the carotenoids seem to be tightly coupled with proteins under the form

*Table 4*

**Stability constants ($K$) and surface collapse pressure increments ($\Delta\pi$) of the regular associations ($AB_n$; $1 \leqslant n \leqslant 6$) and minimum standard deviation ($\Delta$)**

| System | Component A | Component B | $K$ | $\Delta\pi$, mN/m | $\Delta$, mN/m |
|---|---|---|---|---|---|
| (4) | DSL | AX | 1.45 | 1.00 | 0.213 |
| (5) | DGDG | AX | 1.17 | 0.05 | 0.172 |

of caroteno-protein complexes. Moreover, neither the existence of caroteno-lipid-protein complexes can be excluded.

Furthermore, the study of adsorption of soluble proteins dissolved from aqueous phase at either carotenoid or lipid „pure" monolayers, as at caroteno-lipid mixed films, would be of interest — what could bring about a better understanding of the relative magnitudes of the caroteno-protein interactions as compared to the interactions evidenced between carotenoids and lipids in our systems. We expect the caroteno-lipido-protein systems to be more relevant from a biological viewpoint.

## REFERENCES


1. S. J. Singer and G. L. Nicolson, *Science*, **175,** 720 (1972).
2. G. L. Gaines, Jr., "Insoluble Monolayers at Liquid — Gas Interfaces", Interscience, New York, 1966, Chapter 9, p. 348.
3. E. Gorter and F. Grendel, *J. Exp. Med.*, **41,** 439 (1925).
4. D. A. Cadenhead, in "Structure of Biological Membranes" (S. Abrahamsson and I. Pascher, Eds.), Plenum, New York, 1976, p. 63.
5. P. J. Quinn, *FEMS Microbiology Reviews*, **39,** 87 (1986).
6. H. T. Tien, "Bilayer Lipid Membranes: Theory and Practice", Dekker, New York, 1974.
7. C. N. Kossi and R. M. Leblanc, *J. Colloid Interface Sci.*, **80,** 426 (1981).
8. I. Langmuir, *J. Amer. Chem. Soc.*, **39,** 1848 (1917).
9. D. A. Cadenhead, in "Structure and Properties of Cell Membranes", vol. 3, CRC Press, 1985, Chapter 2.
10. D. Chapman, *Quarterly Reviews of Biophysics*, **8** (2), 185(1975).
11. H. E. Ries, Jr., *Nature*, **281,** 287 (1979).
12. F. Müller-Landau and D. A. Cadenhead, *Chem. Phys. Lipids*, **25,** 299(1979); *ibid.*, **25,** 315(1979); D. A. Cadenhead and F. Müller-Landau, *ibid.*, **25,** 329(1979).
13. P. Tancrede, G. Munger and R. M. Leblanc, *Biochim. Biophys. Acta*, **689,** 45 (1982).
14. M. Tomoaia-Cotişel, *Ph. D. Thesis*, University of Cluj-Napoca, 1979.
15. J. T. Davies, *J. Colloid Sci.*, **11,** 377 (1956).
16. B. W. MacArthur and J. C. Berg, *J. Colloid Interface Sci.*, **68,** 201 (1979).
17. E. Chifu, J. Zsakó and M. Tomoaia-Cotişel, *J. Colloid Interface Sci.*, **95,** 346 (1983).
18. J. Zsakó, V. Neagu, M. Tomoaia-Cotişel and E. Chifu, *Rev. Roumaine Chim.*, **32,** 739 (1987).
19. M. Nakagaki and N. Funasaki, *Bull. Chem. Soc. Jpn.*, **47,** 2482 (1974); M. C. Phillips and P. Joos, *Kolloid — Z. Z. Polym.*, **233,** 499 (1970).
20. M. Tomoaia-Cotişel and E. Chifu, *J. Colloid Interface Sci.*, **95,** 355 (1983).
21. M. Tomoaia-Cotişel, E. Chifu and J. Zsakó, *Colloids and Surfaces*, **14,** 239 (1985).
22. E. Chifu, J. Zsakó and M. Tomoaia-Cotişel, *Stud. Univ. Babeş—Bolyai, Chem.*, **31**(2), 90 (1986); M. Tomoaia-Cotişel, J. Zsakó and E. Chifu, *Rev. Roumaine Chim.*, **32,** 663 (1987).
23. M. Tomoaia-Cotişel, I. Albu and E. Chifu, *Stud. Univ. Babeş—Bolyai, Chem.*, **24**(2), 68(1979); E. Chifu and M. Tomoaia-Cotişel, *ibid.*, **26** (2), 3 (1981).
24. M. Tomoaia-Cotişel, J. Zsakó, M. Sălăjan and E. Chifu, in "Water and Ions in Biological Systems" — Proceedings of III-rd International Conference (A. Pullman, V. Vasilescu and L. Packer, Eds.), USMS Press, Bucharest, 1985, pp. 371—381; J. Zsakó, M. Tomoaia-Cotişel, A. Mocanu and E. Chifu, *J. Colloid Interface Sci.*, **110,** 317 (1986); E. Chifu, J. Zsakó, M. Tomoaia-Cotişel, M. Sălăjan and I. Albu, *ibid.*, **112,** 241 (1986); E. Chifu, M. Sălăjan, M. Tomoaia-Cotişel, J. Demeter-Vodnar and J. Zsakó, *Stud. Univ. Babeş—Bolyai, Chem.*, **32** (1), 50 (1987).
25. A. W. Cuthbert, *Pharm. Rev.*, **19,** 59 (1967); J. A. Clements and K. M. Wilson, *Proc. Nat. Acad. Sci. USA*, **48,** 1008 (1962); B. R. Cater, D. Chapman, S. M. Hawes and J. Saville, *Biochim. Biophys. Acta*, **363,**, 54 (1974).

26. H. E. Ries, Jr., M. Matsumoto and N. Uyeda, *Bull. Instit. Chem. Res., Kyoto Univ.*, **53**, 77 (1975); H. E. Ries, Jr., M. Matsumoto, N. Uyeda and E. Suito, *J. Colloid Interface Sci.*, **57**, 396 (1976); H. E. Ries, Jr., *Colloids and Surfaces*, **10**, 283 (1984); H. E. Ries, Jr., *J. Colloid Interface Sci.*, **106**, 273 (1985).
27. M. Tomoaia-Cotişel, A. Sen and P. J. Quinn, *J. Colloid Interface Sci.*, **94**, 390 (1983).
28. M. Montal, *Methods Enzymol.*, **32**, 545(1974); M. Montal and P. Mueller, *Proc. Nat. Acad. Sci. USA*, **69**, 3561 (1972).
29. S. W. White, D. C. Peterson, S. Simon and M. Yafuso, *Biophys. J.*, **16**, 481 (1976).
30. J. M. Mountz and H. T. Tien, *Photochem. Photobiol.*, **28**, 395 (1978).
31. I. Langmuir, *Trans. Faraday Soc.*, **15**, 62 (1920); K. B. Blodgett, *J. Amer. Chem. Soc.*, **57**, 1007 (1935); K. B. Blodgett and I. Langmuir, *Phys. Rev.*, **51**, 964 (1937); I. Langmuir, *Science*, **87**, 493 (1938).
32. J. Zsakó, E. Chifu and M. Tomoaia-Cotişel, *Gazz. Chim. Ital.*, **109**, 663 (1979).
33. M. Tomoaia-Cotişel, J. Zsakó and E. Chifu, *Ann. Chim. (Rome)*, **71**, 189 (1981); M. Tomoaia-Cotişel, E. Chifu and J. Zsakó, in "Water and Ions in Biological System" – Proceedings of II-nd International Conference (A. Pullman, V. Vasilescu and L. Packer, Eds.), Plenum, New York, 1985, pp. 243–250.
34. M. Tomoaia-Cotişel, J. Zsakó, A. Mocanu, M. Lupea and E. Chifu, *J. Colloid Interface Sci.*, **117**, 464 (1987).
35. M. Tomoaia-Cotişel, J. Zsakó, E. Chifu and P. J. Quinn, *Chem. Phys. Lipids*, **34**, 55 (1983).
36. J. T. Davies and E. K. Rideal, "Interfacial Phenomena", Acad. Press, New York, 1963, p. 265.
37. H. E. Ries, Jr. and H. Swift, *J. Colloid Interface Sci.*, **64**, 111 (1978).
38. A. Sen, W. P. Williams and P. J. Quinn, *Biochim. Biophys, Acta*, **663**, 380 (1981); P. J. Quinn and W. P. Williams, *Biochim. Biophys. Acta*, **737**, 223 (1983).
39. H. E. Ries, Jr. and H. Swift, *J. Colloid Interface Sci.*, **89**, 245 (1982).
40. M. Tomoaia-Cotişel, J. Zsakó, E. Chifu and P. J. Quinn, in "Structure, Function and Metabolism of Plant Lipids" (P. A. Siegenthaler and W. Eichenberger, Eds.), Elsevier, B.V., 421 (1984).
41. J. Zsakó, M. Tomoaia-Cotişel and E. Chifu, *J. Colloid Interface Sci.*, **102**, 186 (1984).
42. F. C. Goodrich, "Proceedings Second International Congress Surface Activity", vol. 1, Butterworths, London, 1957, p. 85; I. S. Costin and G. T. Barnes, *J. Colloid Interface Sci.*, **51**, 106 (1975); K. Fukuda, T. Kato, S. Machida and Y. Shimizu, *J. Colloid Interface Sci.*, **68**, 82 (1979).
43. E. Chifu and M. Tomoaia-Cotişel, *Rev. Roumaine Chim.*, **24**, 979 (1979); M. Tomoaia-Cotişel, E. Chifu and J. Zsakó, *Stud. Univ. Babeş–Bolyai Chem.*, **31**(2), 80 (1986).
44. D. J. Crisp, in "Surface Chemistry", Supplement to Research, pp. 17–23, London, 1949.
45. R. Defay, I. Prigogine, A. Bellemans and D. H. Everett, in "Surface Tension and Adsorption", Longmans, Green, London, 1966, chapter 6.
46. M. Tomoaia-Cotişel and E. Chifu, *Gazz. Chim. Ital.*, **109**, 371 (1979).
47. P. Joos and R. A. Demel, *Biochim. Biophys. Acta*, **183**, 447 (1969).
48. I. Prigogine, R. Defay and D. H. Everett, "Chemical Thermodynamics", Longmans Green, London, 1954, chapter 26.
49. E. Chifu, A. Chifu, M. Tomoaia-Cotişel and J. Zsakó, *Rev. Roumaine Chim.*, **32**, 627 (1937); M. Tomoaia-Cotişel, J. Zsakó, E. Chifu and P. J. Quinn, *Biochem. J.*, 1937 in press.
50. A. Milon, G. Wolff, G. Ourisson and Y. Nakatani, *Helv. Chim. Acta*, **69**, 12 (1936).

STUDIA UNIV. BABEŞ-BOLYAI, CHEMIA, XXXII, 1, 1987

# INTERACTIONS OF SOME BIOLOGICALLY ACTIVE COMPOUND MONOLAYERS WITH ELECTROLYTES AT THE AIR/WATER INTERFACE

**EMIL CHIFU*, MARIUS SĂLĂJAN*, MARIA TOMOAIA-COTIŞEL*, JÁNOS DEMETER-VODNÁR* and JÁNOS ZSAKÓ***

*Received: September 8, 1986*

Compression isotherms of xanthophyll (X), viz. zeaxanthin and astaxanthin monolayers, spread at the aqueous buffer solution of pH = 8/air interface, have been recorded in the absence and in the presence of $Co^{2+}$ and of $Cr^{3+}$ ions (M) in the subphase. Results are consistent with the presumption that $MX_4$ type surface complexes are formed. Comparison with the results obtained earlier on subphases with pH = 5.6 shows the complex formation to be favorized by the increase of pH, which means that the anionic form of the surfactant participates in the complex formation. Results obtained plead for the incorporation of the subphase buffer electrolyte into the monolayer and for its squeezing out near to the collapse. On the contrary, the transition metal ions are retained even at the collapse of the monolayer. The effects observed are in good agreement with theoretical expectations, taking into account the presumed structure and electron configuration of the complexes as well as the protolytic equilibria occuring in the monolayers of the xanthophylls studied.

Key-words: *compression isotherms, xanthophylls, surface complexes, transition metal ions, monolayers*

**Introduction.** Compression isotherms, i.e. surface pressure ($\pi$) *vs.* mean molecular area ($A$) curves of surfactant monolayers spread at the air/water interface, are modified by the presence of electrolytes in the aqueous subphase. Electrolytes may have an expanding effect upon the monolayer, i.e. at the same $\pi$ value, $A$ has greater values on electrolyte solutions than on pure water, but also condensing effects may be evidenced, leading to lower $A$ values on electrolyte solutions as compared to the $A$ value observed on pure water. Frequently, the collapse pressure ($\pi_c$) of the monolayer is also affected by the subphase electrolytes. These phenomena reveal the existence of specific interactions of the surfactant molecules, or of their ions, with the ions of the subphase electrolyte. Anionic films interact mainly with the cations [1], the cationic ones with the subphase anions [2]. Cation-anion double long-chain salts spread on concentrated NaCl solutions exhibit an expansion due to the incorporation of both $Na^+$ and $Cl^-$ ions [3]. The condensing effect of $Ca^{2+}$ ions [4] and especially of transition metal ions [5—9] is assigned to the formation of surface complex compounds.

Our previous studies concerning the influence of Na and Mg salts upon the behaviour of uncharged galactolipid monolayers [10] evidenced the incor-

* *University of Cluj-Napoca, Faculty of Chemical Technology, 3400 Cluj-Napoca, Romania*

poration of the subphase anions into the monolayer and their expulsion at greater $\pi$ values, near to collapse.

In the case of two xanthophylls viz. of zeaxanthin (ZX) and astaxanthin (AX) a similar effect was observed with NaCl and $NaNO_3$, as in the case of galactolipid films, but a condensing effect with $Cr(NO_3)_3$ and $CoCl_2$, leading to an increase of $\pi_c$ [11]. The effect of the transition metal salts was explained by the formation of $MX_4$ type surface complexes, where M stands for the transition metal, X for the xanthophyll. The stability of these complexes was observed to increase in the order $Co(ZX)_4 < Cr(ZX)_4$ and $Cr(AX)_4 < Co(AX)_4$. This order was found to be in agreement with the electronic structure of the complexes presumed, by taking into account that ZX can form dative type $\sigma$- and $\pi$-bonds with M, but for AX there is a possibility to also give retrodative $\pi$-bonds [11].

It is worth mentioning that the above given composition of the complexes is consistent with results obtained by means of interfacial tension measurements performed at the benzene/water interface in the case of AX and $Co^{2+}$ [12].

Since both ZX and AX may participate in protolytic equilibria in monolayers spread at the air/water interface [13] and the complex formation might involve a deprotonation of the xanthophyll molecule, one can expect the complex formation to be influenced by the subphase pH. In the present paper compression isotherms are recorded, by using aqueous phosphate buffer solutions of pH = 8 as subphase. In our previous study [11] the subphase pH was of about 5.6, at which the major part of the surfactant molecules is neutral, but at pH = 8 the anionic form is the predominant molecular species [13]. Therefore, if in the complex formation equilibrium the anionic form of the surfactant is involved, at pH = 8 the increase of the stability of the complexes may be expected, and on the contrary, if the neutral molecules participate directly in these equilibria, a decrease of the stability is to be observed. A simple calculation performed on the basis of $pK_a$ values reported earlier [13] shows that by increasing the pH from 5.6 to 8, the fraction of the ionized molecular species increases more in the case of ZX, as compared to AX (see Tab. 1.). Consequently, if the anions are involved in the complex formation equilibria, at pH = 8 a larger stabilizing effect can be expected with ZX, as compared to AX.

**Experimental.** The surfactants used were zeaxanthin (ZX; 3,3′— dihydroxy — β-carotene) and astaxanthin (AX; 3,3′- dihydroxy — 4,4′- dioxo — β-carotene) of all-*trans* configuration, synthetic commercial products (Hoffmann La Roche) of chromatographic purity.

The spreading solvents used were: benzene containing 2 — 3% (v/v) of absolute ethanol for ZX and benzene with 4 — 8% (v/v) chloroform in the case of AX. Spreading solvents were of p.a. purity.

Xanthophyll monolayers were spread at the air/aqueous buffer solution interfaces, at the same molecular area of about 1.3 $nm^2$/molecule, in order to prevent artefacts due to the spreading kinetics [14]. The waiting time necessary for the evaporation of spreading solvents was of about 5 to 15 min.

The electrolytes used were commercial products of p.a. purity, viz. $Co(NO_3)_2.6H_2O$ (Reactivul, Bucharest), $Cr(NO_3)_3 \cdot 6H_2O$ (Merck), $Na_2HPO_4 \cdot 2H_2O$ (Reactivul Bucharest), $KH_2PO_4$ (Merck).

*Table 1*

**Ionization degree ($\alpha$) of the surfactants studied in monolayers spread on subphases of pH = 5.6 and 8, respectively (pH given as lower index of $\alpha$)**

| Surfactant | $\alpha_{5.6}$, % | $\alpha_8$, % | $\alpha_8/\alpha_{5.6}$ |
|---|---|---|---|
| ZX | 5.46 | 93.55 | 17.1 |
| AX | 8.02 | 95.63 | 11.9 |

*Table 2*

**Ionic strength ($J$) of the subphases used**

| Subphase | $J$ | | |
|---|---|---|---|
| | alone | with $Co^{2+}$ | with $Cr^{3+}$ |
| buffer *1* | 0.1959 | 0.1962 | 0.1965 |
| buffer *2* | 0.0196 | 0.0199 | 0.0202 |
| $H_2O$ | 0.0000 | 0.0003 | 0.0006 |

Two phosphate buffers of different ionic strengths were used. Compression isotherms were recorded by means of the Wilhelmy method as described earlier [11], by using buffer solutions alone and subphases containing $10^{-3}$M transition metal salts. We mention that higher Co(II) and Cr(III) concentrations were not used, since at pH = 8 the corresponding salts are sparingly soluble. In the case of $10^{-4}$M solutions no precipitation of hydroxids was observed either with $Co(NO_3)_2$ or with $Cr(NO_3)_3$. Ionic strengths ($J$) of the subphases used both in the present paper (buffers *1* and *2*) and in our previous work ($H_2O$) are presented in Tab. 2.

The experimental results were reproducible and independent of working conditions (such as waiting time before compression, compression rate), indicating a rapid equilibration of the monolayer with the subphases used. Each curve given in the present paper represents the mean result of at least 10 isotherms recorded for the same surfactant on the same subphase.

**Results and discussion.** Compression isotherms of ZX and AX monolayers, spread on different subphases, are presented in Figs. 1 and 2, respectively. Surface characteristics, viz. limiting molecular area ($A_0$) obtained by extrapolation of the high $\pi$ linear portion of the isotherm to $\pi = 0$ (see dashed

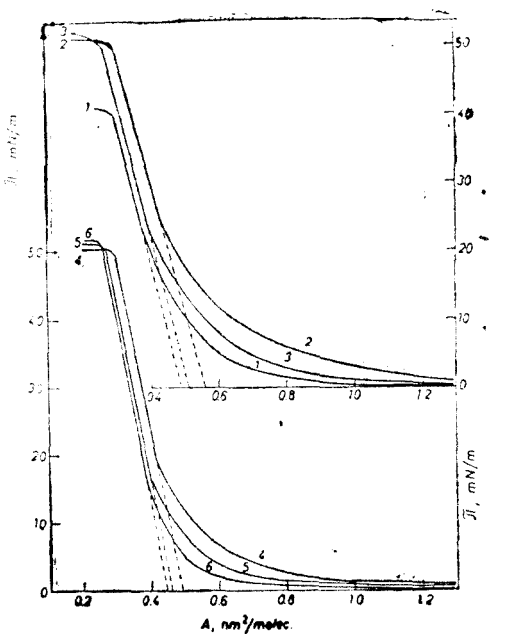


Fig. 1. Compression isotherms of ZX monolayers
Subphase: 1 — $H_2O$; 2 — buffer *1*; 3 — buffer *1* + $Co^{2+}$; 4 — buffer *2*; 5 — buffer *2* + $Co^{2+}$; 6 — buffer *2* + $Cr^{3+}$.

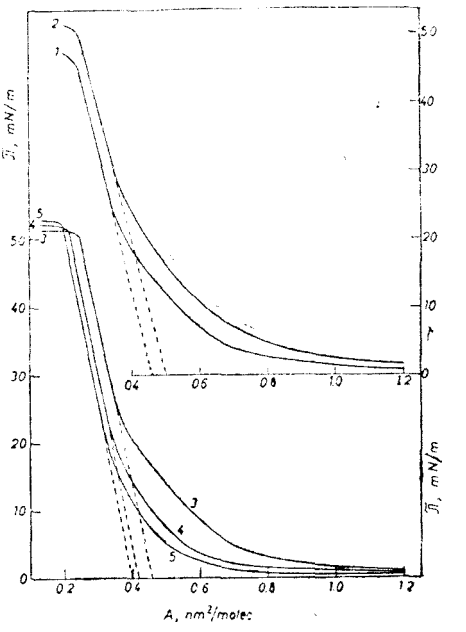


Fig. 2. Compression isotherms of AX monolayers
Subphase: 1 — $H_2O$; 2 — buffer *1*; 3 — buffer *2*; 4 — buffer *2* + $Cr^{3+}$; 5 — buffer *2* + $Co^{2+}$.

*Table 3*

**Surface characteristics of ZX and AX monolayers**

| Subphase | | | ZX | | | | AX | | | |
|---|---|---|---|---|---|---|---|---|---|---|
| pH | buffer | transition metal salt | $A_0$ nm² | $A_c$ nm² | $\pi_c$ mN/m | $C_{so}^{-1}$ mN/m | $A_0$ nm² | $A_c$ nm² | $\pi_c$ mN/m | $C_{so}^{-1}$ mN/m |
| 5.6 | — | — | 0.49 | 0.30 | 40.0 | 103 | 0.46 | 0.25 | 45.0 | 99 |
| 5.6 | — | $CoCl_2$ | 0.48 | 0.28 | 41.0 | 98 | 0.39 | 0.21 | 46.0 | 100 |
| 5.6 | — | $Cr(NO_3)_3$ | 0.46 | 0.27 | 42.0 | 102 | 0.42 | 0.23 | 45.0 | 99 |
| 8 | *1* | — | 0.56 | 0.30 | 49.7 | 107 | 0.50 | 0.25 | 50.7 | 101 |
| 8 | *1* | $Co(NO_3)_2$ | 0.51 | 0.27 | 50.0 | 106 | — | — | — | — |
| 8 | *2* | — | 0.49 | 0.30 | 49.7 | 128 | 0.46 | 0.25 | 50.7 | 111 |
| 8 | *2* | $Co(NO_3)_2$ | 0.46 | 0.28 | 50.0 | 128 | 0.40 | 0.20 | 52.0 | 104 |
| 8 | *2* | $Cr(NO_3)_3$ | 0.44 | 0.26 | 51.0 | 125 | 0.42 | 0.22 | 51.6 | 108 |

lines in Figs. 1 and 2), collapse area ($A_c$) and collapse pressure ($\pi_c$), representing the co-ordinates at which the sudden slope change of the isotherm is observed at high $\pi$ values, and the surface compressional modulus defined as $C_{so}^{-1} = -A_0 (\partial\pi/\partial A)_T = A_0\pi_c/(A_0 - A_c)$, are given in Tab. 3. We mention that data for aqueous subphases of pH = 5.6, are taken from [11].

From Figs. 1 and 2, one can see that the substitution of the aqueous subphase (curves 1) for buffer *1* (curves 2) entails a modification of the compression isotherm, revealing an important expanding effect of the subphase electrolyte for one and the same xanthophyll and an increase of $\pi_c$. The main cause of these effects is the transformation of the neutral surfactant molecules into anions, leading on the one hand to enhanced stability of the monolayer against collapse (increase of $\pi_c$), and on the other hand to expansion of the film due to the electrostatic repulsions between the anionic headgroups. Comparison of curves 2 with curve 4 in Fig. 1 and curve 3 in Fig. 2, recorded on buffer *2*, shows the expanding effect to be also due to the incorporation of buffer electrolyte into the monolayer, since the expanding effect of buffer *1* is greater than that of buffer *2* for each xanthophyll. This effect involving, presumably, the formation of two dimensional lattices containing besides the anionic form of the xanthophyll, as well the ions of the subphase buffer electrolyte, also, is obvious on the basis of $A_0$ values presented in Tab. 3. It is worth mentioning, that $A_c$ is not affected by the buffer solutions, suggesting the idea that the electrolyte incorporated is squeezed out of the monolayer near to the collapse.

Further, Figs. 1 and 2 show the $Co^{2+}$ and $Cr^{3+}$ ions to have an important condensing effect upon the xanthophyll monolayer. In the case of ZX, this effect is greater with $Cr^{3+}$ as compared to $Co^{2+}$. Exactly the opposite is observed with AX, i.e. the condensing effect of $Co^{2+}$ exceeds that of $Cr^{3+}$. As seen from Tab. 3, the $\pi_c$ values are greater in the presence of transition metal ions than in their absence, but they are not affected by the ionic strength of the subphase buffer. The $\pi_c$ values increase in the same order as the condensing effect does. These phenomena are consistent with the presumption that, actually, surface complex compounds of transition metals are formed, having as ligands the xanthophyll molecules and/or their anions.

Concerning the $C_{so}^{-1}$, its values are rather scattered at pH = 5.6, and no clear effect can be observed. On subphases with pH = 8, experimental data are more relevant. On buffer *1* a slight increase of $C_{so}^{-1}$ is observed, as compared to pure water, i.e. monolayers are less compressible. This might be assigned to the electrostatic repulsive forces. On buffer *2*, $C_{so}^{-1}$ values are much greater as compared to the former subphases. Since the electrostatic forces are the same as with buffer *1* the lower compressibility might be due to the lower ionic strength $J$ of the subphase. Thus, the higher is $J$, the greater is the number of ions of the electrolyte, incorporated into the monolayer. Since these ions are gradually expelled when $\pi$ increases, the higher is $J$, the more compressible is the monolayer and the lower will be $C_{so}^{-1}$ as observed in Tab. 2, both with ZX and AX.

The influence of the transition metal ions upon $C_{so}^{-1}$ is rather unsignificant, although a slight decrease of the latter is observed in the presence of the former. If the $Co^{2+}$ and $Cr^{3+}$ ions are thought to co-ordinate xanthophyll anions, the formation of $MX_4$ type complexes entails diminution of the number of electrically charged molecular species. This might lead to the decrease of electrostatic repulsion and to a slight increase of the compressibility, even by taking into account that the formation of surface complexes, i.e. the appearance of more close packed units, had to diminish the compressibility.

As shown in our previous paper [11], the expanding and condensing effects can be easier studied by plotting $\Delta\pi$ *vs.* $A$, where $\Delta\pi = \pi_e - \pi_0$ is the difference of the $\pi$ value on the electrolyte solution ($\pi_e$) and that on a subphase without the electrolyte ($\pi_0$), both obtained for the same mean molecular area of the surfactants. In the present study $\pi_0$ means $\pi$ measured on pure water when the influence of the buffer electrolyte alone is investigated. In the case of the effect of transition metal ions at pH = 8, there is a combined effect of the subphase buffer and of the $Co^{2+}$ or $Cr^{3+}$ ions. Therefore, it is better to take for $\pi_0$ the $\pi$ value measured on the buffer solution alone, having the same ionic strength.

We mention that in the latter case, since $A_c$ values obtained in the presence of transition metal ions are lower than those measured on subphases free of these ions, the construction of $\Delta\pi$ *vs.* $A$ curves is possible only down to a certain $A_c^0$, meaning the collapse molecular area of the surfactant on a subphase having the same pH and $J$ and containing no transition metal ions. Incidentally, in the case of the xanthophylls studied, $A_c^0$ does not depend either on pH or $J$ of the subphase (see Tab. 3).

$\Delta\pi$ *vs.* $A$ curves for ZX and AX monolayers are presented in Figs. 3 and 4, respectively.

In Fig. 3 the curves are obtained by combining the experimental curves given in Fig. 1. Thus, curves 1 and 2 in Fig. 3 are obtained by substracting curve 1, given in Fig. 1, from, curves 2 and 4, respectively, both taken from the same Fig. 1, curves 3 and 4 in Fig. 3 represent curves 5 and 6, respectively, raken from Fig. 1, minus curve 4 from Fig. 1, and curve 5 in Fig. 3 is the diffetence between curves 3 and 2, presented in Fig. 1.

The curves given in Fig. 4 are obtained in a similar way, by using the compression isotherms presented in Fig. 2.

As seen from Figs. 3 and 4, the buffer solutions have an expanding effect (curves 1 and 2), $\Delta\pi$ is positive, and the higher $J$, the higher is also $\Delta\pi$. Ac-

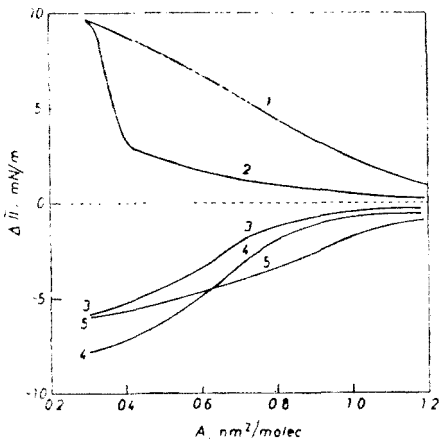


Fig. 3. Expanding and condensing effects in the case of ZX monolayers
Subphase: 1 – buffer *1*; 2 – buffer *2*; 3 – buffer *2* + $Co^{2+}$; 4 – buffer 2 + $Cr^{3+}$; 5 – buffer *1* + $Co^{3+}$.

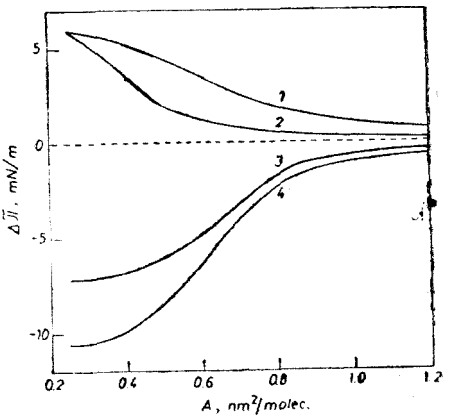


Fig. 4. Expanding and condensing effects in the case of AX monolayers
Subphase: 1 – buffer *1*; 2 – buffer *2*; 3 – buffer *2* + $Cr^{3+}$; 4 – buffer *2* + $Co^{2+}$.

tually, these curves reflect a combined effect, since not only $J$ is modified, but also the pH value, $\pi_e$ is measured at pH = 8, $\pi_3$ at pH = 5.6. Therefore, at the compression $\Delta\pi$ does not pass through a maximum to become vanishingly small at $A_c^0$, as observed earlier with inert electrolytes (Na – salts), indicating the squeezing out of the latters from the monolayer near to the collapse, but it increases up to collapse of the monolayers. The limiting value of $\Delta\pi$ for $A = A_c$ is the difference between the collapse pressures at pH = 5.6 and 8 (of Tab. 3). Since for $A_c$, $\Delta\pi$ has the same value irrespective of $J$, near to the collapse, the squeezing out of the subphase buffer electrolyte from the monolayer seems to be obvious.

In the presence of transition metal ions, $\Delta\pi$ has negative values, indicating a clear condensing effect, consistent with the hypothesis of surface complex formation. At compression $|\Delta\pi|$ increases down to $A_c^0$ (curves 3–5 in Fig. 3 and 3–4 in Fig. 4), which means that the transition metal ions are not squeezed out from monolayers. This is also consistent with the complex formation, leading to covalent bonds between $Co^{2+}$ or $Cr^{3+}$ and the xanthophyll ligands. As shown by curves 3 and 5 in Fig. 3, for $A_c^0$ $\Delta\pi$ approaches the same value, irrespective of $J$, which also means the squeezing out of the buffer electrolyte at high $\pi$ values. Further, it is obvious that at higher $A$ values $\Delta\pi$ is higher in the case of buffer *1* (curve 5), as compared to buffer *2* (curve 3). This effect might be explained by presuming the complex formation to be accompanied by the expulsion of a part of the buffer electrolyte from the monolayer. Consequently, the higher $J$ (i.e. the more expanded the monolayer), the larger will be the condensing effect.

Concerning the correlation between $\Delta\pi$ and the nature of the transition metal ion and of the xanthophyll, the general picture is the same as observed earlier at pH = 5.6 [11]. At $A_c^0$ the following order is observed: in the case

of ZX $|\Delta\pi|$ is higher for $Cr^{3+}$ as compared to $Co^{2+}$, but with AX it is higher for $Co^{2+}$ than for $Cr^{3+}$. By presuming that $|\Delta\pi|$ is a measure of the stability of the surface complex, the above order could be correlated with a formal bond order. For this purpose the formation of $MX_4$ type complexes has been assumed and on the base of the ligand field theory the possibilities of molecular orbital (MO) formations have been studied, by taking into account the geometry of xanthophyll molecules, symmetry properties of the metal ion and of the ligand orbitals as well as the electron configurations. This study revealed the possibility of ZX to give dative type $\sigma$- and $\pi$-bonds with transition metal ions, and that of AX to form dative type $\sigma$-bonds and both dative and retrodative type $\pi$-bonds. By presuming the energy of all bonding MO-s to be lower than the energy of the non-bonding pure ligand MO-s and of the central ion atomic orbitals, and the antibonding MO-s to have higher energies as compared to the above mentioned nonbonding orbitals, the electron configuration of the complexes studied could be established, leading to a formal bond order (B.O.) [11]. This B.O. can be considered as a measure of the stability of the complex and it could be well correlated with the $|\Delta\pi|$ values obtained for $A_{cr}$ separately for each xanthophyll.

The obtained B.O. values [11] are given in Tab. 4. The same table also contains the $|\Delta\pi|$ values obtained at pH = 5.6 and 8, respectively, for $A_c^0$, as well as the ratios $\Delta\pi_8/\Delta\pi_{5\cdot6}$ and $|\Delta\pi|_8$/B.O. As seen, the increase of the pH form 5.6 to 8 entails an important increase of $|\Delta\pi|$, in the case of all complexes. This pleads for the co-ordination of the anionic form of the xanthophyll by the transition metal ion, presumably, leading mainly to neutral complex species or to complex ions with a single positive or negative charge. Since the complex species may be presumed to participate in protolytic equilibria, actually a mixture of different protonated and deprotonated forms must be obtained. The ratios $\Delta\pi_8/\Delta\pi_{5\cdot6}$ show the increase of pH to entail a more important increase of the number of complex molecular species in the case of ZX than with AX. As mentioned in the introduction, this effect could be expected on the basis of the fraction of the ionized surfactant molecular species, given in Tab. 1 and this also pleads for the participation of the surfactant anions in the complex formation equilibria.

Further, Table 4 shows the ratio $|\Delta\pi|_8$/B.O. to be much higher in the case of ZX complexes than with AX ones. This is easy to understand since the B.O. values reported indicates only the number of possible metal-ligand bonds, but they do not reflect the strength of these bonds. The stability of the comple-

*Table 4*

**Characteristics of the surface complexes**

| Complex | B.O. | $\|\Delta\pi\|_{5\cdot6}$ | $\|\Delta\pi\|_8$ | $\Delta\pi_8/\Delta\pi_{5\cdot6}$ | $\|\Delta\pi\|_8$/B.O. |
|---|---|---|---|---|---|
| $Co(ZX)_4$ | 5.5 | 3.7 | 5.8 | 1.57 | 1.05 |
| $Cr(ZX)_4$ | 7.0 | 5.2 | 7.8 | 1.50 | 1.11 |
| $Co(AX)_4$ | 15.5 | 8.0 | 10.6 | 1.32 | 0.68 |
| $Cr(AX)_4$ | 13.5 | 6.0 | 7.2 | 1.20 | 0.52 |

xes must be determined even by the overall strength of the bonds and consequently, the order of these formal B.O. values can indicate an order of stabilities only if the same ligand is involved into the complex formation.

In conclusion, the results obtained on buffered subphases at pH = 8 are in good agreement with our earlier presumptions concerning the formation of $MX_4$ type surface complexes and these results show the anionic form of the xanthophylls studied to participe directly in the complex formation. Further, we can conclude that the concepts of coordination chemistry may be used successfully in the interpretation of surface phenomena, explaining well some specific interactions occuring in monolayers. Since monomolecular films are simplified models of biomembranes, it is obvious that the same concepts may also play an important role in the understanding of some processes occuring in living organism.

## REFERENCES

1. E. D. Goddard, O. Kas and H. C. Kung, *J. Colloid Interface Sci.*, **24**, 297 (1967).
2. E. D. Goddard, G. H. Matteson and G. E. Totten, *J. Colloid Interface Sci.*, **85**, 19 (1982).
3. O. Shibata, *J. Colloid Interface Sci.*, **96**, 182 (1983).
4. H. Hauser, D. Chapman and R. M. C. Dawson, *Biochim. Biophys. Acta*, **183**, 320 (1969).
5. H. Müller, S. Friboy and M. Hellsten, *J. Colloid Interface Sci.*, **32**, 132(1970).
6. Y. Suzuki and H. Matsushita, *Ind. Health*, **7**, 143 (1969).
7. S. A. Gordziel, D. R. Flanagan and J. Swarbrick, *J. Colloid Interface Sci.*, **86**, 178 (1982).
8. T. Smith and R. Serrins, *J. Colloid Interface Sci.*, **23**, 329 (1967).
9. T. Smith, *J. Colloid Interface Sci.*, **25**, 443 (1967).
10. M. Tomoaia-Cotişel, J. Zsakó, E. Chifu and P. J. Quinn, *Chem. Phys. Lipids*, **34**, 55 (1983).
11. E. Chifu, J. Zsakó, M. Tomoaia-Cotişel, M. Sălăjan and I. Albu, *J. Colloid Interface Sci.*, **112**, 241 (1986).
12. J. Demeter-Vodnár, M. Sălăjan, M. Tomoaia-Cotişel, J. Zsakó and E. Chifu, *Studia Univ. Babeş—Bolyai Chem.*, **32**, (1), 92 (1987).
13. J. Zsakó, M. Tomoaia-Cotişel, A. Mocanu and E. Chifu, *J. Colloid Interface Sci.*, **110**, 317 (1986).
14. G. L. Gaines, Jr., "Insoluble Monolayers at Liquid-Gas Interfaces" Interscience, New York, 1966, chapter 4.

STUDIA UNIV. BABEŞ-BOLYAI, CHEMIA, XXXII, 1, 1987

# RELAXATION PHENOMENA IN FATTY ACID MONOLAYERS

**MARIA TOMOAIA-COTIŞEL*, JÁNOS ZSAKÓ*, AURORA MOCANU*, IOSIF ALBU* and EMIL CHIFU***

*Received: September 9, 1986*

Relaxation phenomena occurring in monolayers of fatty acids, viz. of stearic (SA), oleic (OA) and linoleic (LA) acids are studied at constant surface pressure ($\pi$) values, by recording mean molecular area ($A$) *vs.* time ($t$) curves. A calculation procedure is proposed to derive kinetic parameters, by using a Prout-Tompkins type equation, adapted to three mechanisms of relaxation, i.e. micelle formation (*1*), collapse leading to trilayers (*2*) and formation of a collapsed bulk phase (*3*). As observed, during the kinetic run the mechanism may change, e.g. at a certain moment mechanism *2* may replace mechanism *1*. Kinetic parameters are discussed in terms of molecular structure and liquid or solid state of the monolayer. The rate constants of the relaxation process seem to characterize the growth rate of the germs of the new phase, the integration constants are presumed to be correlated to the number of germs of the new phase.

Key-words: *fatty acid monolayers, kinetics of relaxation phenomena, rate constants of the relaxation process, collapse mechanism*

**Introduction.** Monolayers of insoluble surfactants, spread at the air/water interface, present some relaxation phenomena, viz. at a certain mean molecular area ($A$) maintained constant, the surface pressure ($\pi$) decreases in time and if $\pi$ is maintained at a constant value, a decrease of $A$ is observed.

Relaxation phenomena occurring in fatty acid monolayers have been studied by several authors. By following the variation of $\pi$ as function of time, at constant $A$ values, a formal second order kinetics was found in the case of collapse arachidic acid [1] and of palmitic acid [2] monolayers. By maintaining $\pi$ at constant values, the collapse rate, i.e. the rate of the $A$ decrease in time, was found to increase in time in the case of stearic acid [3, 4, 5], and also with $\pi$ [4]. On the contrary, with oleic acid, at $\pi = \text{const}$ the $\ln (A/A_0)$ values were found to be a linear function of $t^{1/2}$ [4], and relaxation phenomena were assigned to dissolution of oleic acid in the aqueous subphase [4]. The collapse rate of stearic acid films, at $\pi = \text{const}$, depends on the subphase pH, viz. it increases with decreasing pH [5]. This is easy to understand, since on neutral and alkaline subphases in the stearic acid monolayers a protolytic equilibrium is established [5,6], leading to the formation of electrically charged surfactant molecular species, and consequently, to the appearance of an electric double layer, having a stabilizing effect upon the film and hindering its collapse.

Since the long chain saturated fatty acids are solid in pure state, the collapse pressure of their monolayers is much higher than the equilibrium spreading pressure (ESP), i.e in the monolayers important overcompressions may

* *University of Cluj-Napoca, Faculty of Chemical Technology, Physical Chemistry Department, 3400 Cluj-Napoca, Romania*

arise. Attempts were made to correlate the collapse rate to this overcompression [7] and to derive kinetic equations based upon the formation and growth of germs of the collapsed bulk phase [4, 5].

Frequently, in the kinetic study of heterogeneous reactions involving the formation and growth of germs of a new phase, the Prout-Tompkins equation [8] is used. This equation has been adapted to the study of collapse kinetics of insoluble monolayers and the following relation has been proposed [9]:

$$\ln \frac{\alpha}{1-\alpha} = k \ln t + \text{const} \tag{1}$$

where $\alpha$ stands for the fraction of monolayer decomposed (collapsed).

At $A = \text{const}$, $\alpha$ can be expressed as function of $\pi$, and a plot of $\ln [\alpha/(1-\alpha)]$ *vs.* $\ln t$ gave a good linearity [9, 10]. By working at $A = \text{const}$, $\pi$ varies during the kinetic run and the physical conditions in the remaining, unaltered portion of the monolayer are changed. This disadvantage does not appear if $\pi$ is maintained at a constant value. In this case $\alpha$ may be given as a function of $A$, by presuming a certain mechanism for the relaxation phenomenon. The validity of the relations derived from Eq.(1) on the basis of these hypotheses was proved in the case of some apocarotenoid monolayers [11].

In the present paper a theoretical study is made with respect to the actual form of Eq.(1), allowing the description of kinetic curves recorded at $\pi = \text{const}$. A method is proposed to derive kinetic parameters from $A$ *vs.* $t$ curves. This method is applied to the study of relaxation phenomena observed at $\pi = \text{const}$ in monolayers of three fatty acids, viz. stearic, oleic and linoleic acids, spread at the air/water interface.

**Experimental.** *Film forming materials.* The fatty acids studied were: stearic (octadecanoic) acid (SA; p.a., Schuchardt), oleic (*cis*-9-octadecenoic) acid (OA; Merck) and linoleic (*cis,cis*-9,12-octadecadienoic) acid (LA; Serva). The declared purity of the unsaturated acids was 98%. Both thin-layer and gas chromatographic tests confirmed this value.

*Spreading solvents.* As spreading solvent benzene for SA, and benzene : *n*-hexane mixtures of different ratios (1 : 4; 1 : 9; 1 : 16, *v/v*) with OA and LA were employed. All solvents were of p.a. purity, used without further purification. The surface tension of the subphase was not altered by spreading of the solvents only, indicating the absence of impurities with surface activity.

*Subphase.* HCl containing bidistilled water was used as subphase. HCl solution of p.a. purity was added to ensure pH = 2.

*Working conditions.* The desired amount of fatty acid solution was placed on the subphase by means of a micropipet. Evaporation of the spreading solvent and the onset of the internal equilibrium in the monolayer occurred during a waiting time of 15—30 min.

Mean molecular area *vs.* time curves were recorded at different constant $\pi$ values, by using the Wilhelmy method. Measurements were made at room temperature, 22±2°C. Reproducibility in the molecular area determination was within ±0.002 nm²/molecule with SA, and within ±0.005 nm²/molecule with OA and LA.

The experimental kinetic curves given in the present paper and used for deriving kinetic parameters are the mean of at least 5—6 individual runs performed in identical conditions.

**Results and discussion.** *Kinetic equations.* Let us denote by $a_0$ the total area of the monolayer at $t = 0$ and at the constant $\pi$ value chosen for the kinetic run, and by $N_0$ the total number of surfactant molecules spread at the interface. Obviously, one has $a_0 = N_0 A_0$, where $A_0$ means the mean molecular area of the surfactant at $t = 0$.

At $t \neq 0$, a number of $N_t^R$ molecules will be in the new phase, appeared as a result of the relaxation phenomenon. Let us denote the mean area necessity of the surfactant molecules in this phase by $A^R$. Since $\pi = \text{const}$, in the remaining portion of the monolayer the mean molecular area remains $A_0$. Consequently, the overall area of the interface can be given as

$$a_t = (N_0 - N_t^R) A_0 + N_t^R A^R$$

and the mean molecular area will be

$$A_t = \frac{a_t}{N_0} = \left(1 - \frac{N_t^R}{N_0}\right) A_0 + \frac{N_t^R}{N_0} A^R \tag{2}$$

The fraction of the monolayer „decomposed", can be defined as

$$\alpha = N_t^R / N_0 \tag{3}$$

The combination of Eqs. (1), (2) and (3) yields:

$$\log B_i \equiv \log \frac{\alpha}{1 - \alpha} = \log \frac{A_0 - A_t}{A_t - A_i^R} = k_i \log t + c_i \tag{4}$$

The lower index $i$ is introduced, since $A^R$, and consequently also $B$, $k$ and $c$, depend on the structure of the new phase, i.e. on the mechanism of the relaxation phenomenon. In respect of the mechanism, the following variants have been advanced [11]:

*Mechanism 1* consists of the formation of micelles, i.e. of islands of close packed, vertically oriented molecules, corresponding to a mean molecular area equal to the collapse area, i.e. $A_1^R = A_c$. This mechanism is observed mainly at low $\pi$ values [5]. In this approximation Eq. (4) takes the following form:

$$\log B_1 \equiv \log \frac{A_0 - A_t}{A_t - A_c} = k_1 \log t + c_1 \tag{5}$$

*Mechanism 2* presumes the incipient collapse of the monolayer to lead to the formation of trilayers [12], i.e. $A_2^R = A_c/3$, and Eq. (4) becomes:

$$\log B_2 \equiv \log \frac{A_0 - A_t}{A_t - A_c/3} = k_2 \log t + c_2 \tag{6}$$

*Mechanism 3* entails the appearance of a collapsed bulk phase, formed by the superposition of a great number of molecular layers, and actually being a droplet of liquid, or a crystallite. In this case the area necessity of the collapsed bulk phase is neglectingly small as compared to the area of the monolayer and one can take $A_3^R = 0$. In this approach Eq. (4) can be written as:

$$\log B_3 \equiv \log \frac{A_0 - A_t}{A_t} = k_3 \log t + c_3 \tag{7}$$

Our study performed with apocarotenoid derivatives at $\pi = \text{const}$ [11] showed the kinetic curves to be well described by means of Eq. (5) at low $\pi$

values. At higher surface pressures Eq. (5) was valid only up to a given time $t_1$ and further Eq. (6) could be applied, by taking $(t - t_1)$ instead of $t$ and $A_{t_1}$ instead of $A_0$.

At higher surface pressures and especially near to the collapse pressure ($\pi_c$), at the beginning Eq. (6) was found to be valid up to a certain $t_2$, and further the experimental curves were described by Eq. (7), by taking $(t - t_2)$ for $t$, and the $A_t$ value corresponding to $t_2$ for $A_0$.

Concerning the rate constants $k_i$ derived, these showed a slight tendency to increase with increasing $\pi$, but they were not very much affected by the change of the mechanism [11].

It is worth mentioning, that in Eqs. (5), (6) and (7), $k_i$ is a dimensionless constant and its numerical value is not affected by the time unit used, since in log $B_i$ *vs.* log $t$ plots the change of this unit entails only a parallel shift of the straight line. On the contrary, $c_i$ representing log $B_i$ for $t = 0$, although it is also dimensionless, depends very much on the units in which time is expressed.

*Theoretical curves and calculation procedure.* In order to obtain a clear image of the influence of both kinetic parameters, $k_i$ and $c_i$, and the relaxation mechanism, theoretical curves $A_t/A_0$ *vs.* $t$ were constructed for a hypothetical case, corresponding to $A_c/A_0 = 0.9$ (a similar situation appears e.g. with OA at about 20 mN/m).

In Fig. 1 theoretical curves, constructed by using Eq. (5), are given to visualize the influence of $k_1$ and $c_1$ upon the shape of kinetic curves. As seen, at the beginning the relaxation rate is very much influenced by the integration constant $c_1$, suggesting the idea that this constant might be related to the number of germs of the new phase (of micelles) or to the rate of the appearance

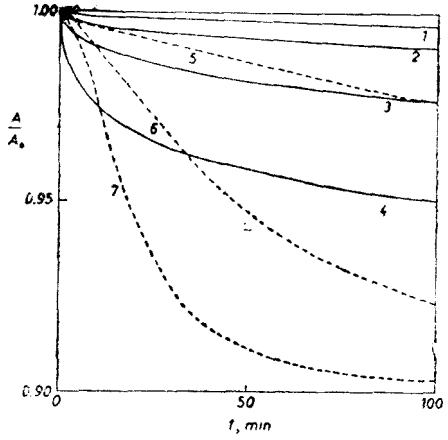


Fig. 1. Theoretical kinetic curves calculated by means of Eq. (5) for $A_c/A_0 = 0.9$. (1)–(4): $k_1 = 0.5$; (5): $k_1 = 1$; (6): $k_1 = 1.5$; (7): $k_1 = 2$.
(1), (5)–(7): $c_1 = -2.5$; (2): $c_1 = -2$; (3): $c_1 = -1.5$; (4): $c_1 = -1$.

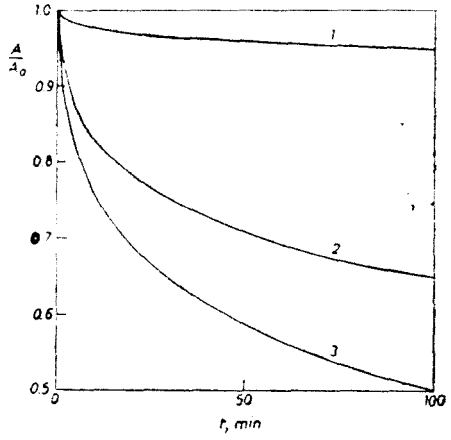


Fig. 2. Theoretical kinetic curves for $A_c/A_0 = 0.9$. $k_1 = k_2 = k_3 = 0.5$; $c_1 = c_2 = c_3 = -1$.
(1)–Eq. (5); (2)–Eq. (6); (3)–Eq. (7).

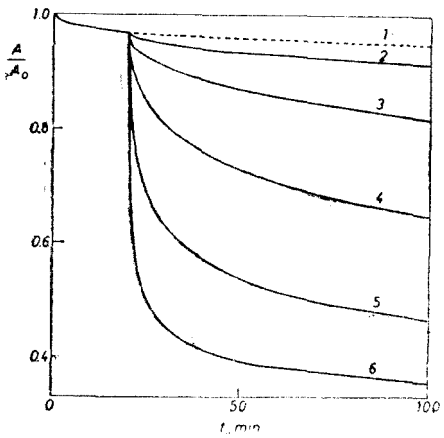


Fig. 3. Theoretical kinetic curves for $A_c/A_0 = 0.9$, calculated by means of Eq. (5) up to $t = 20$ min with $k_1 = 0.5$ and $c_1 = -1$. For $t > 20$ min: curve *1* (dashed line) calculated as for $0 \leq t \leq 20$ min; curves (2)–(6) calculated by means of Eq. (6) with $k_2 = 0.5$; (2): $c_2 = -2$; (3): $c_2 = -1.5$; (4): $c_2 = -1$; (5): $c_2 = -0.5$; (6): $c_2 = 0$.

of such germs. The rate constant $k_1$ might characterize the rate of growth of the germs.

Fig. 2 shows the dependence of theoretical kinetic curves upon the relaxation mechanism, the curves being constructed by using Eqs. (5), (6) and (7), respectively, and by taking $k_1 = k_2 = k_3$, $c_1 = c_2 = c_3$. As seen, the shape of the curves is similar, only the limiting value of $A/A_0$ for $t \to \infty$ is different, viz. $A_c/A_0$, $A_c/3A_0$ and 0, for mechanisms *1*, *2* and *3*, respectively.

In fig. 3 the relaxation is presumed to occur accordingly to mechanism *1* during the first 20 min. From this moment on, an incipient collapse is considered accordingly to mechanism *2*, without the change of the rate constant, i.e. by taking $k_1 = k_2$. Obviously, the general feature of the curve is very much affected by the $c_2$ value. The dashed line curve shows the $A$ values which would arise if the mechanism did not change at $t = 20$ min.

From the examples given above, one can see that there are real possibilities to derive $k_i$ and $c_i$ values from the kinetic curves if the measurements are reproducible and accurate enough.

It is worth mentioning that the change of mechanism actually can occur only gradually, i.e. correctly one has to take into account that simultaneously two mechanisms are acting, the initial one (e. g. *1*), becoming less and less important, and the new one (e.g. *2*), becoming predominant only after a transition period. Nevertheless, as a first approach, one can adopt the following procedure:

By performing a plot of log $B_1$ *vs.* log $t$, if a straight line is obtained, the validity of mechanism *1* may be accepted and $k_1$ and $c_1$ values can be derived graphically, or by linear regression methods. If after a linear portion negative deviations appear, these indicate that the monolayer ceases to „work", i.e. an equilibrium between the micelles and the „expanded" monolayer is gradually established.

In the case of positive deviations from linearity, a change of mechanism might be presumed. By denoting with $t_1$ the time, up to which linearity is observed, and with $A_1$ the corresponding mean molecular area, the experimental data obtained for $t > t_1$, are used to perform a plot of log $B_2$ *vs.* log$(t - t_1)$, by taking $A_0 = A_1$ in the expression of log $B_2$, given by Eq. (6). If the plot is linear, this pleads for mechanism *2* and $k_2$ and $c_2$ values can be derived. Positive and negative deviations from linearity have the same meaning as above. In the case of positive deviations, beginning from $t_2$ on, a plot of log $B_3$ *vs.* log $(t - t_2)$ is to be performed, by taking for $A_0$ the experimental $A_2$ value, corresponding to $t_2$.

Obviously, if the plot log $B_1$ *vs.* log $t$ is not linear for the beginning either, a plot of log $B_2$, or even of log $B_3$, *vs.* log $t$ must be tested.

*Table 1*

**Surface characteristics of the fatty acids studied (pH = 2)**

| Acid | $\pi_c$ mN/m | $A_c$ nm²/molec. |
|---|---|---|
| Oleic | 30.0 | 0.27 |
| Linoleic | 26.0 | 0.31 |
| Stearic | 40.8 | 0.18 |

*Surface characteristics of the fatty acids studied.* Compression isotherms of the fatty acids studied have been reported in our previous paper [6], together with the surface characteristics derived. Collapse pressures and collapse molecular areas are presented in Table 1. We mention that SA presents a liquid condensed → solid phase transition at $\pi = 26$ mN/m.

*Relaxation kinetics in fatty acid monolayers.* At $\pi < 5$ mN/m no relaxation phenomena were observed and $\pi$ remained practically constant for a long time, without a modification of the area to be necessary. At higher $\pi$ values, $\pi$ can be maintained constant only by diminishing the area of the interface. Some examples of kinetic curves, i.e. of $A$ *vs.* $t$ plots are presented in Figs. 4—6 for monolayers of the fatty acids studied. Circles are experimental values, full line curves are calculated ones (see below). The Prout-Tompkins linearization of the kinetic curves is visualized in Fig. 7 in the case of OA. As seen, at low $\pi$ values the first portion, up to a certain $t_1$, can be linearized by means of Eq. (5) and further positive deviations appear, indicating a change of mechanism. Beginning from $t_1$ a linearization is obtained by using Eq. (6) and in the final portion negative deviations may appear, i.e. a relative equilibrium begins

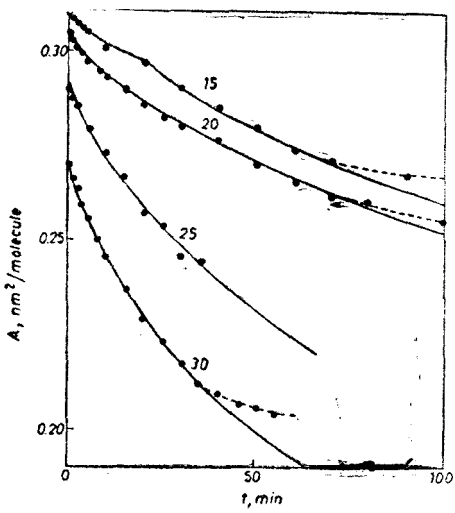


Fig. 4. Kinetic curves for OA. Figures above the curves indicate the constant $\pi$ value in mN/m, at which curves have been recorded. Full line curves calculated by means of Eqs. (5) and (6), by using parameter values given in Tab. 2.

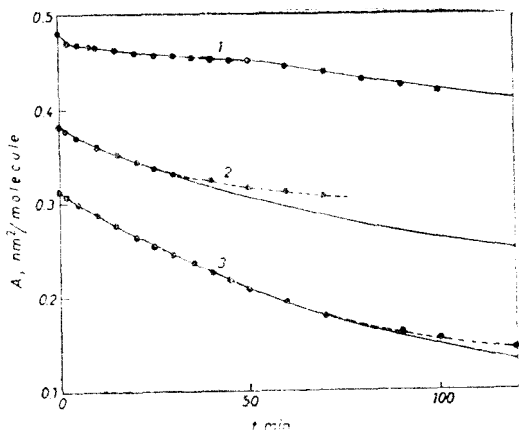


Fig. 5. Kinetic curves for LA. (1): $\pi = 5$ mN/m; (2): $\pi = 20$ mN/m; (3): $\pi = 26$ mN/m. Full line curves calculated by means of Eqs. (5), (6) and (7), by using parameter values given in Tab. 2.

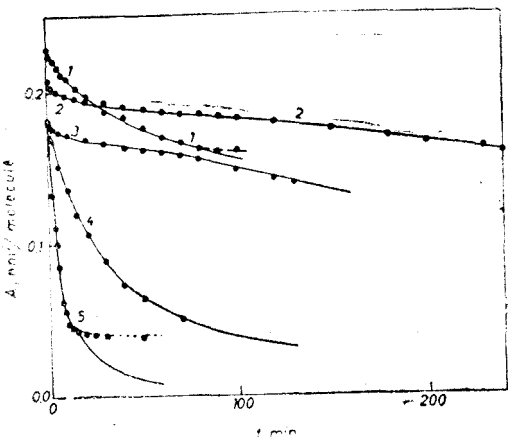

Fig. 6. Kinetic curves for SA.
(1) : $\pi = 10$ mN/m ; (2) : $\pi = 20$ mN/m ; (3) : $\pi = 30$ mN/m ;
(4) : $\pi = 35$ mN/m ; (5) : $\pi = 40$ mN/m.
Full line curves as in Fig. 5.

to establish. At $\pi_c$, linearization is possible only by means of Eq. (6), even from the beginning. The linear portions of the Prout-Tompkins plots were processed by using a linear regression method. The kinetic parameters obtained by means of this procedure are summarized in Tab. 2. We mention that the correlation coefficient was higher than 0.995 in all cases, sometimes depassing even 0.999, which shows a very good linearity.

Tab. 2 contains, besides the constant $\pi$ value at which measurements have been performed, and the $k_i$ and $c_i$ values derived, also the $t_i$ values, corresponding to the maximum time, up to which linearization according to the $i$-th mechanism is very good. The upward arrows after $t_i$ value indicate positive deviations for $t > t_i$, whereas the downward ones are for negative deviations. $A_i$ represents the mean molecular area at $t_i$, taken for $A_0$ in the calculations accordingly to the $(i + 1)$ — th mechanism.

The kinetic parameters have been used to construct theoretical $A$ *vs.* $t$ curves for all fatty acids studied and for all constant $\pi$ values at which kinetic curves have been recorded. These theoretical curves are given with full lines in Figs. 4—6. In the same figures, dashed line curves give the experimental ones in the range where deviations appear. As seen, the theoretical curves describe very well the relaxation phenomena investigated. All systematic deviations appear only in the final portions and they correspond to higher $A$ values as expected on the basis of Eqs. (6) or (7). In the Prout-Tompkins plots these appear as negative deviations, consistent with the establishment of an equilibrium.

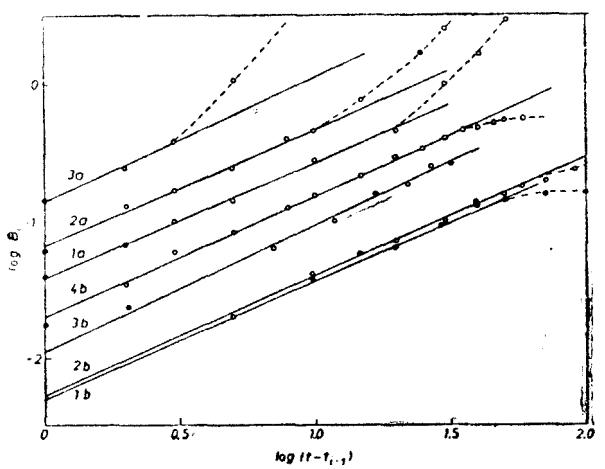

Fig. 7. Prout-Tompkins linearizations for OA.
(1) : $\pi = 15$ mN/m, (2) : $\pi = 20$ mN/m ; (3) : $\pi = 25$ mN/m; (4) : $\pi = 30$ mN/m. *a* : $i = 1$; *b* : $i = 2$. $t_{i-1} = 0$ for *1a*, *2a*, *3a* and *4b*

Inspection of Tab. 2 shows in the case of OA that at $\pi < \pi_c$ the relaxation is due, at the beginning, to the formation of close packed islands. The rate constant $k_1$ has practically the same value, irrespective of $\pi$,

*Table 2*

**Kinetic parameters derived from curves $A$ vs. $t$**

| Surfactant | $\pi$ | $A_0$ | $k_1$ | $c_1$ | $t_1$ | $A_1$ | $k_2$ | $c_2$ | $t_2$ | $A_2$ | $k_3$ | $c_3$ | $t_3$ |
|---|---|---|---|---|---|---|---|---|---|---|---|---|---|
| OA | 15 | 0.310 | 0.841 | −1.417 | 20↑ | 0.2975 | 0.866 | −2.302 | 70↓ | — | — | — | — |
| | 20 | 0.305 | 0.866 | −1.192 | 10↑ | 0.2940 | 0.867 | −2.279 | 80↓ | — | — | — | — |
| | 25 | 0.290 | 0.880 | −0.851 | 3↑ | 0.2845 | 0.898 | −1.925 | 35 | — | — | — | — |
| | 30 | 0.270 | — | — | — | — | 0.885 | −1.696 | 35↓ | — | — | — | — |
| LA | 5 | 0.480 | 0.425 | −1.396 | 50↑ | 0.4500 | 0.994 | −2.688 | 100 | — | — | — | — |
| | 10 | 0.455 | 0.518 | −1.694 | 40↑ | 0.4375 | 1.018 | −3.143 | 120 | — | — | — | — |
| | 15 | 0.380 | 0.870 | −1.218 | 10↑ | 0.3575 | 1.035 | −2.239 | 30↓ | — | — | — | — |
| | 20 | 0.360 | 1.042 | −1.690 | 8↑ | 0.3525 | 0.952 | −2.293 | 35↓ | — | — | — | — |
| | 26 | 0.310 | — | — | — | — | 1.044 | −1.915 | 30↑ | 0.2460 | 1.051 | −2.106 | 70↓ |
| SA | 10 | 0.2270 | 0.455 | −1.004 | 4↑ | 0.2190 | 0.795 | −1.743 | 80↓ | — | — | — | — |
| | 15 | 0.2250 | 0.517 | −0.888 | 2↑ | 0.2175 | 0.596 | −1.583 | 120↓ | — | — | — | — |
| | 20 | 0.2075 | — | — | — | — | 0.452 | −1.579 | 130↑ | 0.1785 | 1.065 | −3.090 | 250 |
| | 25 | 0.1860 | — | — | — | — | 0.457 | −1.612 | 90↑ | 0.1650 | 1.031 | −3.070 | 170 |
| | 30 | 0.1820 | — | — | — | — | 0.450 | −1.502 | 65↑ | 0.1550 | 1.104 | −2.844 | 130 |
| | 35 | 0.1810 | — | — | — | — | — | — | — | — | 1.039 | −1.519 | 70↓ |
| | 40 | 0.1800 | — | — | — | — | — | — | — | — | 1.220 | −0.821 | 12↓ |

*Note:* Units for $A_0$, $A_1$ and $A_2$: nm²/molecule; for $t_1$, $t_2$ and $t_3$: min; and for $\pi$: mN/m.

only a very slight increasing tendency is observed with increasing $\pi$. On the contrary, $c_1$ increases rather significantly at higher $\pi$ values and the time interval of the validity of Eq. (5) is shortened with increasing $\pi$. This suggests the idea that the growth of the islands occurs with a rate constant $k_1$ practically not dependent on $\pi$, but the number of germs, correlated to $c_1$ increases very much with increasing $\pi$. The $k_2$ values are practically equal to $k_1$, but $c_2$ increases with increasing $\pi$, presumably due also to the increase of the number of germs, of the trilayers in this case. The system seems to attain an equilibrium state before of mechanism *3* sets in, even for $\pi = \pi_c$.

The general picture obtained in the case of LA is similar to that found with OA. At $\pi < \pi_c$, one observes also only mechanisms *1* and *2* and $t_1$ decreases with increasing $\pi$, but $k_1$ increases very much with increasing $\pi$. This might be due to the existence of two double bonds in the hydrocarbon chain of LA, which entails the vertical orientation of the molecules to occur with much more difficulty in the case of LA, as compared to OA. Therefore, with increasing $\pi$, in the case of LA the mean molecular area varies more rapidly than with OA, due to the higher compressibility of the monolayer of the former, as compared to the latter. Consequently, in the case of LA monolayers with increasing $\pi$ the role of the intermolecular attraction forces increases significantly, the formation of close packed islands occurs more easily, entailing the increase of $k_1$. The values of $k_2$ are practically the same for all $\pi$ values investigated and equal to the highest value of $k_1$, obtained for $\pi = 20$ mN/m.

At $\pi_c$, mechanism *2* observed for the initial portion is changed for mechanism *3*, with $k_3$ practically equal to $k_2$. As observed, $k_2$ values are higher for LA than for OA, indicating a lower stability of the monolayers of LA, as compared to the OA ones, in agreement with $\pi_c$ values observed experimentally (see Tab. 1). The dependence of $c_i$ values on $\pi$ is not so clear as with OA. The $c_1$ values are rather scattered and no systematic variation is observed. Nevertheless, in the case of $c_2$ an increasing tendency with increasing $\pi$ is rather obvious.

The behaviour of SA films differs quite a lot from that of the unsaturated acids, which is not surprizing by taking into account that SA is solid, and OA and LA are liquids in pure state, at the working temperature. The role of mechanism *1* is insignificant at the $\pi$ values investigated and it is observed only at the very beginning of the relaxation curves, recorded at low $\pi$ values. Presumably, this is due to the condensed character of the monolayer even at $\pi = 10$ mN/m, and $k_1$ has lower values as compared to OA and even to LA at the same $\pi$ values. Unlike the unsaturated acids, the $k_2$ value of SA monolayers exhibit an important decrease, when $\pi$ is increased from 10 to 20 mN/m, but for higher $\pi$ values it becomes practically constant. This constant value is much less than with OA and LA, revealing the high stability of SA films against the collapse involving formation of trilayers. This stability, reflected also by the high $\pi_c$ value, may be due to the close packing of the saturated hydrocarbon chains, leading to very important dispersion type attraction forces. It is interesting to observe, that with SA monolayers mechanism *3* appears already at $\pi = 20$ mN/m and collapse occurs exclusively according to this mechanism at 35 and 40 mN/m. This might be a consequence of the solid state of the monolayer at these surface pressures, and it is consistent with the electron micrographs reported for the collapse of SA [3], evidencing the formation of bulk

crystallites. One might presume that at the collapse of SA monolayers also fracturing processes occur, leading to the formation of multilayers and eventually to the appearance of bulk crystallites. Meanwhile, $k_3$ has rather high values and $c_3$ exhibits a systematic and very important increase with increasing $\pi$. This is consistent with our presumption concerning the physical meaning of $c_i$, since the higher the $\pi$ values, i.e. the overcompression of the monolayer, the higher will be the probability of the formation of germs of the collapsed bulk phase and even the rate of growth of the crystallites might become higher, as compared to the growth of floating lenses of liquid (with LA), due to the more irreversible character of the process. In the case of OA and LA, $\pi_c$ does not differ very much from the ESP and there is a competition between the growth of liquid droplets and their spreading. On the contrary, $\pi_c$ of SA monolayers is very much higher than the ESP, entailing the pronounced irreversibility of the formation of the collapsed bulk phase.

In conclusion, the experimental $A$ *vs.* $t$ curves can be well described by means of Eqs. (5), (6) and (7), or by their successive application for different portions of the kinetic curves. The procedure proposed allows us to derive kinetic parameters $k_i$ and $c_i$, which can be correlated with the molecular structure of the surfactants studied.

## REFERENCES

1. G. Gabrielli, G. G. T. Guarini and E. Ferroni, *J. Colloid Interface Sci.*, **54**, 424 (1976).
2. G. Gabrielli, G. G. T. Guarini and F. Bastianini, *J. Colloid Interface Sci.*, **69**, 352 (1979).
3. R. D. Neumann, *J. Colloid Interface Sci.*, **56**, 505 (1976).
4. R. D. Smith and J. C. Berg, *J. Colloid Interface Sci.*, **74**, 273 (1980).
5. Shuquian Xu, K. Miyano and B. M. Abraham, *J. Colloid Interface Sci.*, **89**, 581 (1982).
6. M. Tomoaia-Cotişel, J. Zsakó, A. Mocanu, M. Lupea and E. Chifu, *J. Colloid Interface Sci.*, **117**, 464 (1987).
7. P. De Keyser and P. Joos, *J. Phys. Chem.*, **88**, 274 (1984).
8. E. G. Prout and F. C. Tompkins, *Trans. Faraday Soc.*, **40**, 488 (1944).
9. P. Baglioni, G. Gabrielli and G. G. T. Guarini, *J. Colloid Interface Sci.*, **78**, 347 (1980).
10. M. Tomoaia-Cotişel, A. Seu and P. J. Quinn, *J. Colloid Interface Sci.*, **94**, 390 (1983).
11. M. Tomoaia-Cotişel, J. Zsakó, E. Chifu, D. A. Cadenhead and H. E. Ries, Jr., in "Progress in Photosynthesis Research", (J. Biggins, Ed.), Martinus Nijhoff, Dordrecht, vol. 2, 1987, pp. 333–337.
12. H. E. Ries, Jr., *Nature*, **281**, 287 (1979).

STUDIA UNIV. BABEŞ-BOLYAI, CHEMIA, XXXII, 1, 1987

# ELECTROROTATION OF LIVING CELLS

C. M. LUCACIU*, I. TURCU* and V. V. MORARIU*

*Received: September 8, 1986*

This is a minireview concerning the electrorotation of living cells, also known as rotational cell resonance. The phenomenon occurs at a characteristic frequency of the external field, which is determined by the relaxation time of the polarization process. The cell membrane capacity and resistance can be evaluated from the characteristic frequency. The advantage of the method is that a single cell can be investigated and it is non-invasive. Examples are given for human erythrocytes and protoplasts. A method of separating cells according to membrane electrical parameters and size is also mentioned. The electrorotation seems to be at a stage when its theoretical bases have been developed, but its practical possibilities are far from being exploited.

Key-words: *rotational cell resonance, electrorotation, cell membrane, cells separation*

**Introduction.** The rotation of cells exposed to alternating electrical fields was reported for the first time by Teixeira-Pinto *et. al.* [1] followed by Füredi and Ahad [2] and Crane [3]. The phenomenon occurs at certain frequencies of the applied field. It is known under different titles such as: cell spin resonance [4], rotational cell resonance [5] or electrorotation [6]. Investigation in this field revealed that electrorotation appeared to be sensitive to cell species, their metabolic state and the influence of various factors. These findings triggered an increased interest in developing a new tool of investigation based on electrorotation. It seems to be generally accepted that such a tool would be useful in the field of membranology either from the biophysical or cell biology side. Therefore, much effort was invested in developing suitable experimental devices and for the understanding of the basic mechanism of rotation.

Holzapfel *et. al.* [7] showed that the electrorotation can be understood in terms of the interaction of the external field with the induced dipoles in the cells. Rotation may only occur when a cell is located in a non-uniform field due to either the vicinity of electrode or another cell.

The electrorotation is a resonance-like phenomenon. The resonance frequency, *i. e.* the external field frequency where maximal rotation occurs, can be used to extract the polarization relaxation time. Further basic electrical parameters of the cell membrane can be evaluated from the relaxation time such as capacity and resistance.

Electrorotation can be achieved in two ways: a) cells are exposed to a non-uniform field created by a two thin electrode system. The number of rotating cells is measured versus the frequency of the external field. This is

* *Institute of Isotopic and Molecular Technology, 3400 Cluj-Napoca, Romania*

known as multicell rotational resonance or multicell electrorotation. b) cells are exposed to a rotating electrical field and therefore the electrorotation of single cells can be investigated. This is the technique in current use.

Until recently, the question of the rotation of single spherical objects in an alternating field was a subject of much controversy. However a theoretical investigation of one of us revealed that such a phenomenon is possible under certain conditions [8].

This paper is intented to be a minireview in the field of electrorotation.

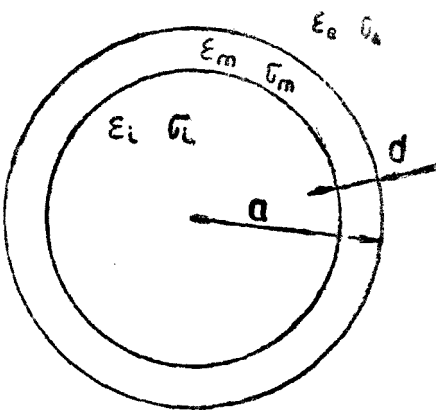


Fig. 1. Spherical model of a living cell

**Theory.** The purpose of this section is to describe the interaction of a simple spherical object with a rotating electrical field. The model is depicted in Fig. 1. The following parameters are considered: the radius a of the sphere; the electrical conductivity $\sigma_i$ and the electrical permitivity $\varepsilon_i$ where $i$ refers to the intracellular volume; the cell is limited by a membrane characterized by $\sigma_m$, $\varepsilon_m$ and thickness $d$. The cell is suspended in a liquid having $\sigma_e$ and $\varepsilon_e$. A dipole is induced when the cell is exposed to an external field $\vec{E}$. The polarization process is characterized by a time constant $\tau$. If $\vec{E}$ changes its orientation there will be a phase difference between $\vec{E}$ and the induced dipole due to the finite relaxation time of the polarization process. This is equivalent to a torque and the cell spins. The rotation will occur at specific frequencies of the external field depending on the polarization mechanism and $\tau$, respectively. The main relaxation mechanism in the $10^3-10^6$ Hz range is the Maxwell-Wagner polarization which is due to the presence of the interfaces and different conductivities in the environments $i$, $m$, $e$, respectively [9]. Clearly the passive electrical properties of the cell are involved in the electrorotation. Therefore, it is possible to estimate such parameters by the investigation of electrorotation. It also should be noted that the electrorotation is a common feature of all living or non-living objects. Fuhr *et al.* investigated, for example, the rotation of glass speres filled with liquids of various conductivities [10].

The electrorotation can be described by the following expression:

$$\frac{d\theta}{dt} = -KE^2 \frac{2\frac{f}{f_0}}{1+\left(\frac{f}{f_0}\right)^2} \tag{1}$$

where $\frac{d\theta}{dt}$ is the angular velocity of the cell, $f$ is the rotational frequency of the field and $f_0$ is a characteristic frequency [11] described by the expression:

$$f_0 = \frac{1}{2\pi r_m c_m} + \frac{\sigma_e \sigma_i}{\pi a c_m (\sigma_i + 2\sigma_e)} \tag{2}$$

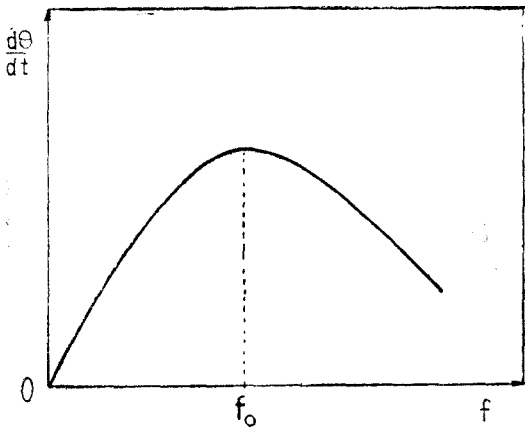


Fig. 2. The frequency dependence of the angular rotation of the cell; $f_0$ is the characteristic frequency of electrorotation.

where $r_m = \frac{d}{\sigma_m}$ and $c_m = \frac{\varepsilon_m}{d}$; $r_m$ and $c_m$ being the specific resistance and the specific capacity of the membrane, respectively. The negative sign in the right hand term shows that the rotation of the cell is opposite to the rotation of the external field. The frequency dependence of the angular velocity of the cell is a resonance like phenomenon. The maximal rotation occurs at $f = f_0$ (Fig. 2).

The angular velocity of the cell is proportional to the square of the field as seen from equation 1.

If the external field frequency is swept, it is possible to determine the value of $f_0$ which is related to the relaxation time $\tau$ of the characteristic polarization process:

$$\tau = \frac{1}{2\pi f_0} \tag{3}$$

When the external conductivity is much smaller than the internal conductivity then (2):

$$f_0 = \frac{1}{2\pi r_m c_m} + \frac{\sigma}{\pi a c_m} \tag{4}$$

It can be noticed that there is a linear dependence between the characteristic frequency and the external conductivity (Fig. 3). If experimental data are available to obtain such a plot then the membrane specific capacity can be measured from the slope and the membrane specific resistance from the intercept of the line with the ordinate axis. If the electrical resistance of the membrane is very large, the term $1/2\ \pi\, r_m c_m$ can be neglected. A non-linear plot suggests that the approximation is not valid, probably due to changes of the membrane parameter.

More detailed calculations of the angular momentum gave the following result [12]:

$$M = 4\pi\varepsilon_0\varepsilon_e a^3 E^2 \left\{ \left( \frac{C_1}{C_2} - \frac{B_1}{B_2} \right) \frac{\frac{f}{f_{01}}}{1 + \left( \frac{f}{f_{01}} \right)^2} + \left( \frac{B_1}{B_2} - \frac{A_1}{A_2} \right) \frac{\frac{f}{f_{02}}}{1 + \left( \frac{f}{f_{02}} \right)^2} \right\} \tag{6}$$

where $f_{01} = \frac{C_2}{2\pi\varepsilon_0 B_2}$; $\quad f_{02} = -\frac{B_2}{2\pi\varepsilon_0 A_2}$

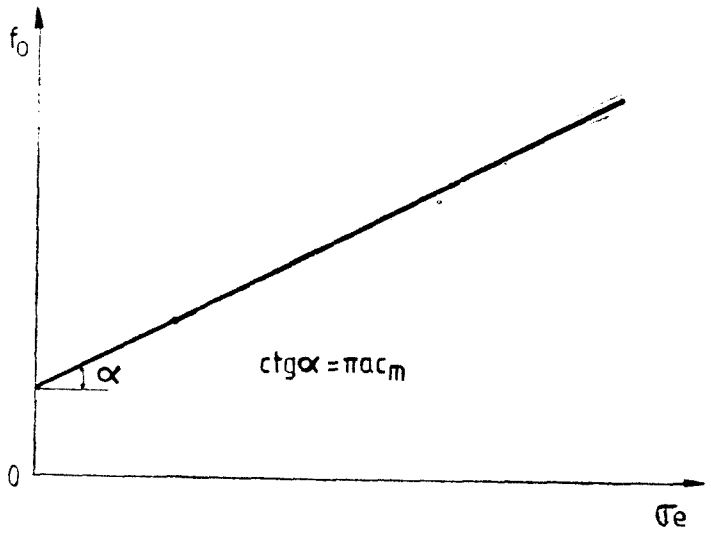


Fig. 3. The external conductivity dependence of the characteristic frequency of electrorotation.

and

$$A_1 = \varepsilon_m(\varepsilon_e - \varepsilon_i) + \frac{d}{a}(\varepsilon_i - \varepsilon_m)(2\varepsilon_m + \varepsilon_e)$$

$$A_2 = -\varepsilon_m(\varepsilon_i + 2\varepsilon_e) - \frac{2d}{a}(\varepsilon_i - \varepsilon_m)(\varepsilon_e - \varepsilon_m)$$

$$B_1 = -\sigma_m(\varepsilon_e - \varepsilon_i) - \varepsilon_m(\sigma_e - \sigma_i) - \frac{d}{a}[(\sigma_i - \sigma_m)(2\varepsilon_m + \varepsilon_e) + (2\sigma_m + \sigma_e)(\varepsilon_i - \varepsilon_m)]$$

$$B_2 = \sigma_m(\varepsilon_i + 2\varepsilon_e) + \varepsilon_m(\sigma_i + 2\sigma_e) + \frac{2d}{a}[(\varepsilon_i - \varepsilon_m)(\sigma_e - \sigma_m) + (\varepsilon_e - \varepsilon_m)(\sigma_i - \sigma_m)]$$

$$C_1 = -\sigma_m(\sigma_e - \sigma_i) - \frac{d}{a}(\sigma_i - \sigma_m)(2\sigma_m + \sigma_e)$$

$$C_2 = \sigma_m(\sigma_i + 2\sigma_e) + \frac{2d}{a}(\sigma_i - \sigma_m)(\sigma_e - \sigma_m)$$

In the case of the biological membranes $\sigma_m \approx 0$ and the first characteristic frequency is:

$$f_{01} = \frac{1}{2\pi a\, c_m\left(\frac{1}{\sigma_i} + \frac{1}{2\sigma_e}\right)} \tag{7}$$

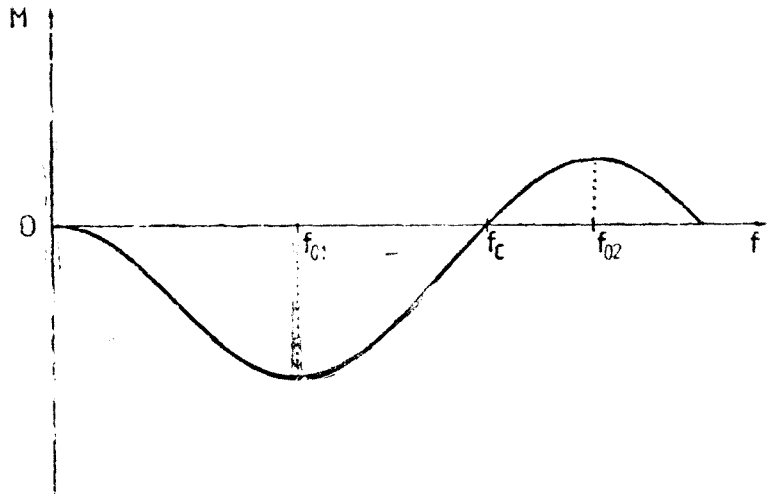


Fig. 4. The angular momentum of a cell versus the rotating field frequency.

which is similar to expression (2) with this condition. The second characteristic frequency is:

$$f_{02} = \frac{(\sigma_i + 2\sigma_e)}{2\pi\varepsilon_0 (\varepsilon_i + 2\varepsilon_e)} \qquad 8)$$

It should be noticed that $f_{02}$ does not depend on the cell membrane characteristics. The frequency dependence of the angular momentum for conditions which are specific for biological cells i. e. $\sigma_m < (\sigma_i, \sigma_e)$ and $\varepsilon_m < (\varepsilon_i, \varepsilon_e)$ is qualitatively illustrated in Fig. 4. The plot shows that the rotation direction of the cell is changed as the rotating field frequency is swept over a large enough range. This theoretical prediction is borne out by experiments on macroscopic models [13]. However, to the best of our knowledge the full frequency dependence has not yet been reported for living cells. The experiments revealed only the lower maximum ($f_{01}$) while the upper maximum ($f_{02}$) which generally occurs at frequencies higher than $10^7$Hz was not detected mainly due to technical limitations.

**Methods.** There are two possibilities to obtain rotating electric fields: a) by applying sine wawes 90° out of phase on a four electrodes system. The platinum electrodes are set at right angles to each other and fastened to a glass microscope slide with an epoxy resin. An alternative possibility is to cover the glass slide with a thin metallic film and obtain the electrode system by using photomicrolithography. Measurement of cell rotation can be done by direct observation at the microscope or by more sophisticated image processing systems /11/. b) Another possibility is to use square-topped pulses applied to a similar square electrode arrangement /14/.

It has been shown that the characteristic frequency detected by either one of the two methods give closely similar values. An essential disadvantage of these methods is the broad maximum in the rotation rate. This makes the determination of the characteristic frequency a slow and rather imprecise procedure. A substantial improvement of the method was proposed and experimented by Michael Arnold *et al.* /15/. They used a special designed generator which „manipulates the frequency and direction of the rotating field so that, when the displayed frequency matches the characteristic frequency of the cell under observation, a sharp null instead of a broad maximum in

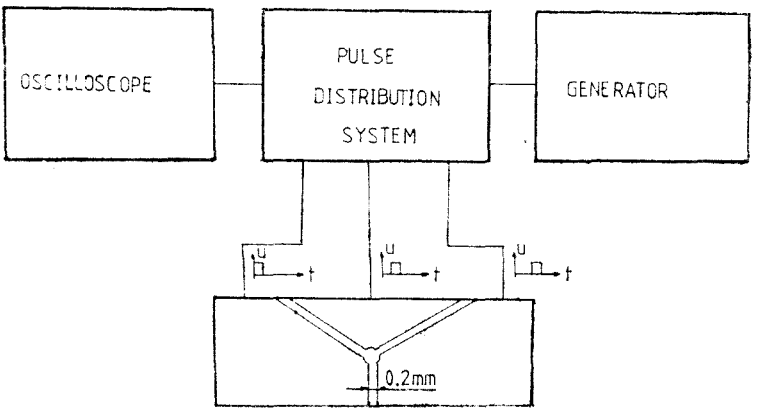


Fig. 5. Experimental set up for the investigation of the electrorotation.

rotation rate is seen." The production of the sharp null allows a quick estimation of the characteristic frequency.

An essential requirement of the electrorotation is the low conductivity of the suspending liquid. At conductivities higher than $10^{-3}\Omega^{-1}cm^{-1}$ strong turbulences are seen near electrodes. It should be understood that full information can be extracted from electrorotation if both the characteristic frequency and the electric conductivity of the suspending liquid are known. The conductivity should be measured in the rotational chamber, but this obviously requires a constant volume chamber. In our laboratory a rotating electric field was produced by using a three electrode system and applying square pulses from a generator. The electrodes system was of the thin film type. The distance between the tip of electrodes was about 0.2 mm. A schematic picture of the experimental set up is illustrated in Fig. 5. The rotation rate was measured by direct observation at the microscope.

**Results.** Experimental data have already been obtained on microorganism, vegetal or animal cells. The basic parameters which can be obtained from electrorotation, as explained in the previous section, are the membrane capacity and resistance. Both depend on the membrane structure. However the intimate relation between the membrane electrical parameters and its structure has not yet been determined. Nevertheless the evaluation of these membrane parameters is of interest for two reasons: the membrane electrical resistance is a measure of the membrane integrity and therefore membrane damaging effects of various factors can be investigated; the membrane capacity is a controlling factor for the dielectric breakdown. This aspect is relevant for cell fusion or electrical permeation.

A. *The evaluation of the electrical passive parameters of cell membranes.* Electrorotation curves for different cell species are illustrated in Fig. 6. The characteristic frequencies were found to be linearly dependent on the external liquid conductivity. This is illustrated for human erythrocytes in Fig. 7. The external conductivity was increased by addition of predetermined amounts of saline solution. The initial suspending solution contained manitol. The membrane capacity can be estimated from this plot being 0.97 $\mu F/cm^2$. Glaser *et al.* [16] reported lower values for human erythrocytes. Probably this is due to the fact that the first term in Eq. (4) was omitted. Errors in the estimation of the erythrocyte membrane capacity could be also due to the nonspherical shape of the erythrocytes [10]. Generally, the typical values for biological membranes

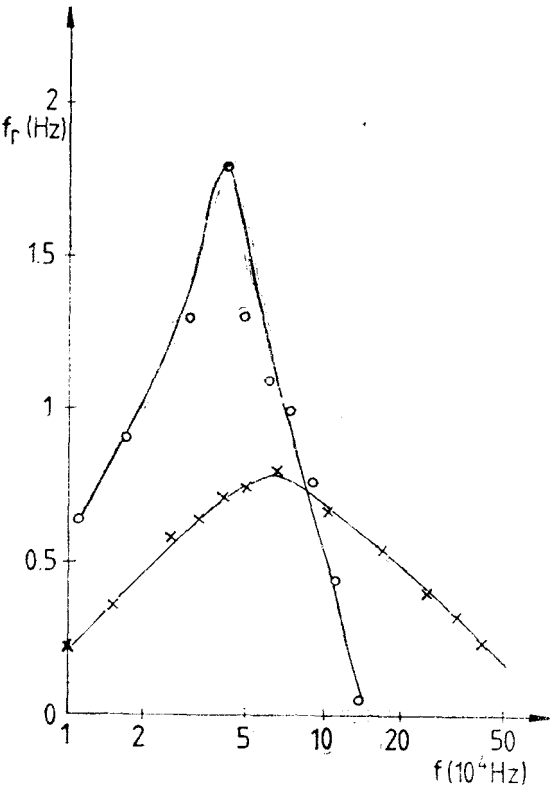


Fig. 6. Electrorotation curves for different cell species obtained with a three electrode system.
○ human erythrocyte $\sigma_e = 1.5\ 10^{-5}\ \Omega^{-1}\ cm^{-1}$
× Zea mays protoplast $\Phi = 31\ \mu m$ $\sigma_e = 6.6\ 10^{-5}\ \Omega^{-1}\ cm^{-1}$

are 1 $\mu F/cm^2$. In the case of plant protoplasts the values of 0.3—0.4 $\mu F/cm^2$ were explained to be due to a more complicated membrane system, also including plasmalemma and tonoplasts. [9, 16, 17]. High values of the membrane resistance are difficult to be estimated from plots of the type shown in Fig. 7.

B. *The effect of chemical agents on passive electrical parameters of the cell membrane.* Arnold *et al.* [18] reported the influence of chemical agents on single swollen thylakoid vesicles prepared from chloroplasts placed in a hypotonic solution. This is a simple model for investigation as it does not contain other internal membranes. In this particular case, $\sigma_i = \sigma_e = \sigma$ and:

$$f_0 = \frac{1}{3\pi a\, c_m}\left(\sigma + \frac{3a}{2r_m}\right) \qquad (8)$$

Following the usual procedure the pH dependence of the membrane capacity was investigated. It was found that the capacity has a minimum at pH 4.4 while near pH 7.0 it is insensitive.

Ionophores such as gramicidin D, valinomycin and nystatin slow down or even stop completely the electrorotation [16, 18]. This can be explained by the reduction of the membrane electrical resistance following the formation of large channels. Thylakoid vesicles treated with ionophores showed practically no effect in respect of the membrane capacity while the membrane resistance decreased. It was possible to estimate the minimum conductance of a single channel ($5 \cdot 10^{-14}$ *S*) which is very close to d.c. estimation ($6 \cdot 10^{-14}$ *S*) [19, 20].

Lipid-soluble ions, such as dipicrylamine, increase the membrane capacity. This effect is concentration dependent.

*Cell separation.* Fuhr *et al.* proposed an unusual method of cell separation based on electrorotation [21, 22]. The method is aimed to separate cells of different types according to their membrane properties (conductivity and capacity) and size. The main idea is to use rotation to bring about translational movement. Unlike usual electrorotation systems, the electrodes are arranged vertically and the lower part is filled with an agar block in such a way that the

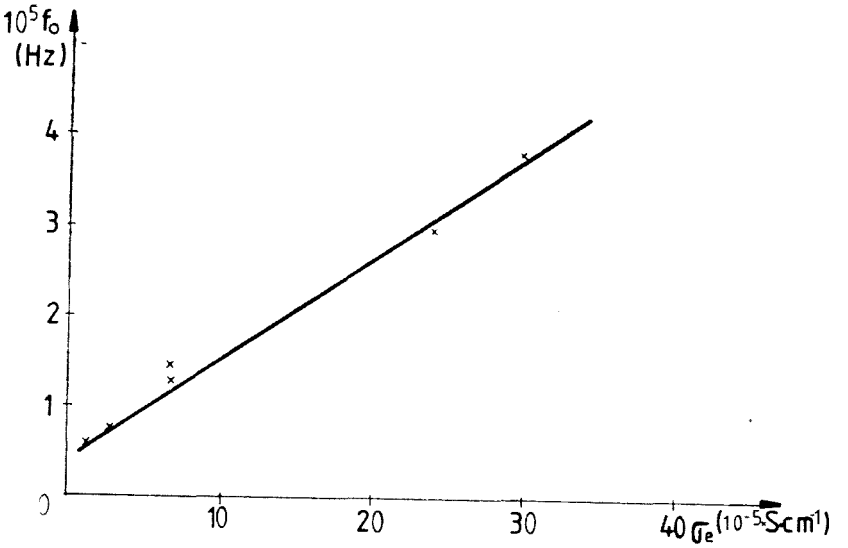


Fig. 7. The characteristic frequency versus the external conductivity for human erythrocyte.

interface was formed in the diagonal direction of the chamber. This interface is used as a rollplane for the cells but other materials may also be used. The contact of the cells with the surface will cause an asymmetric friction and would therefore produce rolling in the presence of the rotating field. If two cells are initially close to one another and they have different characteristic frequencies $f_{01}$ and $f_{02}$, then an applied field $f = f_{01}$ will separate the cells as cell no. 1 rolls faster. Fuhr *et al.* [21] exprimented this type of separation on mesophyll protoplasts. They found that the protoplasts traveled with a velocity of about 3—7 μm/s on the agar surface at a field strenght of $3.5 \times 10^3$ V/m. They succeeded to separate resting cells that were damaged by the isolation procedure from living cells, within about two minutes. The separation distance was about 0.2 mm. It is believed that with improvement of the technique, practical applications like the separation of damaged and intact cells or according to more subtle characteristics should be realized on a large scale.

## REFERENCES

1. A. A. Teixeira-Pinto, N. L. Nejelski, J. D. Cutler, J. H. Heller, *Exp. Cell. Res.*, **20**, 548(1960).
2. A. A. Füredi, J. Ahad, *Biochim. Biophys. Acta*, **79**, 1 (1964).
3. H. A. Pohl, J. S. Crane, *Biophys. J.*, **11**, 711 (1971).
4. H. A. Pohl, T. Braden, *J. Biol. Phys.*, **10**, 17 (1982).
5. U. Zimmermann, J. Vienken, G. Z. Pilwat, *Z. Naturforsch*, **36c**, 173 (1980).
6. R. Glaser, G. Fuhr, J. Gimsa, R. Hagedorn, *Studia Biophys.*, **110**, 1 (1985).
7. C. Holzapfel, J. Vienken, U. Zimmermann, *J. Membrane Biol.*, **67**, 13 (1982).
8. I. Turcu, *J. Phys. A.*, (in press).

9. U. Zimmermann, *Biochim. Biophys. Acta*, **694**,, 227 (1982).
10. G. Fuhr, R. Hagedorn, T. Müller, *Studia Biophys.*, **107**, 104 (1985).
11. R. V. E. Lovelace, Stout D. G., Steponkus, *J. Membrane Biol.*, **82**, 157 (1984).
12. G. Fuhr, R. Glaser, R. Hagedorn, *Biophys. J.*, **49**, 395 (1986).
13. R. Glaser, G. Fuhr, "Electrorotation of single cells a new method for assessment of membrane properties", in *Electric Double Layers in Biology* (M. Blank editor), Plenum Press, New York (1986).
14. G. Fuhr, R. Hagedorn, R. Glaser, *Studia Biophys.*, **102**, 321 (1984).
15. W. M. Arnold, U. Zimmermann, *Patent application official designation P3325 843.O* received at the Patent Office, F.R.G., July 18, 1983 cited in (18).
16. R. Glaser, G. Fuhr, J. Gimsa, *Studia Biophys.*, **96**, 11 (1983).
17. J. Gimsa, G. Fuhr, R. Glaser, *Studia Biophys*, **109**, 5 (1985).
18. W. M. Arnold, B. Wendt, U. Zimmermann, R. Korenstein, *Biochim. Biophys. Acta*, **813**, 117, (1985).
19. B. W. Urban, S. B. Hladky, D. A. Haydon, *Fed. Proc.*, **37**, 2628 (1978).
20. B. W. Urban, S. B. Hladky, D. A. Haydon, *Biochim. Biophys. Acta*, **602**, 331(1980).
21. G. Fuhr, R. Hagedorn, H. Göring, *Plant. Cell Physiol.*, **26**, (8), 1527(1985).
22. G. Fuhr, R. Hagedorn, Th. Müller, *Studia Biophys.*, **107**, 23(1985).

STUDIA UNIV. BABEŞ-BOLYAI, CHEMIA, XXXII, 1, 1987

# THERMAL EFFECTS OF MICELLIZATION OF SURFACTANTS

G. DRĂGAN*, GEORGETA POPESCU* and S. IFRIM*

*Received:* *September 8, 1986*

The evaluation of thermal effects associated to micellization of the amphiphilic surfactants in aqueous solutions is made by considering two types of calorimetric measurements, namely: solution behaviour at infinite dilution and the integral behaviour including several transitions in solution morphology. In view to better detect the contribution of the hydrophil and hydrophob groups, the solution behaviour at infinite dilution of several compounds of the type $(R_i)_n - (X - Y^+)_n$ as a function of the length $i$ and volume $n$ of the alkyl $(R_i)$ and/or ionic group are considered. Two of the recently introduced techniques using the high resolution mixing calorimetry (HRMC) are applied for aqueous solutions of sodium dodecyl sulphate and results to be sensitive to any changes in solute-water interactions as a function of solute concentration. In conclusion, both types of experiments can be used to evaluate kinetic parameters of the micellization process, but preserving standard experimental conditions for a series of homologous compounds.

Key-words: *high resolution mixing calorimetry, surfactants, micellization*

1. **Introduction.** Separation of pure thermal effect of micellization from the integral heat of surfactants-water interactions is a difficult problem due to the composite structure of both components [1—3]. So, in the basic experiments of solution and dilution, many elementary processes occur and their contributions strongly depend on the particular experimental conditions of mixing [4]. A special interest has been focussed on the "iceberg" picture of water and aqueous solutions of solutes with ionic component in molecular structure [1]. The relation between hydrophobic bonding in proteins and water structure has represented the starting point in the study of composite solutes [2]. The composite structure of surfactants is defined by their amphiphilic behaviour in solution experiments in which the micellization transition occurs as a specific process. This process is modulated by structure breaker and/or maker character of the ionic and hydrophobic components.

According to Frank and Wen [5] structure breaking ions orient the neighbouring solvent molecules, restricting their participation in H-bonded water clusters and leading to a region of disorder around the solvated solute molecules. There are many classifications, some of them being contradictory, of the structure breaking/making ions and of the hydrophobic components established on a large variety of experimental techniques [1, 2, 5, 6, 7], but the most correct one should be established in standard experimental conditions and generally depends on the particular measuring system [3, 4].

* *ICECHIM-CCF, Spl. Independenţei 202, Bucharest 77208, Romania*

The comparison of two series of calorimetric measurements in standard experimental conditions on solution and dilution of standard ionic surfactants is presented in this work in view to better separate the contribution of micellization process. The first series refers to the infinite diluted solutions [8, 9], while the second one takes into account the solution and dilution behaviours on a large domain of concentrations [3, 4, 10].

2. **Experimental.** *Calorimetric measurements.* The detailed experimental conditions for the two series of measurements were previously described [8,10] and correspond to the process of mixing in the isothermal conduction calorimeters. The time-resolution is the main characteristic which differs for the two types of calorimeters and this has been thoroughly discussed in the recent works devoted to this types of experiments [3, 4, 10, 11].

*Materials.* The studied standard compounds belong to the general series of alkyl ($R_i$)-ionic ($X^-Y^+$) compounds with pro analysis purity.

3. **Results and discussion.** 3.1. *Behaviour at infinite dilution.* For this limit of behaviour the surfactant molecules can be considered to be perfectly isolated and the solution as a perfect gas of these entities. Taking into account a large number of molecular species in the series of $R_i - X^-Y^+$ with different length of the alkyl ($R_i = C_iH_{2i+1}$) and/or ionic component we can detect their contributions to the solution behaviour.

The integral heat of solution at infinite dilution, $\Delta H_s^0$, is determined at different temperatures close to the ambient temperature in view to maintain unchanged the water structure, and below to the glass transition of solutes [11]. The following relationship can be established in these conditions [8, 9]:

$$d(\Delta H_s^0)/dT = \Delta C_p^0 = C_p^0 - C_p^s \qquad (1).$$

where $C_p^0$ — the molar specific heat of the solute in the infinite diluted solution, $C_p^s$-the molar specific heat of the solute in glassy state, and $\Delta C_p^0$ represents the variation of the molar specific heat of the solute by its molecular isolation by interaction with water. Taking into account that the inter- and intra-molecular interactions in solid solute below $T_g$ essentially by H-bonds are stronger than solute-water interaction, $\Delta H_s^0$ generally results to be endothermal [11]. The dependence of $\Delta H_s^0$ at 25°C for four series of compounds differing by the alkyl length and volume and the ionic nature are represented in Figure 1 as a function of the alkyl length. For small length of the alkyl radical, $\Delta H_s^0$ is endothermal and strongly decreases to exothermal values for $i = 2-4$ excepting for the series of alkyl sodium sulfate. More suggestive is the

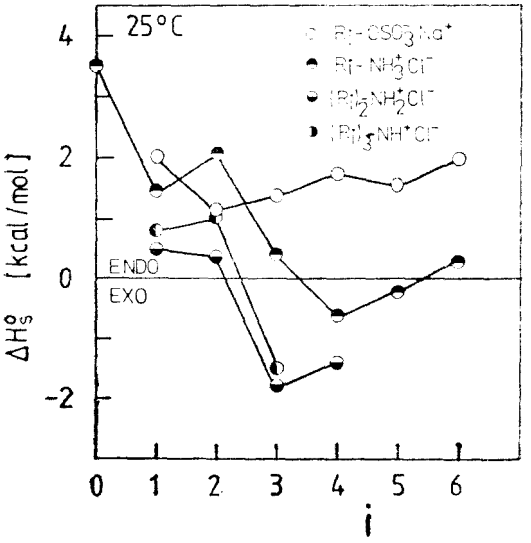


Fig. 1. Dependence of heat of solution at infinite dilution for amphiphilic compounds of type $R_i - X^-Y^+$ as a function of the alkyl length ($R_i = C_iH_{2i+1}$).

dependence of $\Delta C_p^0$ versus $i$ in Figure 2, which shows that $C_p^s > C_p^0$ for the majority of compounds up to $i = 2-3$ and $\Delta C_p^0 > 0$ and proportionally increases with the alkyl length and volume. This means that $R_i$ — radical decreases the density of the van der Waals bonding in the glassy state of solute but increases the density of water-solute bonding.

Similar data are represented for other two pairs of compounds in Figure 3 from which results, in addition, the influence of the nature and volume of the ionic component. We may notice that the ionic part has a reverse effect in respect of the alkyl group. However, from the dependence of $\Delta C_p^0$ versus $i$ it can be observed that the ionic components make stronger interactions also in glassy solute which vanish at higher values of $i$ for greater ions.

These results allow to conclude that the capacity of micellization of amphiphilic surfactants can be described even at infinite diluted solutions by the value of $\Delta C_p^0$ determined in standard experimental conditions [8—10].

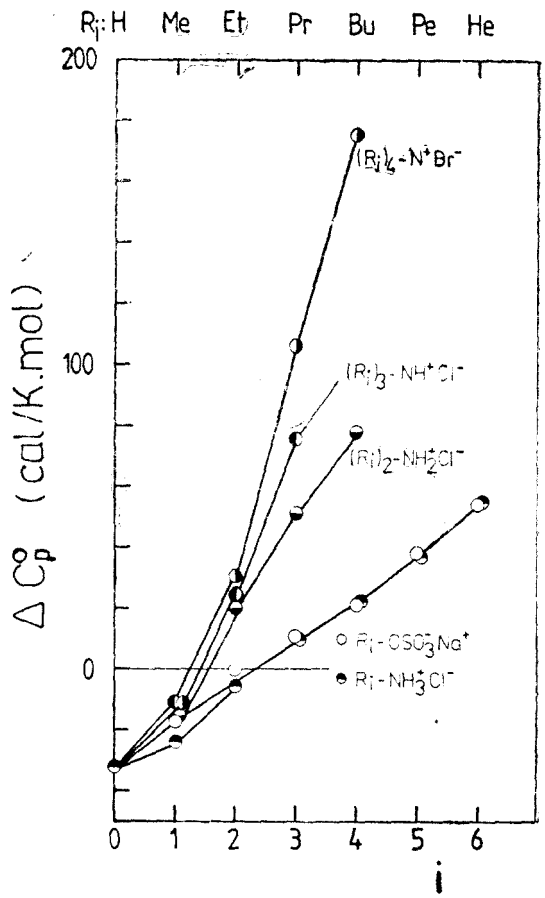


Fig. 2. Dependence of transition value of heat capacity for solution at infinite dilution of glassy amphiphilic solutes of type $R_i-X^-Y^+$ as a function of alkyl length.

3.2. *Integral behaviour.* The integral behaviour for a large domain of solute concentration, which includes the micellization transition values, can be suitably studied by one or many techniques using the high resolution mixing calorimetry (HRMC) recently introduced [10—12]. We will consider in the following representative data in two measuring systems for sodium dodecyl sulfate (SDS). The exact experimental conditions for solution experiments and the obtained results at 30°C for the kinetic HRMC parameters $h$ and $E$ are represented in Figure 4 [3, 10—12]. The following important facts can be revealed in respect of the solution behaviour of pure ionic solutes [4]: (*i*) the overall mixing energy results as endothermal and this is in good agreement with the previously discussed results, (*ii*) dependences $h(m_{st})$ and $E(m_{st})$ show several reproducible transitions even at low values of solute concentration: (*iii*) the transitions in vehaviour become

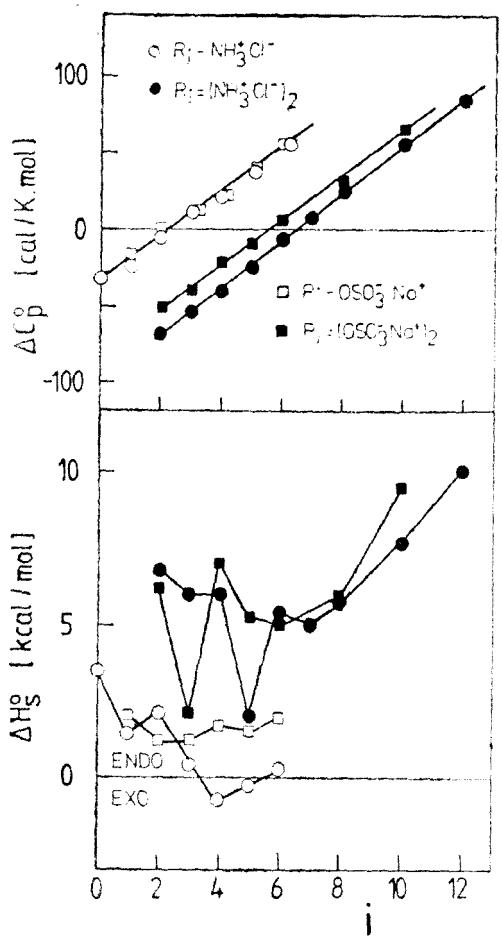


Fig. 3. Dependence of $\Delta H_s^0$ and $\Delta C_p^0$ for solution experiments at infinite dilution of glassy amphiphilic solutes of type $R_i-X^-Y^+$ as a function of alkyl length.

more extended on $m_{st}$ axis at higher concentrations denoting that the molecular clusters have increasing weight distribution, and (*iv*) these experiments can not take into account the rate ratio of $h/E$ which is sensitive to changes in behaviour, because the solute could not be fractionated upon particle sizes [4].

A sensitive and more reproducible study of solute-water interactions for amphiphilic solutes can be performed by HRMC experiments on solutions at different concentrations, $c_{st}$, by mixing with ethanol (EtOH) as water capturer. This technique was extensively used for a large number of pharmaceutically active substances with i. v. and/or i. m. administration [12].

The exact standard experimental conditions are represented with the obtained results for SDS aqueous solutions in Figure 5. We may also notice the following facts: (*v*) the values of $\Delta E = E(c_{st}) - E^0$ ($E^0$ — the mixing energy of pure water and EtOH) really show the transitions in the water-solute interactions as function of $c_{st}$, namely: (*a*) for $\Delta E > 0$, this value includes the additional interaction of $H_2O$-hydrophil groups and (hydrophob/hydrophyl) groups which denotes the solute micellization, and (*b*) for $\Delta E < 0$ denotes the depolymerization of solute clusters; (*vi*) the amplitude and the extension on $c_{st}$ axis of the behaviour transitions decreases and increases, respectively, with the $c_{st}$ increasing, and (*vii*) these expriments can be quantitatively retrieved on the basis of topoenergetic universal procedure [12] and by considering each domain of elementary behaviour between two transitions but with a higher resolution.

**4. Conclusions.** This short but condensed work allows to point out the following concluding remarks:

(*i*) Standard experimental conditions are compulsory in the study of the specific amphiphilic-water interaction by solution and dilution experiments, and;

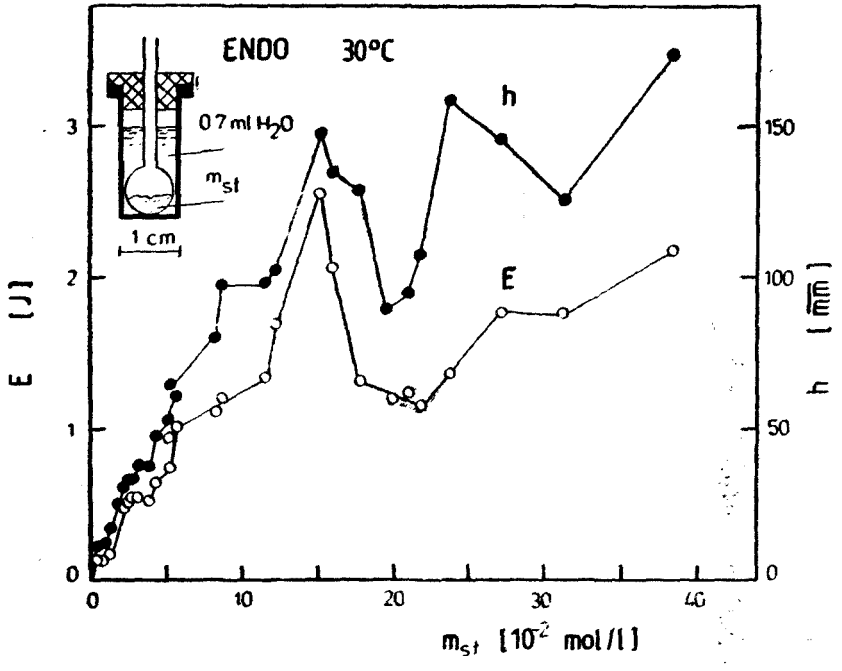


**Fig. 4. The integral solution behaviour of SDS by HRMC experiments expressed by *h* and *E* kinetic parameters [4, 10].**

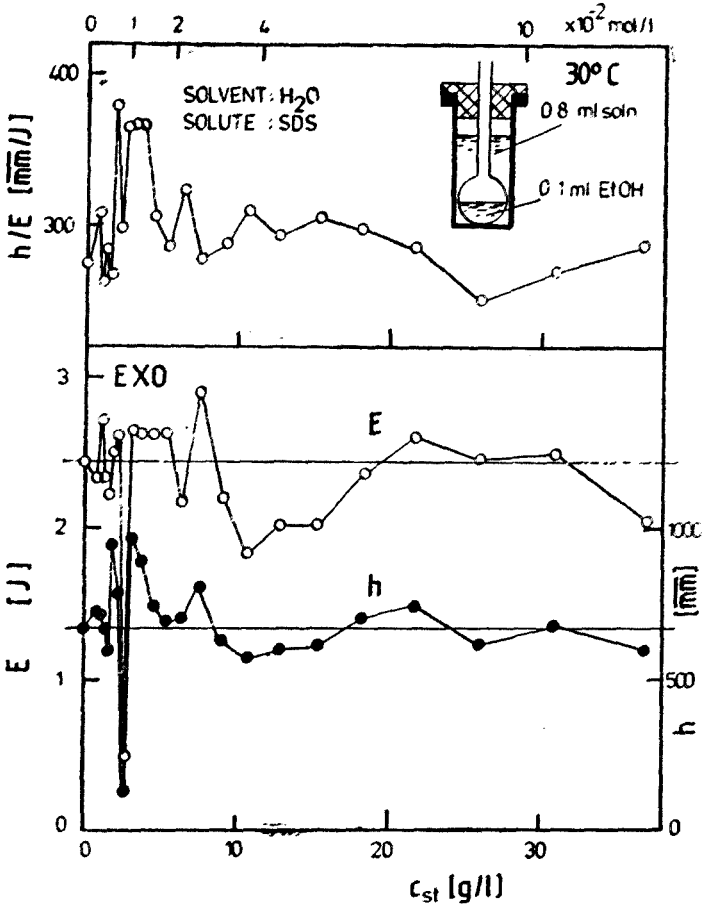


**Fig. 5. The integral compatibility behaviour of SDS-water solutions by HRMC experiments expressed by kinetic parameters of $E$, $h$, and $h/E$ [12].**

*(ii)* Both kinds of experiments on infinite diluted solutions and for the integral range of concentrations allow to determine the kinetic parameters defining the process of solute micellization.

## REFERENCES

1. Frank, H. S., Evans, M. W., *J. Chem. Phys.*, **13**, 507 (1945).
2. Nemethly, G., Scheraga, H. A., *J. Chem. Phys.*, **36**, 3382, 3401 (1962); *J. Phys. Chem.*, **66**, 1772 (1962).
3. Drăgan, G., *Acta Polymerica*, **38**, 467 (1987).
4. Drăgan, G., *J. Thermal Anal.*, **31**, 941 (1986); **32**, 293 (1987).
5. Frank, H. S., Wen, W. Y., *Discussion Faraday Soc.*, **24**, 133 (1957).
6. Schick, M. J., *J. Phys. Chem.*, **68**, 3585 (1964).
7. Luck, W. A. P., *Opt. Pur. Apl.*, **18**, 71 (1985).
8. Tamaki, K., Isomura, Y., Ohara, Y., *Bull. Chem. Soc. Japan*, **45**, 2939 (1972).
9. Tamaki, K., Irie, K., *Bull. Chem. Soc. Japan*, **56**, 2831 (1983).
10. Drăgan, G., *J. Thermal Anal.*, **31**, 677 (1986).
11. Drăgan, G., *The 2-nd National Conference on Colloids and Surface Chemistry, Cluj-Napoca, September*, 8–10, 1986 (High resolution mixing calorimetry in studies of composite systems).
12. Drăgan, G., *The 10-th International CODATA Conference, Ottawa, Canada, July*, 5–8, 1986

STUDIA UNIV. BABEŞ-BOLYAI, CHEMIA, XXXII, 1, 1987

# ADSORPTION MECHANISM OF SOME CAROTENOID DERIVATIVES AT THE LIQUID/SILICA GEL INTERFACE

**SIMION GOCAN*, LILIANA OLENIC**, MARIA TOMOAIA-COTIŞEL* and EMIL CHIFU***

*Received: September 8, 1986*

Separation of some carotenoid derivatives (β—carotene, ethyl ester of β — apo —8′ — carotenoic acid and canthaxanthin), all — *trans* isomers, by thin-layer chromatography, were conducted on silica gel of high efficiency, using eluents of varied polarities. Molecular area values of adsorbed samples calculated from chromatographic data were compared with those obtained by both surface tension measurements at the benzene/water interface and employing molecular models for various configurations of adsorption on silica gel surface. Conclusions were finally drawn about the orientation and adsorption mechanism of carotenoid molecules at organic solvent/silica gel interface. Relying on the theory of Snyder, computed values of the free energies of carotenoid adsorption on silica gel were related to the interactions that occur between the adsorbed carotenoid film and the surface reactive hydroxyl groups of silica gel in agreement with the structure of the studied carotenoids.

Key-words: *thin-layer chromatography of carotenoids, carotenoid films on silica gel surface, carotenoid monolayers at benzene/water interface, adsorption of carotenoid on silica gel surface*

**Introduction.** Chromatographic methods are frequently used in studies on separation of components of biological interest such as carotenoid derivatives, with either analytical or preparative scope. To the end of devising a separation method, as a first step the adsorption mechanism of some carotenoid derivatives, all-*trans* isomers: ethyl ester of β-apo-8′-carotenoic acid (CA), β-carotene (C) and canthaxanthin (4, 4′-dioxo-β-carotene) (CX) (Fig. 1) has been investigated at the organic solvent/silica gel interface by thin-layer chromatography (TLC).

In adsorption chromatography [1], the basic equations take the form:

$$\xi R_F = 1/[1 + (W \cdot K^0/V_M)] \quad (1)$$

and

$$R'_M = \log[(1/\xi R_F) - 1] \quad (2)$$

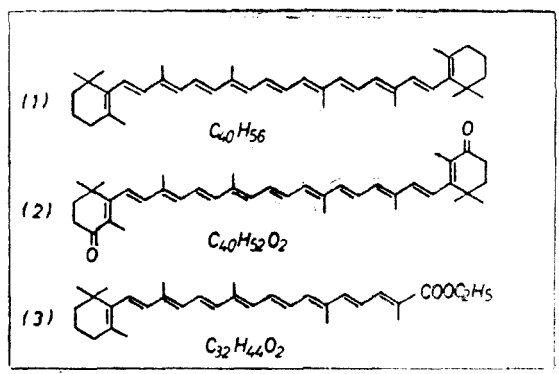


Fig. 1. Structural formulas of some carotenoid derivatives: β-carotene (C:1), canthaxanthin (4,4′-dioxo-β-carotene (CX:2)), and ethyl ester of β-apo-8′-carotenoic acid (CA:3).

* *University of Cluj-Napoca, Faculty of Chemical Technology, 3400 Cluj-Napoca, Romania*
** *Chemistry Institute of Cluj-Napoca, 3400 Cluj-Napoca, Romania*

where $\xi$ stands for a correction factor owed to the concentration gradient of the solvent in thin layer, W is the adsorbent weight in thin layer, $V_M$ is the volume of the mobile phase, and $R_F$ and $R'_M$ have known significance.

As concerns $K^0$, Snyder [1] derived the following equations:

$$\log K^0 = \log V_a + \alpha.f(X, S); \quad f(X, S) = (S^0 - A_s \cdot \varepsilon^0) \tag{3}$$

where $K^0$ is the adsorption distribution coefficient of a certain sample compound at the liquid/solid interface, $V_a$ stands for adsorbent surface volume, $\alpha$ is a function of adsorbent surface activity, $S^0$ is dimensionless free energy of adsorption of a sample on a chosen adsorbent, $\varepsilon^0$ is the solvent strength parameter, $A_s$ is molecular area of the adsorbed compound, and f(X, S) is a quantity which is determined by the particular sample and solvent involved.

By combining Eqs. (1—3), the following equation is obtained:

$$R'_M = \log (V_a \cdot W/V_M) + \alpha (S^0 - A_s \cdot \varepsilon^0) \tag{4}$$

Taking into account that $V_a$, $W$ and $V_M$ are constant values for a given adsoption system and f(X, S) is a function of the sample and solvent used in the system, Eq. (4) can be re-written as:

$$R'_M = a + \alpha (S^0 - A_s \cdot \varepsilon^0) = a + \alpha f(X, S) \tag{4'}$$

where $a = \log (V_a \cdot W/V_M)$.

Thus, $R'_M$ being graphically represented as function of f(X, S) and using some standard samples, the characteristic parameters of the adsorption system used ($a$ and $\alpha$) are determined by means of Eq. (4').

Writing now Eq. (4) for adsorption of a certain sample-component with one and the same adsorbent, in the presence of two differing eluents, by subtraction of the obtained relations, the following equation results:

$$\Delta R'_M = \alpha \cdot A_s (\Delta\varepsilon^0) \tag{5}$$

which is useful both to estimate the effect on sample $R'_M$ values of a change in solvent and to determine the $A_s$, value.

Knowing the values of $a$, $\alpha$, and $A_s$, experimentally obtained from chromatographic data, $S^0$ can be computed by Eq. (4') written this time under the form:

$$S^0 = [(R'_M - a)/\alpha] + A_s \cdot \varepsilon^0 \tag{6}$$

Furthermore, in order to obtain information about the asdorption mechanism of carotenoid derivatives on silica gel surface, both the $A_s$ (Eq. (5)) and $S^0$ (Eq. (6)) values were estimated from chromatographic data. These values were related to the monolayer characteristics of carotenoids adsorbed at the organic solvent/water interface because of the resemblance of the polarity of silica gel surface with that of water. Orientation of the carotenoid molecules on the silica gel surface is discussed by also taking into account the molecular models of carotenoids as well as the various possible configurations of the adsorption of carotenoids on the adsorbent surface.

**Experimental.** Experiments were carried on thin layer of silica gel of high efficiency with a granulation ranging between 5—15 μm, whereas the mobile phase consisted of eluents of varied polarities: petroleum ether ($\varepsilon^\circ = 0$), benzene, ($\varepsilon^\circ = 0.25$), $CH_2Cl_2$ ($\varepsilon^\circ = 0.32$), $CHCl_3$($\varepsilon^\circ = 0.26$) and ethyl acetate ($\varepsilon^\circ = 0.38$). Developings were performed in a saturated N—chromatographic chamber, on plates with thin layers of 10 × 10 cm and 200 μm thick.

**Results and discussion.** With a view to determining characteristic parameters of the adsorption system, i. e. regression curve coefficients, according to Eq. (4'): ordinate intercept $a$ and slope $\alpha$, as standard compounds were chosen: p-amino-azo-benzene, Sudan Red and Sudan Yellow, for which the f(X, S) values are known [2]; the data obtained by TLC are given in Table 1 and their plot in Fig. 2.

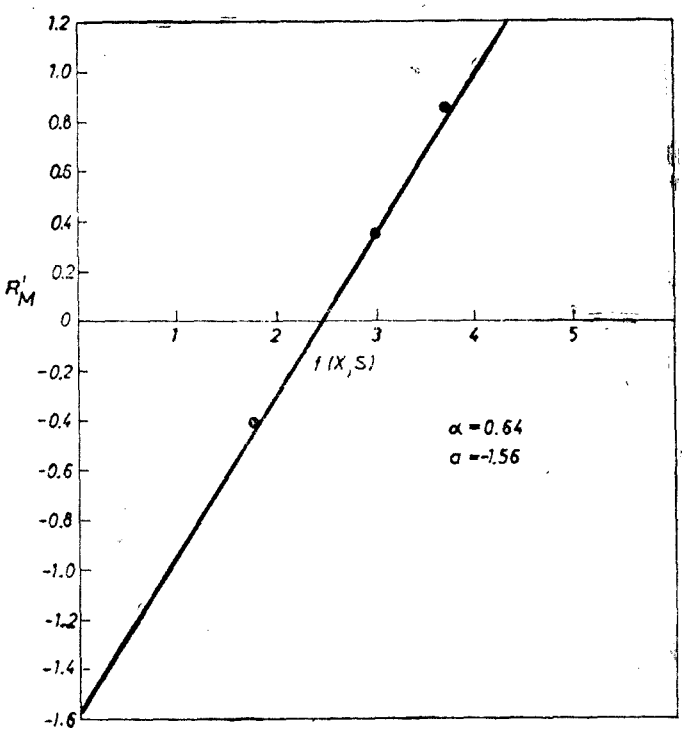


Fig. 2. $R'_M$ vs. f($X$, $S$) for the system of silica gel with benzene as eluent in the presence of standard samples (Table 1). For $a$ and $\alpha$ significances see Eq. (4').

The results obtained by TLC upon separation of the chosen carotenoids, $R_F$ and $R'_M$, are given in Table 2. Relying on the experimental data, and using Eq. (5), the $A_s$ values of the adsorbed carotenoids at the organic solvent/silica gel interface have been computed and they are given in Table 2. It is found that the area ($A_s$) required for an adsorbed molecule at the solution/silica gel interface is quite different with the three carotenoids, and it increases in the order CA < C < CX — which is reasonable having in mind the differing structures of carotenoids and the configurations that could ensue from adsorption of carotenoid on solid. Before molecular area necessities for a given adsorbate can be calculated, the configuration of the sample adsorption must be specified.

An indirect procedure was thus used, by referring to limi-

*Table 1*

$R_F$, $R'_M$ **and f($X$, $S$) values for benzene/silica gel system**

| Standard sample | $R_F$ | $R'_M$ | f($X$,$S$) |
|---|---|---|---|
| p—Amino—azo—benzene | 0.11 | 0.86 | 3.7 |
| Sudan Red | 0.31 | 0.35 | 3.0 |
| Sudan Yellow | 0.66 | —0.40 | 1.8 |

*Table 2*

**Adsorbate molecular areas ($A_s$ and $A_0$) and adsorption energies ($\bar{S}^0$); $R_F$ and $R'_M$ values and solvent strength ($\varepsilon^0$). (For symbols see the text)**

| Sample | $R_F$ | $\varepsilon^0$ | $R'_M$ | $A_s$ | $A_0$ | $\bar{S}^0$ |
|---|---|---|---|---|---|---|
| Ethyl ester of β-apo-8'-carotenoic acid : CA | 0.62 | 0.25 | −0.21 | 10.71 | 8.24 | 4.78 |
| | 0.83 | 0.32 | −0.69 | | | |
| β-Carotene : C | 0.17 | 0.00 | 0.69 | 13.75 | 9.06 | 3.52 |
| | 0.97 | 0.25 | −1.51 | | | |
| Canthaxanthin : CX | 0.16 | 0.26 | 0.72 | 23.18 | 8.71 | 9.61 |
| | 0.92 | 0.38 | −1.06 | | | |

*Note:* Units of 8.5 Å² per unit of $A_s$ and $A_0$

ting molecular area ($A_0$) of these carotenoids adsorbed at the benzene/water interface, previously published by us [3—7], which had been obtained by surface tension measurements. These $A_0$ values correspond to the area of close packed molecules in the adsorbed film at *quasi*-saturation of the liquid/liquid interface, and they are also given in Table 2. Unlike the $A_s$ values, the $A_0$ values for the three carotenoids are close to one another, what pleads for identic orientation of carotenoids in the ordered adsorbed film at the benzene/water interface. Moreover, molecular model studies [3, 6, 7] — on all investigated carotenoids — point to a preferentially vertical orientation of the close packed molecules at values $A_0$ i.e. one of the molecular extremity (Fig. 1) is anchored in the water phase, with CX and C (compounds of symmetric structure), and the ester group is herein anchored in the case of CA (compound of asymmetric structure). The slight differentiation of the $A_0$ values appears to be relating, on the one hand, to the somewhat different geometry of these molecules, which leads to differing area necessities, and on the other hand, to their differing polarity, implied in the interaction with the interfacial water.

As regards the $A_s$ values, estimated from chromatographic data, it is to be noted that they are not as accurate as those obtained by measurements of interfacial tension at the benzene/water interface that is uniform and energetically homogeneous.

For all that, by comparing the $A_0$ values with the $A_s$ values, some conclusions can eventually be drawn about the orientation of the carotenoid molecules in the chromatographic process of adsorption. It can be seen in Table 2 that the $A_s$ values are, generally, greater than the $A_0$ ones — what is realistic taking into account botht he possibilities of orientation of the carotenoids at the solid/liquid interface and the fact that the solid surface is uneven and energetically inhomogeneous. However, the $A_s$ value is close to the $A_0$ one only for the CA sample — what would plead for 'vertical' — prevailing orientation of these molecules at the liquid/silica gel interface, too, with the carotenoid skeleton in the organic liquid phase, orientation that could be ascribed to the strong in-

teractions of the adsorbate with silica gel surface without excluding adsorbate-adsorbate lateral interactions in the inside of the adsorbed layer ; with compound C, $A_s$ is a bit greater then $A_0$, what would suggest a weaker packing in the film of C adsorbed on silica gel than in the one at the liquid/liquid interface ; whereas with the CX sample, $A_s$ is about 2.5 times greater than $A_0$ — which points to a distinctly different orientation of the CX molecules at the two types of interfaces. The great $A_s$ values would suggest a longitudinal adsorption of the molecule of canthaxanthin on the solid, i.e. the molecular chain axis is oriented parallel to the silica gel surface, what would be expected for a cooperative interaction which includes both adsorbate-adsorbent strong interactions and adsorbate-adsorbate lateral interactions in conformity with a simple adsorbed parallel-layer model [8].

Further on, employing the molecular area of carotenoids determined from chromatographic data ($A_s$), the adsorption free energy ($S^0$) of carotenoids on silica gel were computed by Eq. (6), for each eluent used. The $S^0$ values calculated for a certain carotenoid were *not* considerably influenced by the employed eluents, which suggests that the interactions between the carotenoid monolayers adsorbed on silica gel and the bulk solution have no important role. Table 2 gives the mean value of the free energies ($\bar{S}^0$) of carotenoid adsorption at the solution/silica gel interface. The $\bar{S}^0$ values increase in the order C < CA < CX i.e. parallel to the increase of the polarity of these derivatives — which points to occurrence of some specific interactions with surface reactive hydroxyl groups of silica gel e.g. by hydrogen bonds with C = 0 group of compounds CA and CX. In this respect, it is to be noted that value $\bar{S}^0$ for the adsorption of CX is over two times greater than the corresponding value for the adsorption of CA and, especially, for that of C on the silica gel surface, what suggests an alignment and a close packing of the CX molecules, parallel to the silica gel surface. This packing allows for optimizing the interaction of one of the C = 0 polar headgroups through hydrogen bonds to the surface reactive hydroxyl groups of the adsorbent as well as of the other one to the polar group of another nearby CX molecule also longitudinally adsorbed on the solid, in accord to the determined $A_s$ values. This finding is once more indicative that the stability of the adsorbed layer of these carotenoids is due first to the adsorbate — silica gel — prevailing interactions through hydrogen bonds between the C = 0 group and the surface reactive hydroxyls both for CA with the hydrocarbon polyene chain oriented in the bulk solution and for CX lying on the surface, without excluding though the possibility of adsorbate-adsorbate lateral interactions within the adsorbed layer. Such a cooperative interaction can also explain the ordering of carotenoids in the adsorbed layer, i.e. alignment and close packing of the molecules in the ordered CX and CA monolayer on silica gel.

To the end of providing additional information about the adsorption mechanism of carotenoid on silica gel, the $A_s$ values were related to the molecular area necessities required by adsorption, taking into account the different possible configurations for adsorbed all-*trans* carotenoids on silica gel, using molecular geometric models. Carotenoid molecules are considered as rigid plates [3, 6, 7] because of the delocalized $\pi$-bond system of the polyene chain [9]. The molecules are imagined anchored on the silica gel surface, as results from

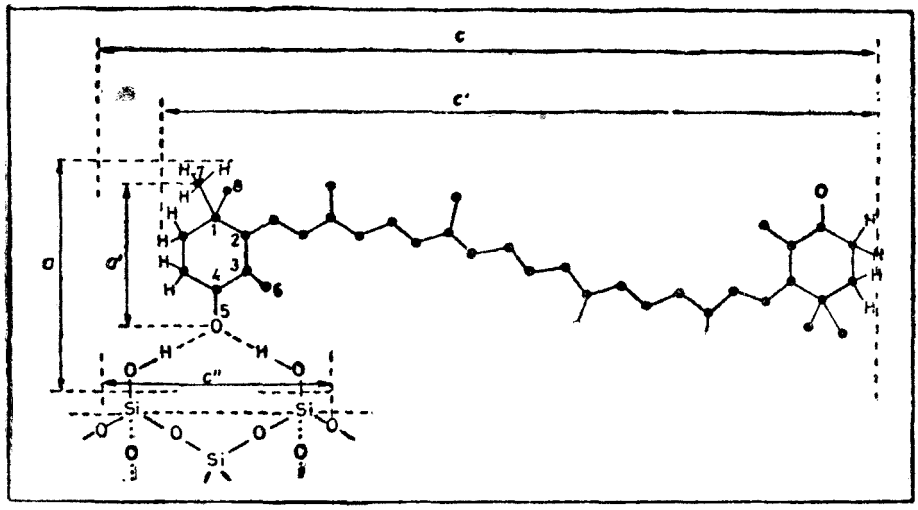


Fig. 3. Shape and dimensions of the canthaxanthin molecule oriented in adsorbed film at the organic solvent/silica gel interface.

the above discussion, by their polar headgroup/headgroups that interact with the hydroxyl groups of the adsorbent surface, which occur in clusters of two or more [1].

To illustrate, one of the possible configurations of canthaxanthin adsorption on the silica gel surface is given in Fig. 3. This "edgewise" configuration seems most likely, considering the canthaxanthin structure (Fig. 1) as well as the $\bar{S}^0$ and $A_s$ values, the possibility of flat or vertical adsorption being however not excluded [1]. The following magnitudes are computed: the width $a$ and thickness $b$ of the molecular plate, as well as the length of the molecular chain $c'$ for the free molecule, the length $c$ of the molecule linked to adsorbent, and $c''$ the length from the molecule that falls as projection on the surface of the adsorbent as a result of the interaction with the OH-surface. For the sake of simplicity the molecular plate thickness $b$ perpendicular on the plane of Fig. 3 has not been drawn. Further on, we are giving the computation of the molecular dimensions for canthaxanthin adsorbed on the silica gel surface. The plane of atoms 1, 2, 3, 4, 5 and 6 is assumed to have a vertical position, and the headgroup axis (width) is presumed to lie along this plane (Fig. 3). By using the bond lengths and bond angles obtained by means of X-ray diffraction [9], the distance between the nucleus of the oxygen atom 5 and the projection of the nuclei of carbon atoms 7 and 8 on the above considered plane is $a' = 5.02$ Å. As there are three hydrogen atoms bound to each of the 7 and 8 carbon atoms, 0.6 Å is added for the C-H bond projection and 0.3 Å for the covalent radius of the terminal hydrogen atoms. At the other end of the head group axis, the oxygen atom can be presumed to interact with two OH-surface groups from the adsorbent. Since the $\pi$-bond of the C=O groups is delocalized, the two hybrid orbitals of the O atom, having the non-participating electron

pairs, must be oriented along the same vertical plane. If the carbonyl group is presumed to interact with the OH surface groups of the adsorbent through the hydrogen bonds on these electron pairs, the vertical projection on the "a" axis of the O...H—O bridge and the covalent radius of the O atom has to be added, i.e. 1.88 Å. The head group width is thus $a = 7.80$ Å. Due to the S shape of the polyene chain (the β-ionone rings are overlaid), the "*a*" width of the polar group is precisely the width of the molecular plate. Thickness *b* of this molecular plate is first determined by the two $CH_3$ groups in positions 7 and 8. Since the binding of the CX molecule to the adsorbent appears to have no contribution when calculating *b*, this size was estimated according to the bond lengths and bond angles taking into account, on the one hand, the covalent radii of the terminal H atoms ($b = 4.9$Å) and, on the other hand, its value (marked by an asterisc) with van der Waals radii of the terminal H atoms ($b^* = 6.3$ Å). Similar to the way employed for studying the behaviour of insoluble monolayers at the air/water interface [3, 6, 7], the polyene chain length (of 23.2 Å) was evaluated, whereat the axis length of the β-ionone rings was aded, i.e. 7.8 Å, obtaining thus the molecule length, $c' = 31$ Å. Furthermore, approximately 1 Å had to be added to this value, representing the contribution of the hydrogen bond to adsorbent, whereof $c = 32$ Å. It is worth mentioning that the *c''* value, computed from the adsorption model, corresponds to 5 Å, which is identic to the one reported [1] for the distance between the O atoms on the surface of silica gel. This fact favours the canthaxanthin adsorption on the silica gel in accord to the $\bar{S}^0$ values.

Computation of the molecular sizes (*a*, *b* and *c*) of the CA compound was performed in a twofold way taking into account the image of the CA molecule: first, this molecule was imagined anchored on the silica gel surface (vertical adsorption) through C=O of the ester group (Fig. 1), which gives hydrogen bonds with the surface OH groups of silica gel — in a similar way to that described with CX (Fig. 3) — and the corresponding values for the "free" CA molecule, values employed in the calculation of area necessities for flat and edgewise configurations. In both cases, the values *a*, *b*, and *c* of the CA molecule were calculated by using for the carotenoid skeleton-containing portion of the molecule the bond lengths and angles found by means of X-ray diffraction, with the canthaxanthin molecule [9], while for the other atoms the values were approximated on the basis of bond lengths given in chemical tables and of the hybridization type, only covalent radii of the terminal atoms being taken into account. For simple bonds in the alkyl portion of the CA molecule a free rotation around them was presumed, and the most stable conformation was considered, also taking into account the possibilities of steric hindrance both for the adsorbed CA molecule on silica gel and for the free CA molecule. For the latter situation, the most stable conformation was considered, corresponding to the minimum molecular section onto a direction perpendicular to the longitudinal axis of the molecule.

In the case of β-carotene molecular dimensions *a*, *b*, and *c* were calculated in a similar way to that used for canthaxanthin, but this time the carotene molecule was considered as a 'free' molecule.

Thus, the molecules were assimilated to a parallelepiped characterized by its sizes: *a*, *b*, and *c* — for varied molecular states, i.e. adsorbed and free

*Table 3*

**Molecular dimensions and areas required by adsorbed carotenoids in various configurations ($A_1$: vertical; $A_2$: flat; $A_3$: edgewise) on silica gel surface**

| Sample | State | $a$, Å | $b$, Å | $c$, Å | $A_1$ | $A_2$ | $A_3$ |
|---|---|---|---|---|---|---|---|
| Ethyl ester of β-apo-8′-carotenoic acid: CA | Adsorbed | 25.0 | 3.6 | 13 | 10.59 | — | — |
| | Free | 5.8 | 4.2 | 26 | — | 15.08 | 12.85 |
| β-Carotene: C | Free | 5.0 | 4.2 | 31 | 2.47 | 18.24 | 15.32 |
| Canthaxanthin: CX | Adsorbed | 7.8 | 4.9 | 32 | 4.49 | 29.36 | 18.45 |
| | Adsorbed | 7.8 | 6.3 | 32 | 5.78 | 29.36 | 23.71 |

*Note:* Units of 8.5 Å² per unit of $A_1$, $A_2$ and $A_3$

molecules, calculated according to the above assumptions — taking for these magnitudes the maximum size in the three perpendicular directions (Table 3).

By means of molecular dimensions the molecular area necessities of the adsorbed sample on silica gel were calculated taking into account the various possible configurations of adsorption such as: vertical ($A_1 = a \times b$), flat ($A_2 = a \times c$) and edgewise ($A_3 = b \times c$) configurations, which, too, are given in Table 3.

By comparing the values of molecular areas of the adsorbed carotenoids — chromatographically computed ($A_s$, Table 2) — with those calculated for different configurations of adsorption (Table 3) one finds that:

— CA is preferentially adsorbed in a vertical configuration ($A_s$ being approximately equal to $A_1$), what is plausible because $A_s$ is also close to the experimentally estimated value for $A_0$ at the liquid/liquid interface (Table 2), as illustrated above;

— β-Carotene appears to be adsorbed randomly on the silica gel surface, $A_s$ being close to $\bar{A} = 12.01$ which is the mean value of the areas for the three configuration of adsorption. This suggestes that β-carotene is not likely to follow preferential adsorption on the silica gel surface, what is in accord with the $A_s$ value greater than $A_0$ — the interaction with the silica gel surface being non specific, which is also evidenced by the smallest $\bar{S}^0$ values of this series of carotenoid derivatives;

— Canthaxanthin appears to be predominantly adsorbed in edgewise configuration, because $A_s \approx A_3$ especially when van der Waals radii are considered for the terminal atoms (Table 3, see $b^*$ values) — in agreement with the values of $A_0$ and the molecular structures, as with the great $\bar{S}^0$ values for its adsorption on silica gel, too.

Therefore, by relating the characteristics of carotenoid film adsorbed on silica gel, namely molecular area of the adsorbed sample and the free energy of its adsorption at organic solvent/silica gel interface, to the properties of the films adsorbed at the solution/water interface and employing molecular geometric models, useful information can be obtained about the orientation and adsorption mechanism of sample molecules in the TLC complex processes.

## REFERENCES

1. L. R. Snyder, "Principles of Adsorption Chromatography", Dekker, New York, 1968.
2. G. Vernin, *La France et ses Parfums*, **64**, 205 (1969).
3. M. Tomoaia-Cotişel, *Ph. D.-Thesis*, University of Cluj-Napoca, 1979.
4. M. Tomoaia-Cotişel, I. Albu, E. Chifu, *Stud. Univ. Babeş—Bolyai, Chem.*, **24**(2), 68(1979).
5. E. Chifu, M. Tomoaia-Cotişel, Z. Andrei, E. Bonciu, *Gazz. Chim. Ital.*, **109**, 365 (1979).
6. M. Tomoaia-Cotişel, E. Chifu, *Rev. Chim.* (Bucharest), **32** (11), 1063 (1981).
7. J. Zsakó, E. Chifu, M. Tomoaia-Cotişel, *Gazz. Chim. Ital.*, **109**, 663 (1979).
8. G. H. Findenegg, M. Liphard, *Carbon*, **25** (1), 119 (1987).
9. O. Isler, "Carotenoids", Birkhäuser Verlag, Basel and Stuttgart, 1971, p. 286.

STUDIA UNIV. BABEŞ-BOLYAI, CHEMIA, XXXII, 1, 1987

# COMPLEX FORMATION AT THE BENZENE/WATER INTERFACE

**JÁNOS DEMETER-VODNÁR*, MARIUS SĂLĂJAN*, MARIA TOMOAIA-COTIŞEL*, JÁNOS ZSAKÓ* and EMIL CHIFU***

*Received: September 8, 1986*

Interfacial tension ($\sigma$) measurements are performed at the benzene (B)/water (W) interface. In system 1, astaxanthin (3,3'—dihydroxy, 4,4'—dioxo-β-carotene (AX)) dissolved in B and $Co^{3+}$ in W, the $\sigma$ *vs* $[AX]_B$ curve recorded at constant $[Co^{3+}]_W$ exhibits a maximum at $[AX]_B : [Co^{3+}]_W \approx 3.5 \ldots 3.75$, pleading for the formation of $Co(AX)_4$-type interfacial complex compound. In system 2, iodo-bisdimethylglyoximino-γ-picolino-Co(III) ([$Co(DH)_2$ I (γ-picoline)] (ID)), dissolved in B and $Hg^{2+}$ in W, a sharp $\sigma$ maximum is formed at $[ID]_B : [Hg^{2+}]_W = 1.95$, consistent with the formation of the interfacial complex ion $[Hg(ID)_2]^{2+}$. Results are in agreement with earlier data concerning both the Co with AX complex formation at the air/water interface, and mechanism of Hg(II) assisted aquation of iodo-cobalt complexes.

Key-words: *interfacial tension, benzene/water interface, interfacial complex, transition metal ions*

**Introduction.** The influence of subphase electrolytes upon the compression isotherms of surfactants (S) insoluble in water, spread at the air/water (A/W) interface was assigned by many authors [1—6] to the formation of surface complexes containig both S molecules/ions and metal ions (M) of the subphase electrolyte. These studies could reveal only the strong interaction between M and S, but they could not tell anything about the composition of the complexes studied.

In the case of water soluble surfactants the molar ratio [S]:[M] can be systematically varied in the subphase and surface tension minima were found with aqueous solutions of mandelic acid [7], lactic acid [8] as ligands (L) and aluminium nitrate at the molar ratios L:Al equal to 3:1, 2:1, and 1:1, respectively. These minima were assigned to complex formation corresponding to the same molar ratios. Surface tension minima were also observed in aqueous solutions of anionic surfactants (sodium dodecylsulfate, sodium alkanesulfonates) and [Fe(1, 10-phenantroline)]$^{2+}$ also suggesting a complex formation at the corresponding ratio [9].

Interfacial tension measurements at oil/water interfaces, as function of molar concentration ratio of S dissolved in the oil phase and of M dissolved in the aqueous phase, showed the interfacial tension to exhibit extreme values at a certain molar ratio. By presuming an interfacial complex formation, having the composition corresponding to molar ratio [S]:[M] at the interfacial tension extremum, with tributylphosphate (TBP) the formation of $Li(TBP)_2$ at the

* *University of Cluj-Napoca, Faculty of Chemical Technology, 3400 Cluj-Napoca, Romania*

hexane/water interface [10] and of $Cu(TBP)_3$ at the benzene/water interface [11] was reported.

A theoretical study of the thermodynamic conditions leading to an interfacial tension extremum has been performed in the case when at the interface of two immiscible liquids A and D, surfactant S soluble in D and a metal ion M, soluble in A may form a complex C, insoluble in both A and D, according to the equation

$$\nu_M M + \nu_S S \rightleftharpoons \nu_C C \qquad (1)$$

To this end, Gibbs-Duhem type equations were written for the 3 phases, viz. for both bulk phases A and D, as well as for the interface. With the interface phase the Guggenheim model [12] was used and the two parallel planes between the interface and the bulk phases A and D, respectively, were placed at equal distances from the physical interface. By using Eq. (1) and the above mentioned Gibbs-Duhem type equations, one can show, that if equilibrium (1) is shifted towards the formation of C, at the interfacial tension extremum the following relation will be valid [13]:

$$\frac{[S]_D}{[M]_A} \approx \frac{\nu_S}{\nu_M}$$

i.e. the molar concentration ratio at which the extremum appears, gives indeed the composition of the interfacial complex obtained.

In the present paper the interfacial tension at the benzene/water (B/W) interface has been studied for two systems. In system 1 the B phase contained astaxanthin and the W phase $Co^{2+}$ ions. In system 2 the B phase contained the nonelectrolytic complex [$Co(DH)_2I$(γ-picoline)] and the W phase $Hg^{2+}$ ions.

These systems have been chosen for the following reasons:

*System* 1. The compression isotherms of astaxanthin (AX) recorded at the air/water interface, both in absence and the presence of $Co^{2+}$ ions in the aqueous subphase, suggested the formation of relatively stable surface complex compounds and on the basis of molecular model and ligand field theory considerations the composition $Co(AX)_4$ seemed to be likely [14]. Consequently, in system 1 an interfacial tension extremum may be expected at the concentration ratio $[AX]_B : [Co^{2+}]_W = 4:1$.

*System* 2. In aqueous solutions, octahedral cobalt (III) and chrom (III) complexes also containing halides as ligand undergo an aquation reaction consisting of the substitution of the halide ions for water molecules. In acid and neutral solutions this reaction is very slow, e.g. for the aquation of *cis*-[$Co(en)_2$ Br(γ-picoline)]$^{2+}$ at 25 °C (en: ethylenediamine) the rate constant is of $k = 2.36 \times 10^{-6}$ $s^{-1}$ [15]. These aquation reactions are very much accelerated by some transition metal ions as $Ag^+$, $Hg^{2+}$, $Pb^{2+}$, $Tl^{3+}$ etc, e.g. the aquation rate of *cis*-[$Co(en)_2$ Br(γ-picoline)]$^{2+}$ increases in the presence of Hg(II) salts up to $10^4$ or even $10^5$ times [16]. The above mentioned ions were found not to catalyze the aquation reaction but to be acceptors of the halide ions and in order to explain the obtained kinetic data the formation of intermediate binuclear complexes was presumed [17].

The formation of such bimolecular complexes with a halide ion bridge might be evidenced at the B/W interface in the case of Co(III) or Cr(III) complexes insoluble in W and soluble in B. Such a complex is e.g. the $[Co(DH)_2 I(\gamma\text{-picoline})]$ non-electrolyte (DH stands for a dimethylglyoxime molecule).

**Experimental.** Materials used were of high purity: benzene and $Co(NO_3)_2 \cdot 6H_2O$ p.a. „Reactivul" Bucharest, $HClO_4$ p.a. „Merck"; astaxanthin (AX; 3,3'-dihydroxy-4,4'-dioxo-β-carotene) Hoffmann–La Roche; the iodo-bis - dimethylglyoximino -γ - picolino - cobalt (III) nonelectrolyte (ID; $[Co(DH)_2I(\gamma\text{- picoline})]$) was obtained on the basis of literature data [18]. Purity of the last compound was ensured by recrystallization and checked by means of chemical analysis. Aqueous solutions were prepared by using twice distilled water. In order to have $Hg^{2+}$ ions in the W phase as Hg(II) salt $Hg(ClO_4)_2$ was used. It was prepared from HgO and $HClO_4$.

Interfacial tension measurements were performed by pendant drop technique. The apparatus used was described elsewhere [19] allowing a reproducibility within 0.1 mN/m. Temperature was maintained at $20 \pm 0.1$ °C.

**Results and discussion.** *System 1.* Interfacial tension ($\sigma$) *vs* time ($t$) curves were recorded at the B/W interface, for different concentrations of AX in the B phase and the same concentration of $Co^{2+}$ in W. Some illustrative examples are given in Fig. 1. As seen, $\sigma$ decreases in time, rather rapidly at the beginning and with increasing $t$ it approaches a limiting value, which was taken for the equilibrium interfacial tension, denoted below simply by $\sigma$. The decrease in time of $\sigma$ is due to the adsorption of the surface active molecules from B phase at the interface, presumably implying the formation of an interfacial complex compound with the W phase transition metal ion. Adsorption equilibrium is reached in about two hours.

By using the equilibrium $\sigma$ values, a $\sigma$ *vs* molar concentration $[AX]_B$ isotherm was constructed, which is given in Fig. 2 (full line curve). For the sake of comparison, in the same figure, also the isotherm obtained for aqueous subphase without $Co^{2+}$ ions [20] is shown (dashed line curve). As seen, up to about $[AX] = 2.5 \times 10^{-4}$ mole/l, both curves are very near to each other,

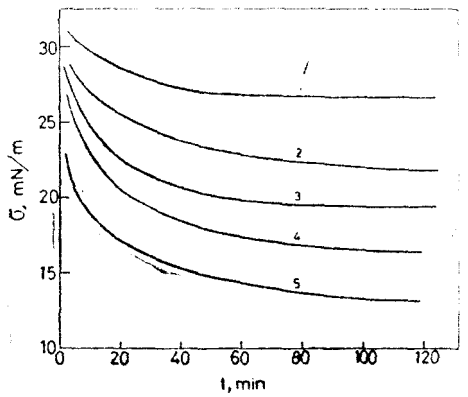


Fig. 1. Interfacial tension *vs.* time curves for system *1*. $[Co^{3+}]_W = 10^{-4}$ mole/l, $[AX]_B \times 10^4$ mole/l: curve (1): 0.71; (2): 1.25; (3): 1.70; (4): 2.59; (5): 4.85.

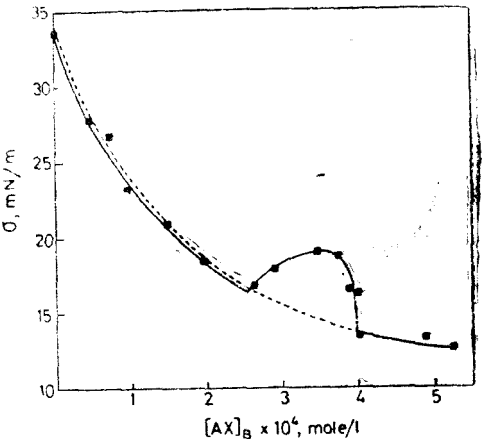


Fig. 2. Equilibrium interfacial tension *vs.* $[AX]_B$ isotherms for system *1*. Full line: $[Co^{3+}]_W = 10^{-4}$ mole/l; dashed line: $[Co^{3+}]_W = 0$.

but at this concentration an increase of $\sigma$ begins, followed by a sudden decrease in the presence of $Co^{2+}$ and at $[AX] \geqslant 4 \times 10^{-4}$ mole/l, the isotherms arrive again near to each other. By taking into account that in the W phase $[Co^{2+}]_W = 10^{-4}$ mole/l, the maximum of the $\sigma$ *vs* $[AX]_B$ curve appears at the molar concentration ratio $[AX]_B : [Co^{2+}]_W$ equal to about 3.5 . . . 3.75. This result is in good agreement with our presumption concerning the composition of the surface complex [14], viz. $Co(AX)_4$. The complete expression obtained for the condition of $\sigma$ extremum is the following [13]:

$$\frac{[S]_D}{[M]_A} = \frac{\nu_S}{\nu_M} \frac{\Gamma_C - \frac{\nu_C}{\nu_S}\Gamma_S}{\Gamma_C - \frac{\nu_C}{\nu_M}\Gamma_M} \tag{2}$$

where $\Gamma_C$, $\Gamma_M$ and $\Gamma_S$ stand for the adsoption of $C$, $M$ and $S$ in the interfaces, respectively. Applied to the interfacial complex $C = Co(AX)_4$, Eq.(2) takes the from:

$$\frac{[AX]_B}{[Co^{2+}]_W} = 4 \frac{\Gamma_C - 0.25\ \Gamma_{AX}}{\Gamma_C - \Gamma_{Co^{2+}}}$$

Since AX is a surface active compound and $Co^{2+}$ is surface inactive, obviously $\Gamma_{AX} \gg \Gamma_{Co^{2+}}$. Consequently, even if $Co(AX)_4$ is a relatively stable complex, involving $\Gamma_C \gg \Gamma_{AX}$, one will have $[AX]_B : [Co^{2+}]_W < 4$ at the extremum of $\sigma$, exactly as obtained experimentally.

Concerning the nature of the interfacial $Co(AX)_4$ complex, it may have neutral molecules, but it might also have an electric charge, since the formation of the Co-O bonds with the O atoms of the OH group in the AX molecules may occur both by substitution of H for Co, leading to the liberation of $H^+$ ions, which pass into the W phase, or simply by using the unshared electron pair of the O atom. Anyhow, the formation of neutral molecules seems to be very likely. In this case two $H^+$ ions are liberated and the other two H atoms could form H bridges between two co-ordinated AX molecules, entailing an enhanced stability of the complex.

*System* 2. From the $\sigma$ *vs* $t$ curves similar to those given in Fig. 1, recorded for different concentrations of ID in the benzene phase, $[ID]_B$, and for the same constant concentration of $Hg(ClO_4)_2$ in the water phase, $[Hg^{2+}]_W = 10^{-3}$ M, the equilibrium values of $\sigma$ were derived. The plot of these equilibrium values *vs* $[ID]_B$ is given in Fig. 3 (full line curve). In this figure the $\sigma$ *vs.* $[ID]_B$ curve, obtained for $[Hg^{2+}]_W = 0$, taken from [20], is also shown (dashed line curve).

As seen, the interfacial tension exhibits a very sharp maximum at the ratio $[ID]_B : [Hg^{2+}]_W \approx 1.95$, pleading for the formation of a $[Hg(ID)_2]^{2+}$ type trinuclear complex ion.

Except the region of the interfacial tension maximum, $\sigma$ values obtained are much lower in the presence of $Hg^{2+}$ in the aqueous subphase, than in its absence. In this respect, there is a great difference between the behaviour of system 2 as compared to system 1, in which the decrease of $\sigma$ due to the W phase

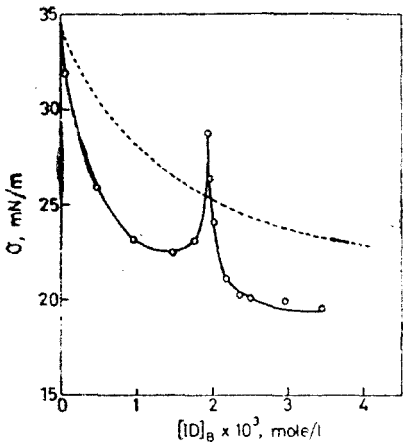


Fig. 3. Equilibrium interfacial tension *vs.* $[ID]_B$ *isotherms for system* 2. Full line: $[Hg^{2+}]_W = 10^{-2}$ mole/l; dashed line: $[Hg^{2+}]_W = 0$.

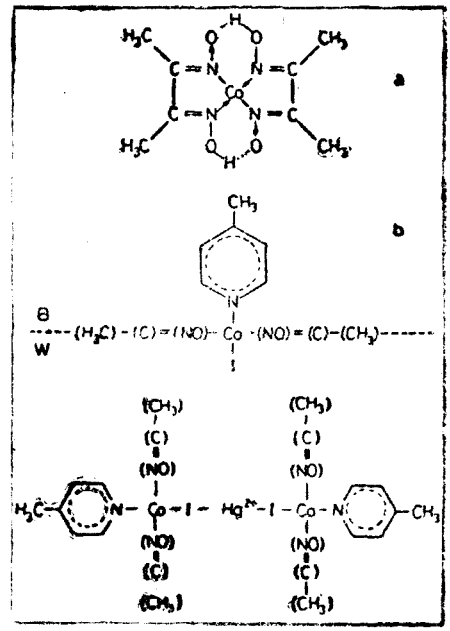


Fig. 4. Molecular structures for system 2: *a,b* — in absence of $Hg^{2+}$ in the W phase; *c* — in the presence of $Hg^{2+}$ in W. *a* — equatorial plane of ID situated in the B/W interface; *b* — axial ligands of ID in a plane perpendicular to the B/W interface. In parantheses: atoms of the equatorial plane situated out of the plane of axial ligands. *c* — the complex $[Hg(ID)_2]^{2+}$. All atoms are situated in the B/W interface except those situated in parantheses. The latter ones belong to the equatorial plane of ID, having in this case an orientation perpendicular to the B/W interface.

electrolyte is very small. This different behaviour might be explained in terms of the interactions of the B phase S molecules with the W phase solvent molecules. Thus, the AX molecules can be thought to be strongly anchored into the W phase, by means of their polar headgroup even in pure monolayer. Presumably, in the case of adsorbed ID molecules, the equatorial plane of the complex, visualized in Fig. 4 a, is situated in the B/W interface and from the axial ligands (Fig. 4 b), the hydrophobic γ — picoline remains in the benzene phase, and the I ligand penetrates into the W phase, due to the polar character of the Co-I bond, but the molecule will be only weakly anchored into the W phase for "pure" monolayers [20]. Therefore, in the absence of W phase electrolyte σ is much lower in the case of AX, as compared to ID, i. e. the surface activity of AX is much largert han that of ID in agreement with our earlier results [20]. Consequently, the co-ordination of AX by the W phase $Co^{2+}$ ions will entail

a less decrease of $\sigma$ than does the co-ordination of ID by the W phase $Hg^{2+}$ ions, exactly as it results from Figs. 2 and 3.

Concerning the structure of the $[Hg(ID)_2]^{2+}$ interfacial complex ion, for the Co-I-Hg-I-Co moiety a linear configuration may be presumed, this being characteristic of the compounds with di-co-ordinated Hg(II). On the base of this hypothesis, the structure given in Fig. 4 c can be imaged. This figure gives the atoms presumed to be in the plane of the B/W interface and the out of plane atoms, belonging to the equatorial ligands are indicated in parantheses (obviously, these atoms appear both in the B and W phases, due to the symmetric character of the equatorial plane; the bridge forming H atoms are omitted in this figure). The enhanced surface activity of these complex ions, as compared to the neutral ID molecules, might be due on the one hand to the stability of the interfacial complex, which can be expected to be insoluble both in B (having an electric charge) and in W (the external ligands having a hydrophobic character) and on the other hand to the possibility of formation of an electric double layer in the side of the W phase (positively charged complex ions in the interface and the corresponding counterions in the adjacent layer of the W phase). Generally, the charged molecular species are considered to have a lower surface activity as compared to the neutral ones, but this is true only if both species are soluble in the same bulk subphase. In our case the interaction between the W phase M ion and the B phase S molecules leads to the retention of the complex ions in the interface, i. e. to an enhanced adsorption.

It is worth mentioning, that accordingly to the molecular models given in Fig. 4, the complex formation leads to a condensing effect since the area necessity of the interfacial complex, corresponding to the configuration given in Fig. 4 c is of about 1.08 $nm^2$/molecule and that of two ID molecules in the configuration of Fig. 4 a would be equal to about 1.18 $nm^2$/molecule [20]. Since both $\gamma$ — picoline and DH ligands are hydrophobic ones, the I-Hg-I bond angle might become less than 180°. In the latter case the area necessity of the complex would be even less than given above.

On the base of both interfacial tension measurements and molecular model considerations, in the system 2 the formation of the interfacial $[Hg(ID)_2]^{2+}$ complex ion can be taken for granted. Therefore, the assumption that in the mechanism of the Hg (II) assisted aquation of iodo-Co (III) complexes, the intermediate formation of binuclear complexes with a Hg-I-Co bridge seems to be likely.

The present study, performed on both systems 1 and 2, reveals that the extreme values of the interfacial tension at the B/W interface, observed at a certain molar concentration ratio $[S]_B : [M]_W$, allows us to evidence the formation of interfacial complex compounds and to determine their composition.

## REFERENCES

1. T. Smith and R. Serrins, *J. Colloid Interface Sci.*, **23**, 329 (1967).
2. T. Smith, *J. Colloid Interface Sci.*, **25**, 443 (1967).
3. Y. Suzuki and H. Matsushita, *Ind. Health*, **7**, 143 (1969).

4. H. Hauser, D. Chapman and R. M. C. Dawson, *Biochim. Biophys. Acta*, **183**, 320 (1969).
5. H. Müller, S. Friberg and M. Hellsten, *J.Colloid Interface Sci.*, **32**, 132 (1970).
6. S. A. Gordziel, D. R. Flanagan and J. Swarbrick, *J. Colloid Interface Sci.*, **86**, 178 (1982).
7. E. Chifu, I. Albu and M. L. Huszár, *Studia Univ. Babeş—Bolyai Chem.*, **16**(2), 15 (1971).
8. E. Chifu and I. Albu, *Studia Univ. Babeş—Bolyai Chem.*, **18**(1), 81 (1973).
9. S. Ozeki, S. Tachiyashiki, S. Ikeda and H. Yamatera, *J. Colloid Interface Sci.*, **91**, 430 (1983).
10. E. Chifu and G. Gabrielli, *Gazz. Chim. Ital.*, **98**, 1213 (1968).
11. M. Tomoaia, Z. Andrei and E. Chifu, *Rev. Roumaine Chim.*, **18**, 1547 (1973).
12. E. A. Guggenheim, "Thermodynamics", 5th ed., North Holland, Amsterdam, 1967, p. 45.
13. E. Chifu, J. Zsakó, M. Tomoaia-Cótişel and I. Albu, unpublished results.
14. E. Chifu, J. Zsakó, M. Tomoaia-Cotişel, M. Sălăjan and I. Albu, *J. Colloid Interface Sci.*, **112**, 241 (1986).
15. J. Zsakó, Cs. Várhelyi and S. Bleoca, *Acta Chim. Sci. Hung.*, **70**, 175 (1971).
16. J. Zsakó, J. Demeter-Vodnár, I. Bâldea and Cs. Várhelyi, *Rev. Roumaine Chim.*, **31**, 443 (1986).
17. J. N. Armor and A. Haim., *J. Am. Chem. Soc.*, **93**, 867 (1971).
18. Cs. Várhelyi and B. Böhm, *Studia Univ. Babeş—Bolyai Chem.*, **9**(1), 55 (1964).
19. E. Chifu, M. Sălăjan, J. Demeter-Vodnár and M. Tomoaia-Cotişel, *Rev. Roumaine Chim.*, **32**, 683 (1987).
20. E. Chifu, J. Zsakó, M. Tomoaia-Cotişel, M. Sălăjan, J. Demeter-Vodnár and Cs. Várhelyi, *Studia Univ. Babeş—Bolyai Chem.*, **32** (2), 1987 (in press).

STUDIA UNIV. BABEŞ-BOLYAI, CHEMIA, XXXII, 1, 1987

# QUANTITATIVE ANALYSIS OF SOME NEUROTRANSMITTERS FROM RAT BRAIN BY GAS GHROMATOGRAPHY – MASS SPECTROMETRY

MONICA CULEA*, N. PALIBRODA* and A. D. ABRAHAM**

*Received: September 8, 1986*

Quantitative methods for the analysis of neurotransmitters — aminoacids (glycine, serine, aspartic acid, glutamic acid, — aminobutyric acid), catecholamines (adrenaline) and anaesthetics (procaine) — by gas chromatography coupled to mass spectrometry have been worked out. Amino acids were analysed as N(O)-trifluoroacetyl-butyl esters. $^{15}$N-lysine was used as internal standard. Adrenaline was analysed as a trimethylsilyl derivative. Procaine was analysed underivatized, using pyrene as internal standard.

Key-words: *GC/MS, neurotransmitters, aminoacids, adrenaline, procaine*

**Introduction.** The classical monoamine neurotransmitters, acetylcholine and the catecholamines, are used by only a small proportion of synapses in mammalian c. n. s. The amino acids GABA (γ-amino — butyric acid) and L-glutamate may be the principal inhibitory and excitatory neurotransmitters used for fast point-to-point transmission in the c.n.s. The monoamines and the large number of neuropeptides (over 30) now known to exist in c. n. s. may be chemical signals used for a different type of chemically addressed form of information transmission between neurons in c.n.s. characterized by less precise spatial connections, a slower time course and a far richer diversity of chemical signals than used in classical synaptic neurotransmission. In this context the brain can be viewed as a neuroendocrine secretory organ of great complexity [1].

The aim of this work was to establish methods to quantitate some of the neurotransmitters of the rat brain using gas chromatography coupled to mass spectrometry (GC/MS).

**Experimental.** A MAT 311 mass spectrometer coupled to a Perkin Elmer model 990 gas chromatograph with flame ionization detector (FID) was used. The GC/MS interface was an effluent separator of the Biemann-Watson type.

Ions were produced by electron impact at 70 eV and accelerated at 3kV. A high voltage of 2 kV was used at the secondary electron multiplier. The ion source was maintained at 200°C.

The following chromatographic columns were used: 1. Ethylene Glycol Adipate (EGA) 1%, glass column 2 m × 4 mm i.d., with temperature program 60°C for 8 min, then 2°C/min up to 200°C.
2. Capillary glass column SE 30 of 15 m length programed from 120°C to 240°C with 8°C/min.

* *Institute of Isotopic and Molecular Technology, 3400, Cluj-Napoca, Romania*
** *Biological Research Center, 3400 Cluj-Napoca, Romania*

3. Capillary glass column Silar 10 C of 24 m length, programmed from 120°C to 225°C with 12°C/min.

Response factors for the quantitative analysis of the aminoacids were determined by preparing derivatives of mixtures containing 100 μg of each aminoacid investigated. The aminoacids were analysed as N(O, S)-trifluoracetylbutyl esters. Derivatization was performed in the first step as esterification with butanol-HCl 3 M at 150°C for 20 minutes, followed by trifluoracetylation in methylene chloride-trifluoracetic anhydride (TFAA) (1:1) at 150°C for 15 minutes and drying at 0°C in an argon stream [2].

The extraction of the aminoacids from the rat brain samples consisted in the following steps: deproteinization for several hours with ethyl alcohol 96% 4:1 v/v alcohol to brain tissue homogenate (0,2 g tissue per ml Krebs Ringer serum) [3], centrifugation, filtration and evaporation of the supernatant to dryness in an argon stream.

During the evaporation $^{15}N$ labelled Lysine 93.3% $^{15}N$ in the position α was added as internal standard for the quantitative analysis of the amino acids in the GC mode in order to avoid possible interferences at the lysine peak in FID detection. Quantitation of lysine was performed by ion monitoring at m/z 320 and 321. Subsequently glutamic acid (Glu) + glutamine (Gln) were determined in a separate run at m/z 180 using total lysine as standard. The remaining aminoacids were finally determined with respect to glutamic acid using FID detection.

Adrenaline was analysed as trimethylsilyl derivative (TMS). Silylation was performed after the extraction step (Curtius *et. al* [4]) at 80°C for 10 minutes in BSA-ethyl acetate (1:1, v/v).

Procaine was analysed in underivatized form using pyrene as internal standard. The GC/MS method was preferred to analyse procaine from brain samples because interferences at the procaine peak were observed in brain samples.

Procaine was extracted from brain homogenates using the procedure of Sundlof *et al.* [5] with a few modifications. Ultrasonication was used to increase extraction efficiency.

For the analysis of underivatized procaine in the nanogram range washing of the injector glass liner and GC/MS interface stainless steel tubing with ethanol: KOH 0,1M (1:1 v/v) were found necessary. The interface tubing was additionally coated with a thin film of OV 17 from a acetone solution. At the begining of each series of determinations the apparatus was conditioned by injecting BSA and triethylamine.

The response factor for procaine vs. pyrene was determined in FID and GC/MS mode by adding known amounts of procaine and pyrene to brain homogenate.

**Results and discussion.** The gas chromatographic separation of a mixture of aminoacids (100 μg each) on column 1, EGA 1%, 2 m length, is shown in Figure 1. Preliminary results of the aminoacid content of brain extracts of 3 month old male Wistar rats are shown in Table 1. The standard errors for a derivatized sample injected repeatedly were of about ± 7%. For different extractions however standard errors were higher, of about ± 25%.

In Figure 2 is shown the GC elution of Adrenaline-TMS on column 2, SE 30, 15 m length, together with the chromatographic conditions. The mass spectrum of adrenaline-$(TMS)_3$ is shown in Figure 3.

The chromatographic separation for the analysis of procaine with pyrene as internal standard, on a capillary glass column with Silar 10 C, 24 m, is shown in Figure 4.

Procaine was analysed in an in vitro experiment of incubated rat brain homogenates containing 0.2 g tissue/ml Krebs Ringer serum and a procaine dose of 5 mg/kg (1 μg/ml homogenate). Table 2 presents procaine concentrations

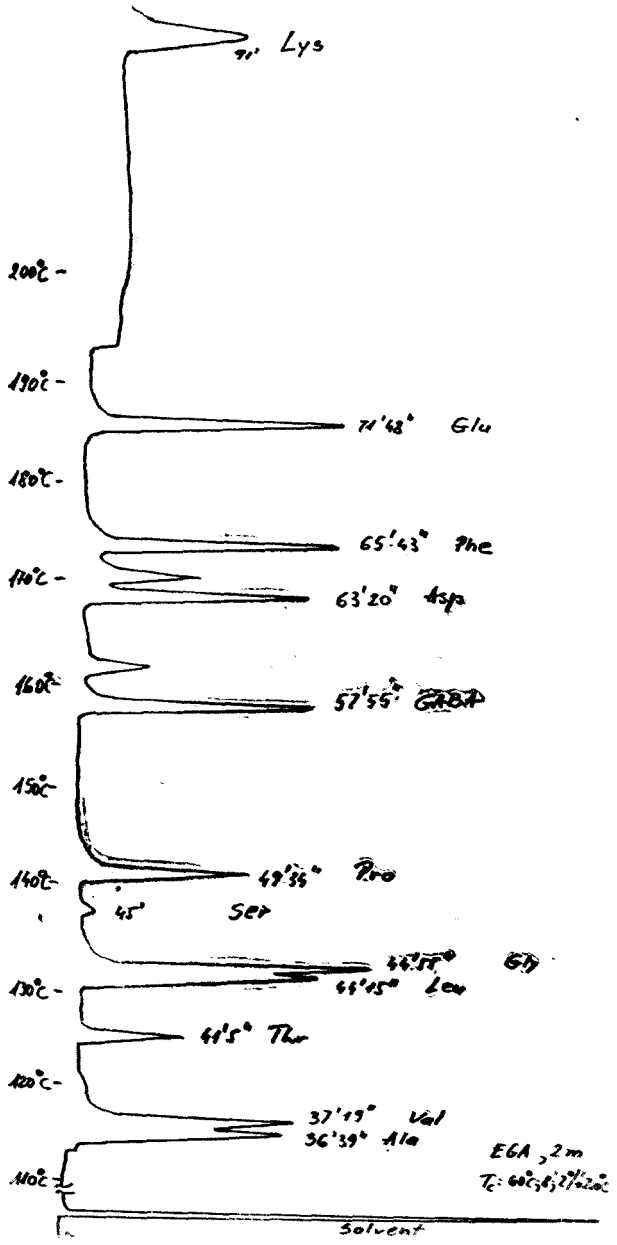


**Fig. 1. Gas chromatographic separation of a mixture of aminoacids (100 µg each).**

*Table 1*

| Amino acids | µg/g | µmol/g |
|---|---|---|
| Gly | 156 | 2,08 |
| Ser | 691 | 6,58 |
| Asp + Asn | 1237 . | 9,30 |
| Glu + Glu | 1611 | 10,95 |
| GaBA | 411 | 4.00 |

found for Wistar rats 3 and 9 month old after 20 min and 60 min incubation in vitro at 38 °C together with the initial values. The data show a significantly higher rate of the concentration decrease in the young rats.

**Conclusions.** Gas chromatography and especially gas chromatography coupled to

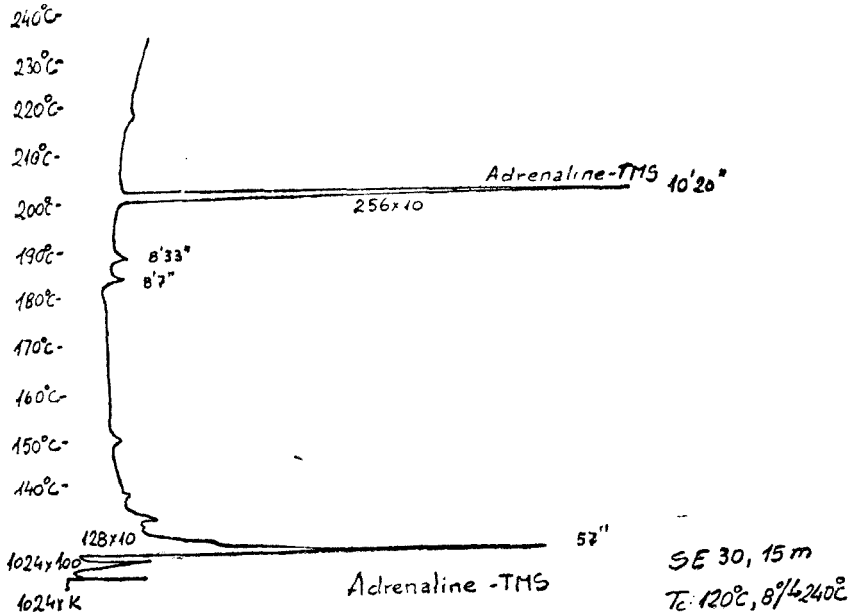


F i g. 2. Gas chromatographic elution of adrenaline TMS.

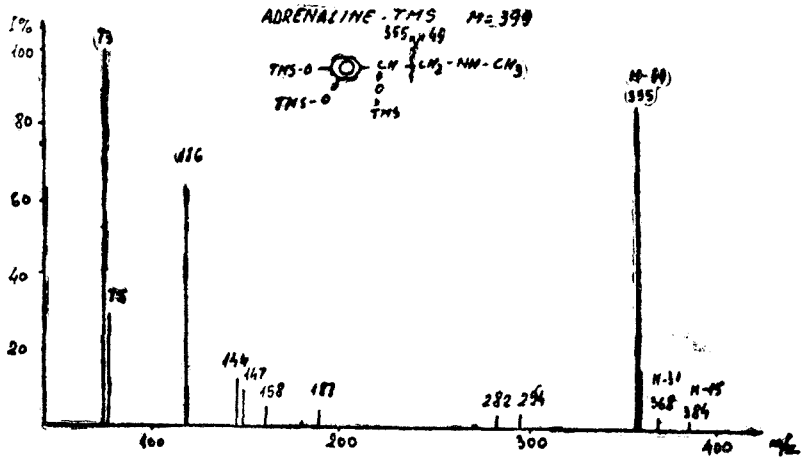


F i g. 3. Mass spectrum of adrenaline—$(TMS)_3$.

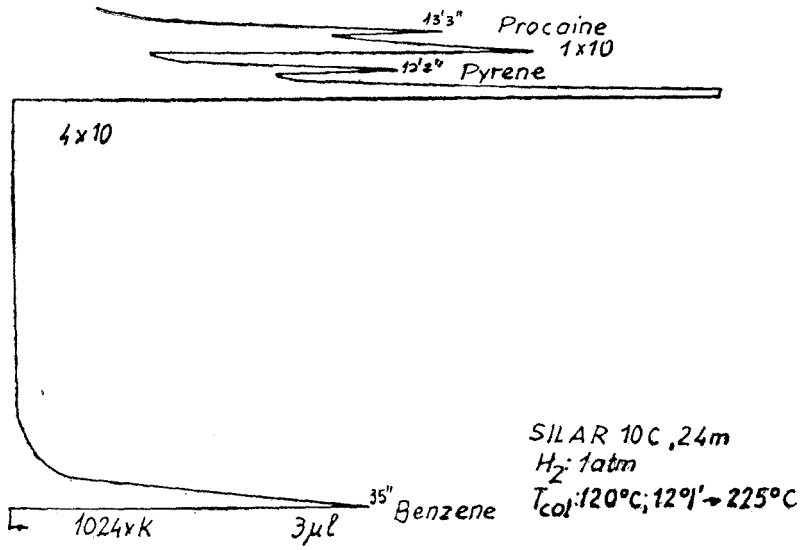


Fig. 4. Gas chromatographic analysis of procaine.

*Table 2*

| Experiment | | $n$ | ng/ml $t = 0$ | $t = 20$ min. | $t = 60$ min. |
|---|---|---|---|---|---|
| Wistar rats (3 month old) | Brain/Procaine HCl | 16 | 780 | 501 | 206 |
| Wistar rats (9 month old) | Brain/Procaine HCl | 6 | 804 | 697 | 525 |
| | Brain/Gerovital $H_3$ | 6 | 929 | 797 | 585 |
| | Brain/Aslavital | 6 | 672 | 607 | 495 |

mass spectrometry together with stable isotope labelled analysis may be successfully used to determine brain neurotransmitters in the microgram and nanogram range.

## REFERENCES

1. Iversen, L. L., *Proc. R. Soc. Lond.*, B **221**, 245 (1984).
2. Gehrke, C. W., Takada, H., *J. Chromatogr.*, **76**, 63 (1973).
3. Hais, I. M., Macek, K., „Cromatografia pe hîrtie", ed. Tehnică, București (1960).
4. Curtius, H. Ch., Wolfensberger, M., Steinmann, B., Redweik, U., Siegfried, J., *J. Chromatogr.*, **99**, 529 (1974).
5. Sundlof, S. F., Duer, W. C., Hill, D. W., Gaucarz, T., Dorvil, M. G., Rosen, P., *Am. J. Vet. Res.*, **44**, 1583 (1983).

# RECENZII

Ionel Haiduc and J. J. Zuckerman, **Basic Organometallic Chemistry**, Walter de Gruyter, Berlin, New York, 1985, XVI + 488 + XXVIII pp.

There are things you can depend on, when looking for top quality; so is the presence of Professor Haiduc's name on the cover of a book. The updating and reediting in English (together with Professor J. J. Zuckerman — another name of resonance in the field) of his well-known text "Chimia Compuşilor Metalorganici", was an event and it became a textbook for the american students. Such a performance is indeed a contribution to the prestige of our University of Cluj on the international arena.

"Basic Organometallic Chemistry", as its name implies, is intended mainly for the newcomer to the field (a fact clearly stressed by the authors in the Preface), so that only the synthesis, reactions, and molecular structure of organometallic compounds are emphasized, giving the reader a really comprehensive overview of this fascinating chapter of modern chemistry.

The book is divided into three parts, with judicious subdividing into lower-level sections, focusing the reader's attention on clear-cut subjects, the way a good textbook should.

In Part I the "rules of the game" are briefly but authoritatively summarized, with special emphasis on the metalcarbon bond — the central structural element of the compounds under scrutiny — and with reference to both laboratory techniques and the routes of access to the ever increasing literature of organometallic chemistry.

Parts II and III, which amount, together, to almost 90% of the book extent, are devoted to the organometallic compounds of non-transition elements and transition metals, respectively. The subdivisions of these two parts follow the Periodic System as a guide line, which is not only very convenient and scientifically sound, but also represents a **sui-generis** tribute to the historic fact that it was the organometallic derivatives that enabled Mendeleev to determine the oxidation states of several of the elements, giving essential clues as to their right placement in the System.

The style is clear and straightforward, the text is rich in structural formulas and contains just the right amount of Tables to provide a synthetic presentation of some aspects. A very good decision was taken when a Professor's Edition was issued (in parallel with the student paperback version) with abundant literature data, enabling the nature scientist to make full use, in both teaching and research, of the precious information contained in this remarkable book.

An extended Subject Index concludes this work giving direct access to selected topics, a feature which ought not to be neglected in any work designed for instruction.

The printing is of high quality, with virtually no errors; this book is, in fact, not only a very enlightening but also an enjoyable reading. It will be, no doubt, of great utility for a wide range of chemists, both beginners and with long experience, and its apparition corresponds to a real necessity, taking into account the large field of practical applications and the outstanding theoretical significance of organometallic chemistry nowadays.

Both the authors and the Publishers are to be congratulated for this success.

IOAN SILBERG

INTREPRINDEREA POLIGRAFICĂ CLUJ,
Municipiul Cluj-Napoca, Cd. nr. 386/1987.

În cel de al XXXII-lea an (1987) *Studia Universitatis Babeş-Bolyai* apare în specialităţile:

matematică
fizică
chimie
geologie-geografie
biologie
filosofie
ştiinţe economice
ştiinţe juridice
istorie
filologie

In the XXXII-nd year of its publication, *Studia Universitatis Babeş-Bolyai* is issued as follows:

mathematics
physics
chemistry
geology-geography
biology
philosophy
economic sciences
juridical sciences
history
philology

Dans sa XXXII-e année (1987), *Studia Universitatis Babeş-Bolyai* paraît dans les spécialités:

mathématiques
physique
chimie
géologie-géographie
biologie
philosophie
sciences économiques
sciences juridiques
histoire
philologie

43 870

Abonamentele se fac la oficiile poștale, prin factorii poștali și prin difuzorii de presă, iar pentru străinătate prin „ROMPRESFILATELIA", sectorul export-import presă, P. O. Box 12—201, telex. 10376 prsfir, București, Calea Griviței nr. 64—66.

**Lei 35**